ANALYSIS AND MODELLING OF SOIL CO2 EMISSIONS WITHIN TEMPERATE CONIFEROUS AND DECIDUOUS FORESTS

By

Yueqian Ma, B.Sc.

A Thesis

Submitted to the School of Graduate Studies

In Partial Fulfillment of the Requirements

For the Degree

Master of Science

McMaster University

MASTER OF SCIENCE (2020) **MCMASTER UNIVERSITY**
(School of Earth, Environment, and Society)
HAMILTON, ON

TITLE: Analysis and Modelling of Soil CO2 Emissions Within Temperate Coniferous and Deciduous Forests

AUTHOR: Yueqian Ma, B.Sc. (Baylor University)

SUPERVISOR: Dr. M. Altaf Arain

NUMBER OF PAGES: v; 133

Abstract

Climate change and extreme weather events have impacted global forest ecosystems' ability to sequester atmospheric carbon dioxide. In this study, the temporal and spatial dynamics of soil CO_2 efflux or soil respiration (Rs) was measured in a temperate coniferous (TP74) and a deciduous forest (TPD) over a six-year period (2014 to 2019). Analysis of Rs trends showed a strong positive correlation with soil temperature (Ts) and soil moisture (SM) at TPD and TP74 causing large pulses of Rs. The average annual temperature sensitivity (Q_{10}) was found to be 2.06 for TPD and 1.87 for TP74. Coherence analysis for both sites from 2017 to 2019 showed that in extreme weather events, TP74's carbon pool was less stable than that of TPD. Dynamics of Rs at both forest sites was further analyzed using thirteen different Rs models (e.g. Ts only, SM only, Ts and SM models, neural network) to evaluate their performance in simulating observed patterns of soil CO_2 effluxes. As compared to other models, the Gaussian – Gamma model consistently reproduced observed dynamics of Rs where on average 70% of variability in Rs was explained.

This study showed that Ts and SM are key determinants of Rs in both forests. Models that incorporate the influence of SM on Rs and were able to better simulate Rs dynamics as compared to Ts only models. Results also suggest that coherence analysis can be utilized to understand temporal variations in Rs. The knowledge of environmental drivers of Rs can be used to determine the impact of climate change and extreme weather events on Rs and assist in developing ecosystem models.

Acknowledgements

This work would not have been possible without the guidance of Professor Altaf Arain, whose knowledge and experience were critical in assisting me with this thesis. I am extremely grateful for the opportunities and experiences that have come from being a part of his group under his supervision.

I am deeply appreciative of extremely valuable discussions and contributions that my friends Shawn McKenzie and Eric Beamesderfer have assisted me over the course of this project to produce meaningful and conclusive analysis of data used for my research.

I would also like to thank the Global Water Futures (GWF) Program and McMaster School of Earth, Environment, and Society for my two years of funding and research scholarships.

Other graduate students in my group also deserve their own share of acknowledgements. Every assisted issue, problem, or question that you have answered or assisted has earned you my gratitude. Thank you, Olivier Champagne, Tariq Deen, Alanna Bodo, Mohamed Rizwan, Nur Hussain, Myroslava Khomik, Stéfan Sauer, and Bing Xu. I would also like to thank our technicians Keegan Smith and Ian Martin for their assistance in field work and data collection.

I also deeply thank my parents, Xianlian Ma and Xiaofei Wu, and my grandparents Tongming Wu and Jianying Li for their support throughout my life, struggles, and successes.

Table of Contents

List of Tables

Chapter 2.

Chapter 3.

List of Figures

Chapter 2.

Chapter 3.

Chapter 1. Introduction

1.1 Forests and the Carbon Cycle

About half the global terrestrial carbon (C) sink is located within forests with the majority (60%) of forest carbon residing within soils (Gomez-Guerrero and Doane, 2018; Canadell et al, 2007; Kindermann et al, 2008). The forest carbon pool consists of 691 pentagrams (Pg) in plant biomass with up to 968 Pg in soils, which is twice as large than that of the atmosphere carbon pool (i.e. 817 Pg) (Lorenz and Lal 2010). Carbon is important for all biological cycles and contributes towards many of Earth's physical processes. Carbon dioxide (CO_2) is taken from the atmosphere by photosynthesis and is sequestered into plant structures. Energy production and biomass storage by plants locks up some carbon while the rest is respired and returned to the atmosphere as carbon. Through litterfall and decomposition, plant carbon enters the soil. Litterfall carbon is utilized by microbes through cellular respiration and CO_2 is released to the atmosphere (Brady and Weil, 2017; Lorenz and Lal, 2010). Forests play a crucial role to regulate carbon fluxes because of their ability to store carbon for extended periods of time within woody biomass and organic matter (Apps and Price, 1996; Yanai et al, 2003; Ontl et al. 2020).

The natural carbon cycle has become unbalanced due to human-induced greenhouse gas emissions, primarily from transportation, electricity production, and burning of fossil fuels (IPCC, 2019). Deforestation due to logging and agriculture has also limited terrestrial carbon sequestration in these ecosystems.

Reduced forest cover can influence the carbon budget within soils by causing increases in soil temperatures and soil water content and affecting microbial activity (MacDougall and Beltrami, 2017). Sequestered carbon within soils can also be released for several decades after deforestation from disturbance (Petrenko and Friedland, 2015).

To mitigate the effects of increasing atmospheric CO_2 concentrations on climate, there have been efforts to restore forest ecosystems and to introduce management strategies such as thinning, afforestation, and natural disturbance control (Bastin et al, 2019; Gonzalez – Benecke et al, 2010; Jandl et al, 2007). Thinning can increase radial growth in remaining trees and decrease litterfall which reduces forest floor accumulation (Assmann, 1961; Sobachkin et al, 2005). Afforestation of former agricultural sites can increase aboveground biomass and total carbon storage (18%) over multiple years (Guo and Gifford, 2002). Natural disturbances primarily fires release stored carbon into the atmosphere and decrease the forest carbon pool. Large-scale wildfire suppression through prescribed burns can decrease the frequency and intensity of fires. These management techniques promote forest ecosystem growth, carbon storage, and soil carbon pool stabilization (IPCC 2014).

1.2 Soil Respiration

Soil respiration (Rs) is the production of CO_2 by microorganisms within the soil. Historically, respiration has been used for the development and testing of fertilizers by measuring the biological activity of organisms (Russell and Appleyard, 1915; Lieth and Ouellette, 1962). Development of the Infrared Gas Analyzer (IGRA) and

its use in chambers have allowed scientists to measure soil CO_2 emissions, conduct experimental studies, and develop empirical relationships between Rs and temperature (Wiant, 1967; Kucera and Kirkham, 1971; Monteith et al, 1964; Medina and Zelwer, 1972; Gonzalez-Ubierna and Lai, 2019; Yan et al, 2019).

Rs occurs via two major processes: autotrophic respiration and heterotrophic respiration. Autotrophic respiration is the release of carbon from symbiotic mycorrhizal fungi within plants and other microorganisms in the rhizosphere, heterotrophic respiration is the production of carbon through decomposition of organic matter by fungi, animals, and bacteria. (Luo and Zhou, 2006). Direct methods of measuring Rs include open and closed soil chambers. Open chambers involve periodic sampling of CO_2 concentrations and efflux is computed from the increase of CO_2 concentrations within the chamber. Closed chambers involve the circulation of air from the chamber to a gas analyzer to measure the rate of change in CO_2 concentrations and CO_2 efflux (Norman et al, 1997).

1.3 Contributing Factors of Soil Respiration

There are two primary sources that affect Rs within forests: abiotic sources and biotic. Abiotic sources are non-organic environmental controls that affect Rs such as temperature, soil moisture, forest type, forest management, pH, and soil texture. Biotic factors result from organic processes such as soil and root microorganism activity.

1.3.1 Environmental Factors

Rs is driven by soil temperature and soil moisture. High soil moisture content facilitates the transport of nutrients within the soil (Orchard and Cook, 1983). Microorganisms utilize water within the soil along with organic material to extract nutrients using aerobic respiration. Drought can also influence Rs. Multiple studies show a decrease in soil respiration in response to lowered precipitation (Borken et al, 2005; Schindlbacher et al, 2012; Knorr et al, 2008; Nikolova et al, 2009). Drought can influence the diffusion of CO_2, cellular enzyme activities, and facilitation of nutrient transport (Selsted et al, 2012; Wang et al, 2014; Sun et al, 2019).

The soil temperature of a forest stand can affect Rs by increasing the rate at which microorganisms decompose organic matter. However, at temperatures greater than 35^{o}C, microbial enzymes that facilitate respiration are denatured, which causes increased vulnerability to changes in climate of traditionally low respiring forest stands such as boreal and alpine forests (Lützow et al, 2009).

The type of soil can influence the amount of respiration depending on the distribution of pore spaces between soil particles. In forests dominated by sandy soils, Rs returns to values before a wet/dry event twice as fast compared to those composed of silt or clay (Bouma and Bryla, 2000). Soils composed of sand cannot maintain water stability compared to soils that are clay-based (Balashov and Bazzoffi, 2003). Other factors such as compaction and root infiltration can also

influence soil pore space by decreasing the amount of nutrients available to microorganisms.

Rs is affected by changing seasons throughout the year. Warming temperatures within the early spring combined with increases in soil moisture from melting snow can cause a dramatic increase in respiration (Makita et al, 2018). Increases in rainfall and ground infiltration causes CO_2 within soil air spaces to be forced out of the soil. During dry-rewetting phases in the summer, increases in soil temperature may promote respiration due to increased root development and decomposition (Ruess et al, 1996; Högberg et al, 2001). Changes in temperature, wind gusts, and plant water uptake affect soil volume storage, which result in CO_2 forcing from differences in pressure potentials (Luo and Zhou, 2006).

Respiration varies with stand age in temperate forests. As a forest ecosystem matures, Rs increases because of succession sequences of plant community replacement, which promotes greater productivity (Johnston, 2017). Forest management practices such as clear cutting or thinning transfers sizeable amounts of organic matter to the soil causing a sharp rise in respiration from decomposition. In mid-successional forests, respiration slows because crown closure shades the soil surface, which causes decreased soil temperatures and water availability (Li, 1926). In old-growth forests, soil respiration increases due to high primary productivity and litter production which contributes to the soil carbon pool (Striegl and Wickland, 2001).

Forest composition is also a determining factor in Rs. A homogenous coniferous or deciduous forest can have different litter decomposition rates and lignin and nutrient composition compared to coniferous forests (Trofymow et al, 2002). Lignin is an organic polymer present in leaves with a rigid carbon structure that is difficult for soil microorganisms to decompose (Poerschmann et al, 2005). Coniferous needles have a greater amount of lignin, which results in slower decomposition and buildup between years (Sahin and Yalcin, 2017; Berg et al, 1984). Deciduous leaves contain more nutrients in loose bound carbon structures formed mostly from cellulose which allows greater rates of decomposition and resultant Rs (Dickinson and Pugh, 1974).

1.3.2 Soil Organic Carbon

Soil organic carbon (SOC) is the amount of measurable organic matter within the soil and can assist in forest productivity through mineralization and decomposition (Schnitzer and Khan, 1978). Globally, SOC contains approximately 1,500 pentagrams of carbon within the top meter of soil which exceeds carbon stored within the atmosphere (~800 pentagrams) and terrestrial vegetation (~500 pentagrams) (FAO and ITPS, 2015).

The amount of SOC within the soil is dependent on decomposition and respiration rates, the erosion and deposition of new soil, and environmental factors such as temperature, and water content. SOC stabilizes the soil horizon by increasing nutrient retention within the soil and regulates soil water capacity. SOC is divided into two pools with different turnover rates: active pools, which have a turnover

rate from a few months to years, and passive pools that have turnover up to thousands of years (Lefèvre et al, 2017). Anaerobic (without oxygen) conditions or soil aggregates can affect turnover times.

Multiple physical and chemical mechanisms can stabilize carbon that enters the soil (Six et al, 2002; Jastrow et al, 2007; Makusa, 2015). Physical stabilization involve isolation with micro- and macro-aggregates causing nutrients to be inaccessible to microorganisms. Chemical stabilization include absorption into clays from formation of chemical bonds. Biogeochemical changes may cause carbon re-formation into chemically inert and complex structures unable to be decomposed.

Although climate change can cause an increase in temperature which can influence increased plant production and litterfall, it also results in increased decomposition of SOC (Keestrea et al, 2016). The frequency of extreme events can be exacerbated with climate change. Increased precipitation can interfere with soil formation by causing compaction by rainfall, changes in soil temperature, vegetation and the availability of micro- and macro-organisms (FAO and ITPS, 2015)

1.3.3 Climate Change and Human Activity

Since the industrial revolution in the 18^{th} century, global atmospheric CO_2 has steadily increased. In response to this increase, ecosystems have experienced increased respiration rates. For example, an analysis of 54 sites in multiple ecosystems and locations had an average of 12–40.6% respiration increase in response to higher atmospheric CO_2 (King et al, 2004). Temperature increases in

parts of the world by climate change can affect all biogeochemical process within an ecosystem. Warming temperatures can extend growing season length (Oberbauer et al, 1992; Norby et al, 2003), stimulate plant growth (Wan et al, 2005), and increase soil nitrogen while reducing soil water content (Rustad et al, 2001).

Climate change can also increase wildfire frequency in an ecosystem. Wildfires reduces Rs by decreasing soil moisture, surface litter, and vegetation (O'Neill et al, 2002). Parro et al, (2019) showed that following a forest fire, average respiration in burned forest areas is half of that compared to unburnt plots. In colder climates such as the Arctic where soil contain sizeable amounts of organic carbon, wildfire causes permafrost to thaw. This process causes trapped organic material to release, enhancing decomposition and increasing Rs (Shaver et al, 2001).

Thinning or clear cutting can change the forest's hydraulic redistribution and passive water movement. When dominant trees are removed, there is a decrease in water movement from deeper layers to shallow layers of soil (Peichl et al, 2010). This movement within soil pores is important for the transference of nutrients and organic matter (Hartge and Stewart, 1995). Thinning can also cause increases in water evaporation and soil temperature sensitivity by exposing previously shaded areas (Campbell et al, 1977).

1.4 Soil Respiration Measurement Methods

Automatic soil chambers involving one or multiple chamber systems can be utilized to measure soil respiration. Single systems use an automatic chamber installed

permanently at the soil surface. The chamber closes when measuring CO_2 efflux but remains open to allow precipitation. A multi-chamber system utilizes an IGRA to measure CO_2 efflux. The chamber system can be custom made to suit research interests and has reference gas canisters for calibration and to close the chamber during measurement. Automatic measuring methods are expensive but has low variability due to multiple chambers.

Errors in chamber soil sampling is primarily caused by wind gusts creating air turbulence. This process creates an impossibility to mimic the soil surface before installation. Davidson et al, (2000) showed that chamber measurement is usually 15% or less compared to surrounding CO_2 efflux. However, increased amount of measurements and curve fitting can decrease data variability.

Indirect methods used to estimate respiration can be derived from the night – time net ecosystem exchange (NEE). An eddy covariance system can measure the net CO_2 exchanges between the atmosphere and the canopy (Burba, 2013). The system can be utilized to measure RE during winter in absence of chamber measurements. The Bowen ratio-energy balance method (BREB) can also be used to determine the heat, CO_2, and water vapor flux in an ecosystem (Dugas et al, 1997).

1.5 Respiration Modeling and Variable Selection

Models are commonly used to estimate soil respiration in ecosystems. Early models correlated SM to the rate of nitrogen mineralization as a linear function (Stanford and Epstein). Other commonly used models such as the Ratkowsky (1982) model

incorporates a minimum temperature for microbial growth. However, later common models such as Rs Q10 (modified version of the Van't hoff (1884) equation; Davidson et al. 2006; Yuste et al. 2010), the Lloyd and Taylor (1994) model, and Arrhenius equation (Rs Ts; 1889) explain Rs as an exponential growth with Ts. Later studies such as Tuomi et al. (2008) suggested improvements to the Arrhenius model by including an additive parameter as a simple solution. These models fail to account for the biological activity of microorganisms at high Ts values where Rs declines due to enzyme denaturing by heat stress (Atkin et al. 2000; Davidson et al. 2006). This presents the need for a model that is dependent on other environmental variables to explain spatial and temporal variability. Models such as the Bunnell (1997) model, the Gaussian – Gamma (Khomik et al, 2017) model, and Rs Ts SM (Khomik et al, 2010) model addressed the drought effects on Rs by incorporating SM. Other models such as the Rs Ts SM GEP model (Huang et al, 2014) suggested including the effects of plant carbon loss through photorespiration by including the ecosystem GEP from the growing season. Neural networks have also been utilized to estimate soil respiration based on non-linear environmental relationships and the estimation of complex ecosystems (Song et al. 2014; Zhou et al. 2013; Melesse and Hanley, 2005).

Multiple environmental factors can exert influences on Ts and SM. For example, net radiation is the difference between the amount of radiation absorbed by the earth's surface and the energy reflected to space. When radiation enters the earth, it is partitioned into different fluxes such as sensible and latent heat fluxes. Sensible

heat can be absorbed by the soil surface causing an increase in Ts and latent heat flux can affect SM by causing evaporation. Both of these fluxes are dependent on albedo and vegetation cover (Melesse and Hanley, 2005). Additionally, in earlier studies Ts are shown to closely correlated with air temperature and follows the same trends throughout the seasons (Parkin and Kaspar, 2003; Zheng et al. 1993). Higher air temperature is often accompanied by an increase in precipitation due to increased evaporation. This can also influence SM especially during a drought where the amount and distribution of precipitation can exert control over the upper soil horizon where the majority of biological activity occurs (Yuste et al. 2003). Furthermore, temperate ecosystems are most sensitive to precipitation distribution during drought due to consistent precipitation received through the year (Borken et al. 1999; Longdoz et al. 2000; Lee et al. 2002).

1.6 Study Significance

An understanding of Rs is of acute interest to climate change science due to considerable uncertainty in how Rs will respond to extreme environmental conditions from climate change (Warner et al, 2019). Extreme weather patterns can cause shifts in both temperature and precipitation, which affects forest productivity and carbon loss. With improper management, forests can become carbon sources instead of carbon sinks. Modeling and prediction using empirical soil carbon flux data is difficult because of high variability, general inaccessibility to soil carbon measurements in the winter, and lack of long – term data (Bond–Lamberty et al, 2010).

Analysis and understanding of Rs is traditionally performed by empirically derived models and correlation with soil temperature (Ts). However, there are many studies that show multiple other factors such as soil moisture (SM) can have an influence on Rs (Bunnell et al, 1977; Stanford and Epstein 1974; Khomik et al, 2009; Jia et al, 2013). To improve model prediction, there is a need to understand how environmental variables affect Rs at various temporal scales.

1.7 Study Objectives

The objective of this study is to measure the dynamics of Rs within managed conifer and deciduous forests in Southern Ontario, Canada and determine the effects of key environmental variables such as Ts and SM as well as extreme weather impacts on Rs. Other objectives include the comparison of thirteen different Rs models with varying complexity to determine the best model fit to observed patterns of Rs and associated uncertainties due to variations in Rs between chambers and measurements. Forest sites include a white pine (*Pinus strobus*) coniferous stand planted in 1974 (TP74) and naturally regenerated managed 90 – year – old white oak (*Quercus* alba) dominated deciduous stand (TPD). The soil in both sites are classified as Brunisolic Gray Brown Luvisol consisting more than of 90% sand.

In this study, thirteen different models of Rs were used to simulate observed patterns of Rs at both sites. A neural network was constructed and compared with multiple models to determine fit and estimation in TPD from 2014 to 2018. Neural networks are algorithms designed to recognize patterns using neurons and back

propagation. Automated neural networks have been used to model fluxes within forests and potentially utilize eddy covariance data to simulate a spatial pattern of carbon fluxes within an ecosystem (Van Wijk and Bouten, 1999; Van Wijk et al, 2002; Papale and Valentini, 2003; Melesse and Hanley, 2005; Song et al, 2014; Ebrahimi et al, 2019).

In addition, wavelet coherence was applied for TP74 and TPD from 2017 to 2019 which included a year of extreme weather, to analyze for environmental variable effects. Continuous wavelet transform (CWT) is a mathematical method of analyzing stationary and non-stationary time series (Mallat, 2009). Wavelet coherence is based on CTW and plots two time series at the same time scale to determine cross correlations and can be utilized within forests to determine the sensitivity of Rs to environmental influences (Grinsted et al, 2004; Wood et al, 2013; Vargas et al, 2011; Jia et al, 2018).

Specific objectives of this study are to:

1) Measure soil CO_2 efflux over the extended growing season (April – October) in a coniferous (TP74) and deciduous (TPD) forest ecosystem using automatic chamber systems.
2) Determine the impacts of environmental variables and extreme weather events on Rs in both forests.
3) Examine the validity of different Rs models in simulating observed dynamic of Rs at both sites and its uncertainty.

With respect to the organization of this thesis, introduction and background is given in Chapter 1, study results are presented in Chapters 2 and 3 in the form of two journal articles, and conclusions are summarized in chapter 4. References are self – contained within each chapter because this dissertation is composed of two manuscripts where there is overlap in the introduction, site details, and methodology.

1.8. References

Apps, M. J., & Price, D. T. (1996). *Forest ecosystems, forest management, and the global carbon cycle*. *NATO ASI series. Series I, Global environmental change: vol. 40*. Berlin, New York: Springer. https://doi.org/10.1007/978-3-642-61111-7

Ashton, M. S., Tyrrell, M. L., Spalding, D., & Gentry, B. (2012). *Managing Forest Carbon in a Changing Climate*. Dordrecht: Springer Netherlands. https://doi.org/10.1007/978-94-007-2232-3

Assmann, E. (1961). *Waldertragskunde : organische Produktion, Struktur, Zuwachs und Ertrag von Waldbeständen*: München : BLV. Retrieved from http://lib.ugent.be/catalog/rug01:000289135

Balashov E., & Bazzoffi P. (2003). Aggregate water stability of sandy and clayey loam soils differently compacted with and without wheat plants.

Bastin, J.-F., Finegold, Y., Garcia, C., Mollicone, D., Rezende, M., Routh, D., . . . Crowther, T. W. (2019). The global tree restoration potential. *Science (New York, N.Y.), 365*(6448), 76–79. https://doi.org/10.1126/science.aax0848

Berg, B., Ekbohm, G., & McClaugherty, C. (1984). Lignin and holocellulose relations during long-term decomposition of some forest litters. Long-term decomposition in a Scots pine forest. IV. *Canadian Journal of Botany, 62*(12), 2540–2550. https://doi.org/10.1139/b84-345

Binkley, D., & Menyailo, O. (Eds.) (2005). *NATO science series. Series IV, Earth and environmental sciences: vol. 55. Tree species effects on soils: Implications for global change /-edited by Dan Binkley and Oleg Menyailo*.

Dordrecht, Great Britain: Springer in cooperation with NATO Public Diplomacy Division. https://doi.org/10.1007/1-4020-3447-4

Bond-Lamberty, B., & Thomson, A. (2010). Temperature-associated increases in the global soil respiration record. *Nature*, *464*(7288), 579–582. https://doi.org/10.1038/nature08930

Borken, W., Xu, Y.-J., Brumme, R., & Lamersdorf, N. (1999). A Climate Change Scenario for Carbon Dioxide and Dissolved Organic Carbon Fluxes from a Temperate Forest Soil Drought and Rewetting Effects. *Soil Science Society of America Journal*, *63*(6), 1848–1855. https://doi.org/10.2136/sssaj1999.6361848x

Borken, W., Savage, K., Davidson, E. A., & Trumbore, S. E. (2006). Effects of experimental drought on soil respiration and radiocarbon efflux from a temperate forest soil. *Global Change Biology*, *12*(2), 177–193. https://doi.org/10.1111/j.1365-2486.2005.001058.x

Bouma, T. J. (2000). On the assessment of root and soil respiration for soils of different textures: interactions with soil moisture contents and soil CO2 concentrations. *Plant and Soil*, *227*(1/2), 215–221. https://doi.org/10.1023/A:1026502414977

Brady, N. C., & Weil, R. R. (2017). *The nature and properties of soils* (Global edition). Boston: Pearson.

Bunnell, F. L., Tait, D.E.N., & Flanagan, P. W. (1977). Microbial respiration and substrate weight loss—II. *Soil Biology and Biochemistry*, *9*(1), 41–47. https://doi.org/10.1016/0038-0717(77)90059-1

Burba, G. (2013). Eddy covariance method for scientific, industrial, agricultural, and regulatory applications: A field book on measuring ecosystem gas exchange and areal emission rates. Lincoln, Nebraska: LI-COR Biosciences.

Campbell, R. E., Baker, Jr., M. B., Ffolliott, P. F., Larson, F. R., & Avery, C. C. (1977). Wildfire effects on a ponderosa pine ecosystem: An Arizona case study.

Canadell, J. G., Le Quéré, C., Raupach, M. R., Field, C. B., Buitenhuis, E. T., Ciais, P., . . . Marland, G. (2007). Contributions to accelerating atmospheric CO2 growth from economic activity, carbon intensity, and efficiency of natural sinks. *Proceedings of the National Academy of Sciences of the United States of America*, *104*(47), 18866–18870. https://doi.org/10.1073/pnas.0702737104

Curiel Yuste, J., Janssens, I. A., Carrara, A., Meiresonne, L., & Ceulemans, R. (2003). Interactive effects of temperature and precipitation on soil respiration in a temperate maritime pine forest. *Tree Physiology*, *23*(18), 1263–1270. https://doi.org/10.1093/treephys/23.18.1263

Davidson, E. A., Verchot, L. V., Cattânio, J. H., Ackerman, I. L., & Carvalho, J.E.M. (2000). Effects of soil water content on soil respiration in forests and cattle pastures of eastern Amazonia. *Biogeochemistry*, *48*(1), 53–69. https://doi.org/10.1023/A:1006204113917

Dickinson C. H, & Pugh G. J. F. Biology of Plant Litter Decomposition. Volume 2 (1974).

Dugas, W. A., Reicosky, D. C., & Kiniry, J. R. (1997). Chamber and micrometeorological measurements of CO2 and H2O fluxes for three C4 grasses. *Agricultural and Forest Meteorology*, *83*(1-2), 113–133. https://doi.org/10.1016/S0168-1923(96)02346-5

Ebrahimi, M., Sarikhani, M. R., Safari Sinegani, A. A., Ahmadi, A., & Keesstra, S. (2019). Estimating the soil respiration under different land uses using artificial neural network and linear regression models. *CATENA*, *174*, 371–382. https://doi.org/10.1016/j.catena.2018.11.035

FAO and ITPS. 2015. Status of the World's Soil Resources (SWSR) – Main Report. Food and Agriculture Organization of the United Nations and Intergovernmental Technical Panel on Soils, Rome, Italy

Fontaine, S., Barot, S., Barré, P., Bdioui, N., Mary, B., & Rumpel, C. (2007). Stability of organic carbon in deep soil layers controlled by fresh carbon supply. *Nature*, *450*(7167), 277–280. https://doi.org/10.1038/nature06275

Gómez-Guerrero, A., & Doane, T. (2018). The Response of Forest Ecosystems to Climate Change. In W. R. Horwath & Y. Kuzyakov (Eds.), *Developments in Soil Science: Vol. 35. Climate change impacts on soil processes and ecosystem properties* (Vol. 35, pp. 185–206). Amsterdam: Elsevier. https://doi.org/10.1016/B978-0-444-63865-6.00007-7

Gonzalez-Benecke, C. A., Martin, T. A., Cropper, W. P., & Bracho, R. (2010). Forest management effects on in situ and ex situ slash pine forest carbon balance. *Forest Ecology and Management*, *260*(5), 795–805. https://doi.org/10.1016/j.foreco.2010.05.038

González-Ubierna, S., & Lai, R. (2019). Modelling the effects of climate factors on soil respiration across Mediterranean ecosystems. *Journal of Arid Environments*, *165*, 46–54. https://doi.org/10.1016/j.jaridenv.2019.02.008

Goodale, C. L., Apps, M. J., Birdsey Richard A., Field, C. B., Heath, S. L., Houghton, Richard, A., . . . Shvidenko, A. Z. Forest Carbon Sinks In The Northern Hemisphere.

Grinsted, A., Moore, J. C., & Jevrejeva, S. (2004). Application of the cross wavelet transform and wavelet coherence to geophysical time series. *Nonlinear*

Processes in Geophysics, *11*(5/6), 561–566. https://doi.org/10.5194/npg-11-561-2004

Gulde, S., Chung, H., Amelung, W., Chang, C., & Six, J. (2008). Soil Carbon Saturation Controls Labile and Stable Carbon Pool Dynamics. *Soil Science Society of America Journal*, *72*(3), 605–612. https://doi.org/10.2136/sssaj2007.0251

Guo, L. B., & Gifford, R. M. (2002). Soil carbon stocks and land use change: a meta-analysis. *Global Change Biology*, *8*(4), 345–360. https://doi.org/10.1046/j.1354-1013.2002.00486.x

Hartge, K. H., & Stewart, B. A. (1995). *Soil Structure: Its Development and Function*. *Advances in soil science*. Boca Raton Fla., London: Lewis.

Högberg, P., Nordgren, A., Buchmann, N., Taylor, A. F., Ekblad, A., Högberg, M. N., . . . Read, D. J. (2001). Large-scale forest girdling shows that current photosynthesis drives soil respiration. *Nature*, *411*(6839), 789–792. https://doi.org/10.1038/35081058

Horwath, W. R., & Kuzyakov, Y. (Eds.) (2018). *Developments in Soil Science: Vol. 35*. *Climate change impacts on soil processes and ecosystem properties*. Amsterdam: Elsevier.

Hou, Z. S. , Engel D. W., Lin G., Fang Y. L., and Fang Z. F.. 2013. An uncertainty quantification framework for studying the effect of spatial heterogeneity in reservoir permeability on CO2 sequestration. Math. Geosci. 45:799–817

IPCC, 2014: Climate Change 2014: Synthesis Report. Contribution of Working Groups I, II and III to the Fifth Assessment Report of the Intergovernmental Panel on Climate Change [Core Writing Team, R.K. Pachauri and L.A. Meyer (eds.)]. IPCC, Geneva, Switzerland, 151 pp.

IPCC, 2019: Climate Change and Land: an IPCC special report on climate change, desertification, land degradation, sustainable land management, food security, and greenhouse gas fluxes in terrestrial ecosystems [P.R. Shukla, J. Skea, E. Calvo Buendia, V. Masson-Delmotte, H.-O. Pörtner, D. C. Roberts, P. Zhai, R. Slade, S. Connors, R. van Diemen, M. Ferrat, E. Haughey, S. Luz, S. Neogi, M. Pathak, J. Petzold, J. Portugal Pereira, P. Vyas, E. Huntley, K. Kissick, M. Belkacemi, J. Malley, (eds.)]. In press.

J. M. Norman, C. J. Kucharik, S. T. Gower, D. D. Baldocchi, P. M. Crill, M. Rayment, K. Savage, R. G. Striegl (1997). A comparison of six methods for measuring soil-surface carbon dioxide fluxes.

Jandl, R., Lindner, M., Vesterdal, L., Bauwens, B., Baritz, R., Hagedorn, F., . . . Byrne, K. A. (2007). How strongly can forest management influence soil

carbon sequestration? *Geoderma*, *137*(3-4), 253–268. https://doi.org/10.1016/j.geoderma.2006.09.003

Jastrow, J. D., Amonette, J. E., & Bailey, V. L. (2007). Mechanisms controlling soil carbon turnover and their potential application for enhancing carbon sequestration. *Climatic Change*, *80*(1-2), 5–23. https://doi.org/10.1007/s10584-006-9178-3

Jia, X., Zha, T., Wang, S., Bourque, C. P.-A., Wang, B., Qin, S., & Zhang, Y. (2018). Canopy photosynthesis modulates soil respiration in a temperate semi-arid shrubland at multiple timescales. *Plant and Soil*, *432*(1-2), 437–450. https://doi.org/10.1007/s11104-018-3818-z

Jia, X., Zha, T., Wu, B., Zhang, Y., Chen, W., Wang, X., . . . He, G. (2013). Temperature response of soil respiration in a Chinese pine plantation: Hysteresis and seasonal vs. Diel Q10. *PloS One*, *8*(2), e57858. https://doi.org/10.1371/journal.pone.0057858

Johnston, J. D. (2017). Forest succession along a productivity gradient following fire exclusion. *Forest Ecology and Management*, *392*, 45–57. https://doi.org/10.1016/j.foreco.2017.02.050

Keesstra, S. D., Bouma, J., Wallinga, J., Tittonell, P., Smith, P., Cerdà, A., . . . Fresco, L. O. (2016). The significance of soils and soil science towards realization of the United Nations Sustainable Development Goals. *SOIL*, *2*(2), 111–128. https://doi.org/10.5194/soil-2-111-2016

Khomik, Myroslava. (2004). Soil CO2 Efflux From Temperate and Boreal Forests in Ontario (Master's Thesis). McMaster University. Hamilton, Ontario.

Khomik, M., Arain, M. A., Brodeur, J. J., Peichl, M., Restrepo-Coupé, N., & McLaren, J. D. (2010). Relative contributions of soil, foliar, and woody tissue respiration to total ecosystem respiration in four pine forests of different ages. *Journal of Geophysical Research*, *115*(G3). https://doi.org/10.1029/2009JG001089

Khomik, M., Arain, M. A., Liaw, K.-L., & McCaughey, J. H. (2009). Debut of a flexible model for simulating soil respiration–soil temperature relationship: Gamma model. *Journal of Geophysical Research*, *114*(G3). https://doi.org/10.1029/2008JG000851

Kindermann, G., Obersteiner, M., Sohngen, B., Sathaye, J., Andrasko, K., Rametsteiner, E., . . . Beach, R. (2008). Global cost estimates of reducing carbon emissions through avoided deforestation. *Proceedings of the National Academy of Sciences of the United States of America*, *105*(30), 10302–10307. https://doi.org/10.1073/pnas.0710616105

King, J. S., Hanson, P. J., Bernhardt, E., DeAngelis, P., Norby, R. J., & Pregitzer, K. S. (2004). A multiyear synthesis of soil respiration responses to elevated atmospheric CO 2 from four forest FACE experiments. *Global Change Biology*, *10*(6), 1027–1042. https://doi.org/10.1111/j.1529-8817.2003.00789.x

Knorr, K.-H., Oosterwoud, M. R., & Blodau, C. (2008). Experimental drought alters rates of soil respiration and methanogenesis but not carbon exchange in soil of a temperate fen. *Soil Biology and Biochemistry*, *40*(7), 1781–1791. https://doi.org/10.1016/j.soilbio.2008.03.019

Kucera, C. L., & Kirkham, D. R. (1971). Soil Respiration Studies in Tallgrass Prairie in Missouri. *Ecology*, *52*(5), 912–915. https://doi.org/10.2307/1936043

Lal, R. (2004). Soil Carbon Sequestration Impacts on Global Climate Change and Food Security.

Lal, R. (2008). Carbon sequestration. *Philosophical Transactions of the Royal Society of London. Series B, Biological Sciences*, *363*(1492), 815–830. https://doi.org/10.1098/rstb.2007.2185

Lee, M.-s., Nakane, K., Nakatsubo, T., Mo, W.-h., & Koizumi, H. (2002). Effects of rainfall events on soil CO 2 flux in a cool temperate deciduous broad-leaved forest. *Ecological Research*, *17*(3), 401–409. https://doi.org/10.1046/j.1440-1703.2002.00498.x

Lefèvre, C., Rekik, F., Alcantara Cervantes, V., & Wiese, L. (2017). *Soil organic carbon: The hidden potential*. Rom: Food and Agriculture Organization of the United Nations. Retrieved from http://www.fao.org/3/a-i6937e.pdf

Li, Tsi-Tung. (1926). Soil temperature as influenced by forest cover.

Lieth, H., & Ouellette, R. (1962). Studies On The Vegetation Of The Gaspé Peninsula: II. The Soil Respiration Of Some Plant Communities. *Canadian Journal of Botany*, *40*(1), 127–140. https://doi.org/10.1139/b62-014

Longdoz, B., Yernaux, M., & Aubinet, M. (2000). Soil CO2 efflux measurements in a mixed forest: impact of chamber disturbances, spatial variability and seasonal evolution. *Global Change Biology*, *6*(8), 907–917. https://doi.org/10.1046/j.1365-2486.2000.00369.x

Lorenz, K., & Lal, R. (2010). *Carbon sequestration in forest ecosystems*. Dordrecht: Springer.

Luo, Y., & Zhou, X. (2006). *Soil respiration and the environment*. Amsterdam, Boston: Elsevier Academic Press.

Lützow, M. von, & Kögel-Knabner, I. (2009). Temperature sensitivity of soil organic matter decomposition—what do we know? *Biology and Fertility of Soils*, *46*(1), 1–15. https://doi.org/10.1007/s00374-009-0413-8

MacDougall, A. H., & Beltrami, H. (2017). Impact of deforestation on subsurface temperature profiles: implications for the borehole paleoclimate record. *Environmental Research Letters*, *12*(7), 74014. https://doi.org/10.1088/1748-9326/aa7394

Makita, N., Kosugi, Y., Sakabe, A., Kanazawa, A., Ohkubo, S., & Tani, M. (2018). Seasonal and diurnal patterns of soil respiration in an evergreen coniferous forest: Evidence from six years of observation with automatic chambers. *PloS One*, *13*(2), e0192622. https://doi.org/10.1371/journal.pone.0192622

Makusa, G. P. (2015). Soil Stabilization Methods and Materials.

Mallat, S. G., & Peyré, G. (2009). *A wavelet tour of signal processing: The sparse way / Stéphane Mallat ; with contributions from Gabriel Peyré* (3rd ed.). Amsterdam, Boston: Elsevier/Academic Press.

Medina, E., & Zelwer, M. (1972). Soil respiration in tropical plant communities.

Melesse, A. M., & Hanley, R. S. (2005). Artificial neural network application for multi-ecosystem carbon flux simulation. *Ecological Modelling*, *189*(3-4), 305–314. https://doi.org/10.1016/j.ecolmodel.2005.03.014

Monteith, J. L., Szeicz, G., & Yabuki, K. (1964). Crop Photosynthesis and the Flux of Carbon Dioxide Below the Canopy. *The Journal of Applied Ecology*, *1*(2), 321. https://doi.org/10.2307/2401316

Morris, S. J., Bohm, S., Haile-Mariam, S., & Paul, E. A. (2007). Evaluation of carbon accrual in afforested agricultural soils. *Global Change Biology*, *13*(6), 1145–1156. https://doi.org/10.1111/j.1365-2486.2007.01359.x

Nay, S. M., Mattson, K. G., & Bormann, B. T. (1994). Biases of Chamber Methods for Measuring Soil CO2 Efflux Demonstrated with a Laboratory Apparatus. *Ecology*, *75*(8), 2460. https://doi.org/10.2307/1940900

Nikolova, P. S., Raspe, S., Andersen, C. P., Mainiero, R., Blaschke, H., Matyssek, R., & Häberle, K.-H. (2009). Effects of the extreme drought in 2003 on soil respiration in a mixed forest. *European Journal of Forest Research*, *128*(2), 87–98. https://doi.org/10.1007/s10342-008-0218-6

Norby, R. J., Hanson, P. J., O'Neill, E. G., Tschaplinski, T. J., Weltzin, J. F., Hansen, R. A., . . . Johnson, D. W. (2002). Net Primary Productivity of a CO2-Enriched Deciduous Forest and the Implications for Carbon Storage. *Ecological Applications*, *12*(5), 1261–1266. https://doi.org/10.1890/1051-0761(2002)012[1261:NPPOAC]2.0.CO;2

Oberbauer, S. F., Gillespie, C. T., Cheng, W., Gebauer, R., Serra, A. S., & Tenhunen, J. D. (1992). Environmental effects on CO2 efflux from riparian tundra in the northern foothills of the Brooks Range, Alaska, USA. *Oecologia*, *92*(4), 568–577. https://doi.org/10.1007/BF00317851

Oelkers, E. H., & Cole, D. R. (2008). Carbon Dioxide Sequestration A Solution to a Global Problem. *Elements*, *4*(5), 305–310. https://doi.org/10.2113/gselements.4.5.305

O'Neill, K. P., Kasischke, E. S., & Richter, D. D. (2002). Environmental controls on soil CO 2 flux following fire in black spruce, white spruce, and aspen stands of interior Alaska. *Canadian Journal of Forest Research*, *32*(9), 1525–1541. https://doi.org/10.1139/x02-077

Ontl, T. A., Janowiak, M. K., Swanston, C. W., Daley, J., Handler, S., Cornett, M., . . . Patch, N. (2020). Forest Management for Carbon Sequestration and Climate Adaptation. *Journal of Forestry*, *118*(1), 86–101. https://doi.org/10.1093/jofore/fvz062

Orchard, V. A., & Cook, F. J. (1983). Relationship between soil respiration and soil moisture. *Soil Biology and Biochemistry*, *15*(4), 447–453. https://doi.org/10.1016/0038-0717(83)90010-X

Pachauri, R. K., & Mayer, L. (Eds.) (2015). *Climate change 2014: Synthesis report*. Geneva, Switzerland: Intergovernmental Panel on Climate Change.

Papale, D., & Valentini, R. (2003). A new assessment of European forests carbon exchanges by eddy fluxes and artificial neural network spatialization. *Global Change Biology*, *9*(4), 525–535. https://doi.org/10.1046/j.1365-2486.2003.00609.x

Parkin, T. B., & Kaspar, T. C. (2003). Temperature Controls on Diurnal Carbon Dioxide Flux. *Soil Science Society of America Journal*, *67*(6), 1763–1772. https://doi.org/10.2136/sssaj2003.1763

Parro, K., Köster, K., Jõgiste, K., Seglinš, K., Sims, A., Stanturf, J. A., & Metslaid, M. (2019). Impact of post-fire management on soil respiration, carbon and nitrogen content in a managed hemiboreal forest. *Journal of Environmental Management*, *233*, 371–377. https://doi.org/10.1016/j.jenvman.2018.12.050

Peichl, M., Arain, M. A., ULLAH, S., & MOORE, T. R.I.M. (2010). Carbon dioxide, methane, and nitrous oxide exchanges in an age-sequence of temperate pine forests. *Global Change Biology*, *16*(8), 2198–2212. https://doi.org/10.1111/j.1365-2486.2009.02066.x

Petrenko, C. L., & Friedland, A. J. (2015). Mineral soil carbon pool responses to forest clearing in Northeastern hardwood forests. *GCB Bioenergy*, *7*(6), 1283–1293. https://doi.org/10.1111/gcbb.12221

Poerschmann, J., Gathmann, A., Augustin, J., Langer, U., & Górecki, T. (2005). Molecular composition of leaves and stems of genetically modified Bt and near-isogenic non-Bt maize--characterization of lignin patterns. *Journal of Environmental Quality*, *34*(5), 1508–1518. https://doi.org/10.2134/jeq2005.0070

Pumpanen, J., Kolari, P., Ilvesniemi, H., Minkkinen, K., Vesala, T., Niinistö, S., . . . Hari, P. (2004). Comparison of different chamber techniques for measuring soil CO2 efflux. *Agricultural and Forest Meteorology*, *123*(3-4), 159–176. https://doi.org/10.1016/j.agrformet.2003.12.001

Rayment, M. B., & Jarvis, P. G. (1997). An improved open chamber system for measuring soil CO 2 effluxes in the field. *Journal of Geophysical Research*, *102*(D24), 28779–28784. https://doi.org/10.1029/97JD01103

Rochette, P., Ellert, B., Gregorich, E. G., Desjardins, R. L., Pattey, E., Lessard, R., & Johnson, B. G. (1997). Description of a dynamic closed chamber for measuring soil respiration and its comparison with other techniques. *Canadian Journal of Soil Science*, *77*(2), 195–203. https://doi.org/10.4141/S96-110

Ruess, R. W., van Cleve, K., Yarie, J., & Viereck, L. A. (1996). Contributions of fine root production and turnover to the carbon and nitrogen cycling in taiga forests of the Alaskan interior. *Canadian Journal of Forest Research*, *26*(8), 1326–1336. https://doi.org/10.1139/x26-148

Russell, E. J., & Appleyard, A. (1915). The Atmosphere of the Soil: Its Composition and the Causes of Variation. *The Journal of Agricultural Science*, *7*(1), 1–48. https://doi.org/10.1017/S0021859600002410

Rustad, L., Campbell, J., Marion, G., Norby, R., Mitchell, M., Hartley, A., . . . Gurevitch, J. (2001). A meta-analysis of the response of soil respiration, net nitrogen mineralization, and aboveground plant growth to experimental ecosystem warming. *Oecologia*, *126*(4), 543–562. https://doi.org/10.1007/s004420000544

Sahin, H., & Yalcin, O. (2017). Chemical Composition and Utilization of Conifer Needles-A Review. *Journal of Applied Life Sciences International*, *14*(3), 1–11. https://doi.org/10.9734/JALSI/2017/37076

Schindlbacher, A., Wunderlich, S., Borken, W., Kitzler, B., Zechmeister-Boltenstern, S., & Jandl, R. (2012). Soil respiration under climate change: prolonged summer drought offsets soil warming effects. *Global Change*

Biology, *18*(7), 2270–2279. https://doi.org/10.1111/j.1365-2486.2012.02696.x

Schnitzer, M., & Khan, S. U. (1978). Soil Organic Matter.

Selsted, M. B., Linden, L., Ibrom, A., Michelsen, A., Larsen, K. S., Pedersen, J. K., . . . Ambus, P. (2012). Soil respiration is stimulated by elevated CO2 and reduced by summer drought: three years of measurements in a multifactor ecosystem manipulation experiment in a temperate heathland (CLIMAITE). *Global Change Biology*, *18*(4), 1216–1230. https://doi.org/10.1111/j.1365-2486.2011.02634.x

Shaver, G. R., Bret-Harte, M. S., Jones, M. H., Johnstone, J., Gough, L., Laundre, J., & Chapin, F. S. (2001). Species Composition Interacts with Fertilizer to Control Long-Term Change in Tundra Productivity. *Ecology*, *82*(11), 3163–3181. https://doi.org/10.1890/0012-9658(2001)082[3163:SCIWFT]2.0.CO;2

Six, J., Conant, R. T., Paul, E. A., & Paustian, K. (2002). Stabilization mechanisms of soil organic matter: Implications for C-saturation of soils. *Plant and Soil*, *241*(2), 155–176. https://doi.org/10.1023/A:1016125726789

Sobachkin, R. S., Sobachkin, D. S., & Buzykin, A. I. (2005). The Influence of Stand Density on Growth of Three Conifer Species. In D. Binkley & O. Menyailo (Eds.), *NATO science series. Series IV, Earth and environmental sciences: vol. 55. Tree species effects on soils: Implications for global change / edited by Dan Binkley and Oleg Menyailo* (Vol. 55, pp. 247–255). Dordrecht, Great Britain: Springer in cooperation with NATO Public Diplomacy Division. https://doi.org/10.1007/1-4020-3447-4_14

Song, X., Peng, C., Zhao, Z., Zhang, Z., Guo, B., Wang, W., . . . Zhu, Q. (2014). Quantification of soil respiration in forest ecosystems across China. *Atmospheric Environment*, *94*, 546–551. https://doi.org/10.1016/j.atmosenv.2014.05.071

Stanford, G., & Epstein, E. (1974). Nitrogen Mineralization-Water Relations in Soils. *Soil Science Society of America Journal*, *38*(1), 103–107. https://doi.org/10.2136/sssaj1974.03615995003800010032x

Striegl, R. G., & Wickland, K. P. (2001). Soil respiration and photosynthetic uptake of carbon dioxide by ground-cover plants in four ages of jack pine forest. *Canadian Journal of Forest Research*, *31*(9), 1540–1550. https://doi.org/10.1139/x01-092

Sun, S., Lei, H., & Chang, S. X. (2019). Drought differentially affects autotrophic and heterotrophic soil respiration rates and their temperature sensitivity. *Biology and Fertility of Soils*, *55*(3), 275–283. https://doi.org/10.1007/s00374-019-01347-w

Totsche, K. U., Amelung, W., Gerzabek, M. H., Guggenberger, G., Klumpp, E., Knief, C., . . . Kögel-Knabner, I. (2018). Microaggregates in soils. *Journal of Plant Nutrition and Soil Science*, *181*(1), 104–136. https://doi.org/10.1002/jpln.201600451

Trofymow, J. A., Moore, T. R., Titus, B., Prescott, C., Morrison, I., Siltanen, M., . . . Visser, S. (2002). Rates of litter decomposition over 6 years in Canadian forests: influence of litter quality and climate. *Canadian Journal of Forest Research*, *32*(5), 789–804. https://doi.org/10.1139/x01-117

Van Wijk, M. T., & Bouten, W. (1999). Water and carbon fluxes above European coniferous forests modelled with artificial neural networks. *Ecological Modelling*, *120*(2-3), 181–197. https://doi.org/10.1016/S0304-3800(99)00101-5

Van Wijk, M.T., Bouten, W., & Verstraten, J.M. (2002). Comparison of different modelling strategies for simulating gas exchange of a Douglas-fir forest. *Ecological Modelling*, *158*(1-2), 63–81. https://doi.org/10.1016/S0304-3800(02)00174-6

Vargas, R., Carbone, M. S., Reichstein, M., & Baldocchi, D. D. (2011). Frontiers and challenges in soil respiration research: from measurements to model-data integration. *Biogeochemistry*, *102*(1-3), 1–13. https://doi.org/10.1007/s10533-010-9462-1

Wan, S., Hui, D., Wallace, L., & Luo, Y. (2005). Direct and indirect effects of experimental warming on ecosystem carbon processes in a tallgrass prairie. *Global Biogeochemical Cycles*, *19*(2), n/a-n/a. https://doi.org/10.1029/2004GB002315

Wang, H., Lin, H., & Liu, D. (2014). Remotely sensed drought index and its responses to meteorological drought in Southwest China. *Remote Sensing Letters*, *5*(5), 413–422. https://doi.org/10.1080/2150704X.2014.912768

Warner, D. L., Bond-Lamberty, B., Jian, J., Stell, E., & Vargas, R. (2019). Spatial Predictions and Associated Uncertainty of Annual Soil Respiration at the Global Scale. *Global Biogeochemical Cycles*, *33*(12), 1733–1745. https://doi.org/10.1029/2019GB006264

Welles, J. M., Demetriades-Shah, T. H., and McDermitt D. K.: Considerations for measuring ground CO2 effluxes with chambers, Chem. Geol., 177, 3–13, 2001.

Wiant, H. V. (1967). Has the Contribution of Litter Decay to Forest "Soil Respiration" Been Overestimated?

Wood, T. E., Detto, M., & Silver, W. L. (2013). Sensitivity of soil respiration to variability in soil moisture and temperature in a humid tropical forest. *PloS One*, *8*(12), e80965. https://doi.org/10.1371/journal.pone.0080965

Yan, T., Song, H., Wang, Z., Teramoto, M., Wang, J., Liang, N., . . . Peng, S. (2019). Temperature sensitivity of soil respiration across multiple time scales in a temperate plantation forest. *The Science of the Total Environment*, *688*, 479–485. https://doi.org/10.1016/j.scitotenv.2019.06.318

Yanai, R. D., Currie, W. S., & Goodale, C. L. (2003). Soil Carbon Dynamics after Forest Harvest: An Ecosystem Paradigm Reconsidered. *Ecosystems*, *6*(3), 197–212. https://doi.org/10.1007/s10021-002-0206-5

Yim, M. H., Joo, S. J., & Nakane, K. (2002). Comparison of field methods for measuring soil respiration: a static alkali absorption method and two dynamic closed chamber methods. *Forest Ecology and Management*, *170*(1-3), 189–197. https://doi.org/10.1016/S0378-1127(01)00773-3

Zheng, D., Hunt, E. R., & Running, S. W. (1993). A daily soil temperature model based on air temperature and precipitation for continental applications. *Climate Research*, *2*, 183–191. https://doi.org/10.3354/cr002183

Chapter 2:

Evaluating environmental controls on soil respiration in a deciduous forest in the Great Lakes region using various modeling approaches

2.1 Abstract

Soil Respiration (Rs) is a major component of the carbon cycle, where carbon dioxide (CO_2) is released into the atmosphere though heterotrophic and autotrophic processes dependent on soil type, depth, and time of production. Understanding of these soil CO_2 emission processes and the development of an appropriate Rs model can help in the assessment of environmental controls and climate change impacts on forest ecosystems. In this study, half-hourly CO_2 data was measured in a 90-year deciduous forest in the Great Lakes region using an automated CO_2 efflux chamber system and a closed – path eddy covariance system from July 2014 to December 2018. Mean Rs varied from a maximum value of 7.50 µmol C m^{-2} s^{-1} in July to a minimum value of 1.11 µmol C m^{-2} s^{-1} in December and demonstrated a clear seasonal trend that was driven by soil temperature and availability of water content. These data were used to evaluate the performance of seven different Rs models in predicting the soil CO_2 emission from the forest. The models included are: 1) Gaussian – Gamma model, derived from a Gaussian function with Rs and temperature combined with a Gamma function combining Rs and soil water content using an exponential and power function, 2) Rs Q_{10}, which accounts for increase in Rs per 10^{o}C increase in temperature, 3) Rs Ts SM, which is the Q_{10} response of Rs

is constrained using a logistic soil water content function, 4) Rs Ts, which is a general exponential regression model of Rs, 5) Bunnell Model, which is a generalized Rs model account for temperature and soil water content effects, 6) Rs Ts SM GEP, which is a model that simulates Rs during the growing season and accounts for photosynthesis activity or gross ecosystem productivity (GEP), and 7) NARX, which is a nonlinear autoregressive neural network function with exogenous inputs. Comparison of these seven different models showed that the Gaussian – Gamma model performed the best by capturing the seasonal variations of Rs quite well and having an annual model testing average coefficient of determination (R^2) of 0.71. Performance of the Bunnell model and NARX was also adequate with an annual average testing R^2 of 0.70 and 0.69, respectively. This study highlights the challenges and significance of environmental controls such as temperature and soil water content on the simulation of Rs in forest ecosystems.

2.2 Introduction

The earth's surface area contains 3.7 billion hectares of forests which cover around 31% of its land surface. Forests provide vital services such as wood production, clean water and air, and play a major role in biogeochemical cycling of carbon dioxide (CO_2) (Apps and Price, 2013; Matsumono et al, 2008).

Knowledge of atmospheric CO_2 movement or exchanges is imperative for greater understanding of carbon sources and sinks. Net carbon within a forest stand is characterized by uptake from photosynthesis and release by respiration. CO_2 is absorbed from the atmosphere and through photosynthesis, reacts with water to

produce oxygen and carbohydrates which is stored. Some carbon is released as CO_2 through respiration of living plant components (autotrophic respiration) and is returned to the atmosphere. The remaining carbon is allocated to different plant pools such as leaves, stem, and roots which is eventually decomposed to release CO_2 back into the atmosphere (heterotrophic respiration) (Brady and Weil, 2008; Lorenz and La, 2010). Therefore, forests are considered climate regulators due to their ability to sequester atmospheric carbon, holding it in large pools for long periods of time and then releasing it back (Apps and Price, 2013).

Soil respiration (Rs) is the release of CO_2 through both heterotrophic and autotrophic activity and accounts for 30 – 80% of net CO_2 release within forests (Davidson et al, 2006; Luo and Zhou, 2006). Within the carbon cycle, 10% of the atmospheric CO_2 is passed through the soil each year primarily through organic matter decay (Raich and Potter, 1995). Variability of Rs is influenced by diurnal processes such as photosynthetic activity, shade from trees, and proximity to tree trunks (Khomik, 2004). When compared to the atmosphere and biotic sinks the soil carbon sink is 3.2 and 4 times larger, respectively (Lorenz et al, 2010). Therefore, due to improper management techniques such as clear cutting and extreme weather events from climate change causing shifts in temperature and precipitation, a small release in Rs can result in a large release of CO_2 into the atmosphere (Peng et al, 2008).

Rs is comprised of heterotrophic respiration; the microbial decomposition of organic matter and autotrophic respiration; the growth and maintenance of plant

roots and associated mycorrhizae. Rs is primarily affected by abiotic and biotic sources. Biotic sources include soil and root microorganism activity and deposit of organic material from litterfall. Abiotic sources such as energy heat flux, temperature (soil and air), precipitation, and soil moisture can influence Rs by affecting the facilitation of nutrient transport and microorganism activity. By mapping, modeling, and monitoring flux movement, forest management techniques such as thinning can be utilized to decrease the amount of CO_2 released into the atmosphere (Reichstein and Beer, 2008; Peng et al, 2008). Changes in Rs rates can indicate activities that may have caused disturbance to the ecosystem (Schlesinger and Andrews, 2000). Multiple studies have indicated that autotrophic and heterotrophic respiration show similar seasonal trends though heterotrophic respiration increases slightly earlier in the growing season (Hogberg et al, 2001; Hanson et al, 2000).

The introduction of eddy covariance techniques can determine flux exchange throughout an entire ecosystem by calculating vertical fluxes from wind that contains rotating eddies of different sizes (Running et al, 1999; Geider et al, 2001). Total CO_2 uptake and release can be calculated from the technique and can be integrated into soil CO_2 emissions or Rs to estimate the effects of respiration under changing climate conditions (Burba, 2013). In empirical models, Rs is a function of temperature and scales with secondary environmental factors such as soil moisture. Previous studies have utilized models to fit measured respiration data in

individual sites (Janssens and Pilegaard, 2003; Del Grosso et al, 2005; Richardson and Hollinger, 2005).

Rs models can be classified into two types: empirical and mechanistic. Empirical models typically use regression analysis of Rs with temperature and soil moisture which is derived from observed data. Mechanistic models are processes based and created using environmental and biological factors that contribute to Rs. These models can be categorized into two parts: the CO_2 production model; which consider factors that produce CO_2, and the CO_2 production-transport models; which considers CO_2 production along with its transport to the soil surface.

Early Rs models utilized the relationship between enzyme activity of microorganisms and temperature as an exponential equation (Van't Hoff, 1884). However, the equation underestimates Rs at low temperatures and overestimates it a high temperature (Lloyd and Taylor, 1994). Moreover, it is impossible for Rs to continuously increase exponentially as temperature increases. Eventually, Rs starts declining when the temperature reaches beyond the optimum temperature due to microorganism death. Lloyd and Taylor created another Rs equation that represented Rs within a wide range of ecosystems and across different temperature ranges (Thierron and Laudelout, 1996; Savage and Davidson, 2001; Hollinger and Richardson, 2005). Davidson et al, (2006) discovered that Rs is highly correlated with temperature and radiation during the growing season along with multiple abiotic and biotic interactions and factors. Skopp et al, (1990) conducted a laboratory experiment that showed Rs increases with soil water content up to 0.7

then declines. They showed that the response of Rs is caused from an increase in diffusion facilitating the transport of nutrients at lower soil moisture. However, at higher soil moisture levels Rs starts to decrease due to the limitation of oxygen diffusion.

Neural networks are composed of artificial neurons that stimulate a biological neural system (Hebb, 1949). Automated neural networks (ANN) utilize machine learning for recognition, prediction, and classifying patterns. Weights are assigned to input values to "train" the network into recognizing similar values (Rosenblatt, 1958). Some ANN utilize hidden layers that consists of one output layer sending its input to many hidden layers. The hidden layers then pass their output to another hidden layer or an output layer. Hidden layers are described as such because only their output is seen and allows the network to find features within the data. These layers allow following layers to operate with these features and splits individual tasks within different layer. Within machine learning techniques, data is commonly split using feature extraction where a different useful feature is extracted to facilitate learning.

ANN techniques may use supervised or unsupervised methods for recognition of parameters and hence predictions (Russell et al, 2010). The Nonlinear autoregressive model with exogenous inputs (NARX) is a variant of a recurrent network that has been utilized in time series prediction problems (Lin et al, 1996; Gao and Meng, 2005). Neural networks have the benefit of providing an alternative to conventional models that are limited by linearity, variable dependencies, etc.

ANN can allow users to model complex relationships and phenomena quickly and easily that may be otherwise impossible to predict (Sinanoğlu, 2004).

The specific objectives of this study are to (1) obtain an understanding of spatial and temporal dynamics of Rs, (2) determine how Rs responds to its main controlling variables (i.e. soil temperature and soil moisture), (3) assess the impact of extreme weather events on Rs, (4) to compare several different models with varying complexity using a wide range of parameters, and (5) to determine which model produces the best fit and Rs estimation according to coefficient of determination (R^2), slope, and y-intercept.

2.3 Materials and Methods

2.3.1 Site Description

This study is conducted in a 90 – year – old mature deciduous forest northwest of Long Point Provincial Park in Southern Ontario established in the 1930s (TPD; 42.64^{o}N, 80.56^{o}W). The naturally – regenerated forest resides on sandy (Brusonic Gray Brown Luvisol) soil. Parts of forested land were previously agricultural fields that were converted to forest. Predominant tree species include white oak (*Quercus alba*), sugar and red maple (*Acer saccharum*, *A. rubarum*), American beech (*Facus grandifolia*), red oak (*Q. veluntia*, *Q. rubra*), and white ash (*Fraxinus Americana*). The understory species include young deciduous trees as well as Canadian mayflower (*Maianthemum canadense*), putty root (*Aplectrum hymale*), yellow mandarin (*Disporum lanuginosum*), red trillium (*Trillium erectum*), and horsetail (*Equistrum*). Average tree height is 25.7 cm with a stand density of 504 ± 18 trees

per hectare. Average tree diameter at breast height is 22.3 cm. Soil drainage is rapid to well – drained and has a bulk density of 1.15 g m^{-3}. Further details are provided in Beamesderfer et al, (2020).

The climate in the region is humid continental with warm summers and cool winters. The 30 – year (1981 to 2010) mean annual air temperature and total precipitation measured at a weather station in Delhi, Ontario (~25 km north of the site) is 8.0^{o}C and 997 mm, respectively. Precipitation is evenly distributed over the year, with 13% falling as snow (Environment and Climate Change Canada).

2.3.2 Soil and Ecosystem Flux Measurements

Continuous half – hourly Rs measurements were recorded using an automated CO_2 flux measurement system on top of permanent collars from July 2014 to November 2018 for the snow free growing season. Measurement equipment is comprised of three main components: the gas analyzer (LI – 8100A), long – term measurement chambers (LI 8100 – 104), a multiplexer for multiple chamber measurements (LI – 8150). Each chamber is located 15 m from the measurement equipment and is equipped with a soil temperature and soil moisture probe (LI – 8150 – 203 and GS – 1, respectively) that were installed outside the collar at a depth of 5 cm. Two measurement chambers were deployed from July to December 2014 and the other tree since April 2015 (five total). The soil collars are comprised of PVC with a diameter of 20 cm, a thickness of 1 cm, and height of 11.5 cm. The collars are inserted 7 – 8 cm within the soil surface with 3 cm remaining above. Throughout

the growing season, any vegetation growth is removed from inside the collar to eliminate photosynthesis effects. Further details are provided in Daly (2016).

Ecosystem CO_2 fluxes were measured using a closed – path eddy covariance system (CPEC) which consisted of a sonic anemometer (CSAT3, Campbell Scientific Inc. (CSI)), an infrared gas analyzer (LI – 7200, Li – COR Inc.), and an automatic weather station (CSI). Instruments were installed above the canopy at 36 m on top of a scaffolding tower. A mid – canopy infrared gas analyzer (IGRA; LI – 820, Li – COR Inc.) was used to measure mid – canopy CO_2 at 16 m above ground. Half – hourly eddy covariance flux measurements were recorded at 20 Hz. Metrological data was sampled every 5 seconds and averaged half – hourly using a data logger (CR3000, CSI). Air temperature and relative humidity (HMP155A, Campbell Scientific Inc. (CSI)) and net radiation using four dome net radiometers (CNR4, Kipp and Zonen) is also measured. Soil heat flux is obtained suing four soil heat flux plates (HFT3, Campbell Scientific Inc. (CSI)) buried 3 cm below the soil surface at two different locations.

Soil temperature and soil moisture is measured year – round at two locations at 2, 5, 10, 20, 50, 100 cm depths near the eddy covariance flux tower and CO_2 chamber locations. GEP calculations are derived from modeled ecosystem respiration (RE) and net ecosystem exchange (NEE). The NEE is calculated as the sum of CO_2 flux and the rate of CO_2 storage change. RE is estimated from Ts at 5 cm with SM from measurements made at 5, 10, 20, and 50 cm. GEP gaps are filled using predicted values derived from Ts, SM, photosynthetically active radiation (PAR), vapor

pressure deficit (VPD), photosynthetic flux per quanta, and light saturated rate of CO2 fixation. Further details of flux, meteorological, and soil data measurements are provided in Beamesderfer et al, (2020).

2.3.3 Data Analysis

Soil CO_2 emissions data was processed using Soil Flux Pro software (4.0.1; Li – COR Inc.). The rate of increase in CO_2 concentration during chamber closure was analyzed. An exponential curve was fitted and the resulting plot was fit with a non – linear regression equation that solved for C_∞, t_o, and α where C_o is the starting measured CO_2 concentration. The CO_2 flux based on the slope of the regression equation was reported as the exponential flux.

$$C(t) = C_\infty + (C_o - C_\infty)e^{-\alpha(t-t_0)}$$

Measurements that reported a high exponential iteration (>10) were processed further by changing the start time until the exponential iteration is less than 10. Measurements from one chamber were excluded from 2014 to 2017 due to a hidden wasp nest in the nearby ground that resulted in unusually increased CO_2 emissions.

2.3.4 Rs Models

Linear and non – linear analysis was performed on daily measured Rs. Seven models were derived to determine the correlation between Rs and its environmental controls. The first model was a simple, exponential regression between Rs and Ts (Rs Ts; Van't Hoff, 1884). The second is the Q10 model (Rs Q10; Yuste et al, 2005), the third is a modified Q10 model that incorporates soil moisture (Khomik et al,

2009), the fourth is a model for a temperate deciduous forest that accounts for plant photosynthesis (Rs Ts SM GEP), the fifth is the Bunnell model (Bunnell et al, 1977), the sixth is a Gaussian – Gamma model that was based on Ts and a gaussian function whose dependence on soil moisture was represented by a gamma function (Khomik et al, 2010), the seventh was a NARX neural network model that incorporated latent heat flux (LE), sensible heat flux (H), net radiation (Rn), air temperature above the canopy (Ta) at 36 m, Ts and SM at 5 cm depths and daily precipitation (PPT) and was derived from Melesse and Hanley (2005). This model was trained using a scaled conjugate gradient algorithm.

The models were evaluated using 70% of observed measurements for training and 30% for testing based on studies performed by Gholamy et al (2018). The NARX neural network was created with the neural network time series toolbox from Matlab (2018a) which uses 70% of data for training, 15% for validation, and 15% for testing. Two hidden layers were used within the network with eight hidden neurons and an input and output delay of 2. Further model analysis was performed using the coefficient of determination (R^2), sum of squares (SSE), standard deviation (STD), relative error (RE), slope intercept relating to normal linear model (Y = x), and yearly fit to observed daily Rs. Model equations are shown in Table 2.1.

2.4 Results

2.4.1 Meteorological Measurements

Annual and monthly values of meteorological and soil variables are shown in Figure 2.1. Monthly average temperature (Ta; Figure 2.1a) ranged from -4.37 and 0.21^{o}C in the winter seasons to 19.36 and 21.39^{o}C in the summer. Mean annual Ta values were 7.93, 9.04, 10.64, 9.93, and 9.22^{o}C from 2014 to 2018, respectively. Ta increased above 0^{o}C in April, peaked in August, and declined for the remainder of the year. Photosynthetically active radiation (PAR; Figure 2.1a) and soil temperature (Ts; Figure 2.1b) followed closely to Ta trend with the exception of late winter (January to March) where Ts remained consistently near 0^{o}C. Monthly average values of Ts ranged from -0.03 to 20.61^{o}C for all years.

Maximum values for incoming PAR (Figure 2.1a), Ta, and Ts occurred in the summer. PAR values reached maximum levels in June for 2014, 2016, and 2017, July for 2015, and late May for 2018.

Total annual PPT (Figure 2.1c) was 1429, 810, 777, 1153, and 1644 mm from 2014 to 2018 respectively. SM (Figure 2.2) peaked in early spring with a maximum value of 0.23 (April 2014), 0.22 (January 2015), 0.20 (March 2016 and May 2017), and 0.24 m^3 m^{-3} (February 2018). SM in subsequent years had high values in the beginning of the year (January to April) before decreasing in July for 2016 and 2017 and June in 2018. SM in the summer months reached a minimum value of 0.031 (July 2014), 0.026 (September 2015), 0.021 (August 2016), and 0.022 m^3 m^{-3}(July 2018). There was a second SM peak (0.14 m^3 m^{-3}) in late 2014 October and

in November from 2015 to 2018 (0.17, 0.13, 0.18, 0.20 m^3 m^{-3} respectively). Average SM values are 0.12, 0.10, 0.09, 0.11, and 0.11 m^3 m^{-3} from 2014 to 2018.

2.4.2 Annual and Seasonal Trends in Rs

Daily Rs measurements made during this study are shown in Figure 2.3. Rs seasonality followed closely with Ta and Ts, peaking in the summer and declining throughout the rest of the year. The maximum mean daily Rs was 13.15 µmol CO_2 m^{-2} s^{-1} on August 5, 2014, 10.02 µmol CO_2 m^{-2} s^{-1} on June 15, 2015, 8.68 µmol CO_2 m^{-2} s^{-1} on August 17, 2016, 10.96 µmol CO_2 m^{-2} s^{-1} on October 10, 2017, and 11.86 µmol CO_2 m^{-2} s^{-1} on September 5, 2018. Minimum mean daily Rs was 0.86 µmol CO_2 m^{-2} s^{-1} on November 28, 2014, 1.27 µmol CO_2 m^{-2} s^{-1} on November 20, 2015, 0.95 µmol CO_2 m^{-2} s^{-1} on May 7, 2016, 1.74 µmol CO_2 m^{-2} s^{-1} on May 8 2017, and 1.01 µmol CO_2 m^{-2} s^{-1} on April 29, 2018.

Increases in Rs corresponded to all precipitation events, which caused an increase in SM. For example, on October 9, 2017 there was a 11.7 mm precipitation pulse where SM increased from 0.1 to 0.39 m^3 m^{-3}, causing a 78% increase in Rs (5.97 vs 10.63 µmol CO_2 m^{-2} s^{-1}). Pre – precipitation Rs levels were not reached until 20 days after the rain event (Figure 2.4). Additionally, large fluctuations in Rs was occured after long periods without precipitation. Figure 2.9 shows that after September 2017 (a period of 19 days; figure 2d), a precipitation event caused a spike in Rs greater than those seen in early to mid – summer. Total Rs coverage at the site is 36.71%, 55.07%, 55.07%, 50.68%, and 55.62% from 2014 to 2018.

A strong exponential relationship was displayed between Rs and Ts during 5 years of study (Figure 2.5). Analysis showed that the temperature sensitivity (Q_{10}) from 2014 to 2018 was 2.06, 1.76, 1.70, 1.67, and 2.36. The basal rate of respiration at 10^oC (R_{10}) was found to be 4.73, 3.14, 2.84, 4.36, and 3.51 from 2014 to 2018. The difference in R_{10} and Q_{10} values between 2014 and 2015 could be related to the high percentage (46%) of missing data in 2014 resulting in a loss of early growing season data. The removal of one chamber due to high reported CO_2 can cause low sample size (one chamber used instead of two) which also affected the overall Rs. The increase in temperature sensitivity in 2018 could be caused by the addition of another chamber (four to five). The Coefficient of Variation (CV) was found to be 45%, 43%, 42%, 32%, and 43% from 2014 to 2018.

2.4.3 Comparison of Rs Models

Seven models were utilized to fit Rs data from 2014 to 2018. A comparison of observed and modeled daily mean Rs is shown in Figure 2.6. Modeled vs observed regression analysis with the coefficient of determination (R^2) is shown in Table 2.2. Model relative error is shown in Figure 2.7. Model statistical analysis is outlined in Table 2.5.

In 2014, the model that best fit the data was found to be the Gaussian – Gamma model producing the highest correlation with measured values (R^2 = 0.76) and produced the lowest SSE (111.1; Table 2.4). Comparison of testing linear equations using observed and predicted Rs show that the Gaussian – Gamma model produced a slope closest to 1 and a low intercept (Table 2.3a). The Rs Ts SM model and the

Bunnell model produced a similar testing equation to the Gaussian – Gamma model and a lower intercept with a lower STD (2.63 and 2.62 respectively) with a similar SSE (111.2 and 112.0; Table 2.4). The NARX Neural Network was the worst fitting model with a low coefficient of determination (0.37), low testing slope and intercept (Table 2.3a) with high SSE (134.2). However, STD values (1.46) are lower than the three models mentioned previously and closest with the STD values of the observed data (1.84, Table 2.4).

In 2015, where more complete measured Rs data was available, the model that produced the best fit was the Rs Ts SM model with a high correlation (R^2 = 0.83) and low SSE (54.52) and STD (1.63). The Bunnell model produced a similar testing equation (Table 2.3a) with the same correlation and STD and a lower SSE (53.69). The NARX Neural network testing equation (Table 2.3a) produced a very close slope to 1 and a low intercept with a correlation similar to the previously discussed models. However, the model had a higher SSE (138.7) and STD (2.12). The Rs Ts SM GEP model produced the worst fit with extremely low coefficient of determination (R^2 = 0.056) and slope and intercept (Table 2.3a). However, the equation produced the lowest SSE and STD (15.19 and 0.25 respectively). The model that produced the closest STD to observed data (1.41) was the Rs Q_{10} and Rs Ts models (~1.25; Table 2.4).

In 2016, where temperatures are higher and low overall SM and PPT throughout the year (Figure 2.2c), the model that produced the best fit was the NARX Neural Network. The network produces a low SSE (75.38), high coefficient of

determination (R^2 = 0.79), low STD (1.47), with low intercept on the testing equation. However, the slope of the testing equation is not as close to 1 as the Gaussian – Gamma model which produces similar STD (1.44) and slightly higher SSE (77.83). The Rs Ts SM GEP model produced the worst fit similar to that of 2015 with an extremely low correlation (R^2 = 0.016), a negative slope within the testing function, and a high SSE (174.80). The Rs Ts SM model produced a STD (1.24) closest to observed STD (1.33; Table 2.4).

In 2017 temperatures stabilized with one high precipitation event (Figure 2.2d). The model that produced the best fit was the Gaussian – Gamma model with a relatively high coefficient of determination (R^2 = 0.55) and testing slope matching 1 with low intercept (Table 2.3b). However, the SSE and STD were higher when compared to other models (92.62 and 2.14 respectively). The NARX neural network was also a viable model with a higher correlation (R^2 = 0.63) and closer testing slope to 1 with a low intercept. However, the model produces the highest SSE (248.0) and STD (2.83) from the rest of the models. The Rs Q_{10} and Rs Ts models both produce the worst results with the lowest correlation (R^2 = 0.41) along with similar low testing slope and high intercept (Table 2.3b). The models' SSE and STD are relatively similar as well (~57.08~ and 1.56). The Rs Q_{10} model produced the closest STD (1.55) to the observed STD (1.46; Table 2.4).

In 2018, with the additional chamber added, the model that produced the best fit was the NARX Neural Network with a correlation of 0.83, high slope and low intercept. The network created a relatively low SSE (167.6) and STD (2.44). When

compared to the Gaussian – Gamma model, the model created a slightly lower correlation (0.82) and slightly lower testing slope with slightly higher intercept (Table 2.3b). The model produces slightly higher SSE and STD (181.80, 2.66 respectively). The Rs Q_{10} and Rs Ts models both produced the worst result with a low testing model and intercept and correlation (R^2 = 0.72). Both models produced similar SSE (~233.5) and the same STD (2.63). The closest STD to the observed STD (1.89) is the Rs Ts SM GEP model (1.51; Table 2.4).

Overall, the Gaussian – Gamma model had the best fit explaining an average of 56.50%, 81.50%, 70.50%, 59.00%, and 82.50% of the Rs variability from 2014 to 2018. The Gaussian – Gamma model obtained an R^2 of 0.76 while the NARX neural network obtained an R^2 of 0.37 in 2014. This is probably due to insufficient data coverage for network training. In 2015 (with an additional 3 chambers) and in 2018 (with 1 chamber re-incorporated) the R^2 of both models were similar with a difference of 0.01. In 2016 and 2017, a year with multiple droughts and high precipitation, the neural network (R^2 = 0.79 and 0.63) was able to surpass the Gaussian – Gamma model (R^2 = 0.62 and 0.55) indicating factors such as latent heat, relative humidity, net radiation has an impact on Rs.

Model relative error is shown in figure 2.7. Models for all years showed positive relative error in the summer (June, July, and August) representing Rs underestimation. In April/May and at the end of August, a negative relative error was produced indicating overestimation. Large relative error at the end of 2014, beginning of 2015, and at 2016 and 2018 could be the result of instrumentation

problems causing a loss of data producing gaps that inhibit accurate Rs prediction. Of the seven models, the Gaussian – Gamma and neural network have the lowest relative error.

Daily relative error as a function of temperature is shown in Figure 2.9. The Gaussian – Gamma model showed a uniform relative error across all Ts ranges (0 to 23^{o}C). From 2014 to 2016 and 2018, the Rs TS SM GEP model showed largely positive relative error at low Ts and positive error at higher Ts. The 6 other models produced negative relative errors at low Ts which slowly increased to positive error at high Ts.

Seasonal and growing season Rs emissions were analyzed with each model which are summarized in Table 2.6. Across all years, spring 2016 had the lowest carbon emissions (113 to 232 µmol CO_2 m^{-2} s^{-1}) and summer 2018 had the highest (634 to 680 µmol CO_2 m^{-2} s^{-1}). All models estimated above 1200 µmol CO_2 m^{-2} s^{-1} with the exception of 2015 and 2016. The lowest carbon emissions estimated by the Gaussian – Gamma and neural network was in 2015 (~1084 µmol CO_2 m^{-2} s^{-1}).

2.5 Discussion

2.5.1 Temporal Rs Patterns

Seasonal Rs variation at the site showed increases in the spring that coincided with PAR, Rn, Ta, and Ts. Declines in Rs in the autumn closely followed that of Ts similar to that measured in other temperate forests such as in Taylor et al (2015)

and Shabaga et al (2015) which suggests influence of temperature on Rs production (Davidson et al, 2006).

Rs can be quantified using the soil basal respiration rate at 10^{o}C (R_{10}) and temperature sensitivity (Q_{10}) from the Q_{10} model. R_{10} is the emission of carbon dioxide caused by microorganism activity within the soil. Q_{10} is the temperature sensitivity of Rs, which is the increase in Rs for a 10^{o}C increase in temperature (Jia et al, 2003). Q_{10} obtained at the site ranged from 1.70 to 2.36 and R_{10} ranged from 2.84 to 4.73 (Table 2.2b). These values followed seasonal trends and are within ranges reported in literature (Tang et al, 2014; Greco and Baldocchi, 1996; Goulden et al, 1996; Xu and Baldocchi, 2004).

R_{10} values increased with Ts values while Q_{10} decreased similar to previous temperate forest studies (Yuste et al, 2004; Gaumont – Guay et al, 2006; Jia et al, 2013). A greater sensitivity to temperature (Q_{10}) at lower Ts can be explained by the increased sensitivity of biological activity (microbiota and roots) from temperature fluctuations (Jia et al, 2013). Photosynthesis is the main driver of autotrophic respiration, but sensitivity to environmental factors such as light and temperature can cause change in root biomass influencing autotrophic respiration (Hogberg et al, 2001; Mo et al, 2005; Wei et al, 2010). Additionally, Q_{10} varied between the years probably due to fluctuating seasonal changes, processes, and plant activity (Yuste et al. 2004). It is possible that variations in SM can affect the Q_{10} values due to dry and wet years (Ignace, 2019). In years with multiple drought periods Q_{10} values are shown to be low and higher in years with multiple wet

periods (Craine et al. 2010). Furthermore, the amount of accumulated biomass can also affect Q_{10} by influencing the amount of water available in the soil (Ignace, 2019). The R_{10} and Q_{10} value for the site is 3.27 and 2.41 respectively for all years. The R_{10} value is similar to the yearly average and the Q_{10} value is a closer to that of 2018 which indicates a greater influence of SM on temperature sensitivity at the site.

Seasonal differences were observed between mean Ts, R_{10}, and Q_{10}. For example, May and October 2015 had similar mean Ts (12^oC) but R_{10} and Q_{10} were lower in May. Studies in literature show that high R_{10} values are reported in the autumn regardless of Ts due to summer warming of deeper soil layers and accumulation of fresh litter causing increased microbial activity (Jia et al, 2013; Mo et al, 2005). Seasonal variations in Rs can be accounted by Ts, but other inconsistencies such as increase in Rs following decreases in Ts can be explained by other environmental factors such as soil moisture (Davidson et al, 1998; Xu and Qi, 2001; Pumpanen et al, 2008; Van der Molen et al, 2011). An example is from Rs increase following large rainfall events (Figure 2.4) which is consistent with other reports (Lee et al, 2004; Gaumont – Guay et al, 2006; Yan et al, 2014). Following a rain event, CO_2 within soil pores are replaced with rainwater causing displacement of soil gasses such as CO_2. Lingering rainwater afterwards facilitates the transport of nutrients and causes an increase in microbial population and activity. Decomposition of carbon compounds within the organic soil horizon utilizes aerobic respiration

consuming oxygen and producing a surge in CO_2 efflux (Yan et al, 2014; Orchard and Cook, 1983).

Few studies have quantified the effects of Rs pulses following PPT events. Lee et al, (2002) reported a 16 – 21% increase in Rs following rain events in a temperate deciduous forest in Japan. Borken et al, 2005 found that excluding a throughfall of 168 and 344 mm in a mixed deciduous forest caused a significant decrease of 10 – 30% in mean annual Rs. Furthermore, dry periods caused by drought can also influence Rs. Liu et al, (2016) reported an increase in both soil and heterotrophic respiration in response to precipitation events following a spring drought. The study concluded that longer drought periods resulted in larger increases in Rs.

The site experienced a significant increase in Rs after PPT events compared to those reported for temperate deciduous forests in literature (~60 mm vs 168 and 344 mm in Borken et al, 2006), which could be the result of the site's sandy soil composition and climatic conditions. TPD also receives half the amount of PPT compared to the study performed by Lee et al, (2002) suggesting that a combination of low SM (0.23 $m^3\ m^{-3}$) and good drainage can result in a Rs pulse following a PPT event greater than those typically seen in areas susceptible to frequent drying and rewetting. In a drought, a portion of soil microorganisms die and are decomposed during rewetting from precipitation (Van Gestel et al, 1991; Jeong et al, 2018). Additionally, the

availability of trapped organic matter can also contribute to increased Rs (Borken et al, 1999). In temperate forests where precipitation occurs consistently throughout the year, low SM values may contribute to labile organic matter accumulation. When precipitation occurs, this can cause dissolved organic matter to percolate rapidly into the soil in well drained plots leading to large and rapid Rs pulses.

The variability of Rs in response to change in SM is discussed within literature (Xu et al, 2004; Khomik et al, 2006; Raich et al, 2002; Ohashi and Gyokusen, 2007; Thorne et al, 2020). Analysis indicates that SM accounts for 20% of Rs variability and could be a control in the early growing season during normal climatic periods. This suggests that Ts accounts for approximately 60 – 70% of variability while SM is a secondary control. However, during periods of long drought or high PPT, other factors such as energy balance (e.g. Rn, LH, and H) and Ta may explain further 13% of variability.

2.5.2 Spatial Variability

There are advantages and disadvantages with automated chamber use when dealing with Rs variability. Automated chambers provide temporal measurements but capture less spatial variability compared to manual chambers. For ecosystem – wide scaling from automated chambers, spatial variations must be considered (Wang et al, 2006). There can differences in measured values from a couple of meters apart even within a homogenous area due to differences in shading, soil biomass accumulation, and other factors (Davidson et al, 2002). One indicator of the spatial variability within chambers is the coefficient of variation (CV). The CV was found

to be comparable to other studies. For example, Shi and Jin (2016) reported a CV of 20 – 52% in temperate northeastern forests in China and Ngao et al, (2012) reported a CV of 9 – 62% in a European temperate beech forest. Spatial variation of Rs and its driving factors is under – researched, due to financial difficulties (multiple chamber requirements) and methodology and variability in factors such as soil organic matter content, pH, root distribution, and soil moisture (Bowden et al, 2004; Luan et al, 2014; Shin and Jin, 2016). However, high CV values obtained in this study as well as in literature indicate that spatial variability should be of concern.

2.6 Modeled Rs

2.6.1 Comparison of Model Results

The models that produced the best fit are the Gaussian – Gamma and the NARX neural network, providing better performance than the other five models (Rs Ts, Rs Q10, Rs Ts SM, Rs Ts SM, GEP, Bunnell Model).

In 2014, models produced a poor yearly fit and coefficient of determination mainly because of three factors: the lack of data coverage from measurement later in the season, the removal of one chamber due to high CO2 measurement from a wasp nest, and the smaller number of chambers (3 in 2014 compared to 5 in 2015). This caused a decrease in the amount of data available for training and testing producing a worse fit with observed data. More complex models (Bunnell Model, Gaussian – Gamma, NARX neural network, Rs Ts SM) followed two spikes in Rs during October 17th and the 24th whereas models such as Rs Ts and Rs Q10 produced a

constant increase and decrease throughout the year. This is likely due to seasonal bias such as sharp increases in precipitation and temperature causing models to underestimate indicating that in years with no extreme events or anomalies, a simpler model is suitable for estimation.

In 2015, models on average produced a higher coefficient of determination with the exception of Rs Ts SM GEP model with the addition of more chambers. The Rs Ts SM GEP model produced a worse yearly fit due to uncertainties related to GEP. Similar to 2014, the NARX neural network produced a noisy Rs before and after the growing season whereas the Gaussian – Gamma model produced consistent values. The fluctuations in estimated Rs from the neural network may be due to an assumption of plant growth and respiration during periods where there is little to none. In areas where there is a gap in Rs following a decline, the NARX neural network creates a more pronounced decline than the rest of the models (with the exception of Rs Ts SM GEP). This is probably due to the inclusion of other factors such as Ta and PPT creating an influence on Rs which is reflected due to a decline in Ta and a period of drought because of the positive correlation between the variables (Raich et al, 1992). Afterwards, a sharp increase in Rs is measured which all of the models predict. However, the Rs Q10 and Rs Ts model produced a much lower increase indicating that the Q10 model may not show true temperature sensitivity since other seasonal factors such as precipitation, root size, litterfall, and photosynthesis can interfere (Yuste et al, 2004; Gaumont – Guay et al, 2006). When incorporating SM, the models produced a better yearly fit. SM is an important factor

that can influence Rs and ecosystem growth. Lower Rs can be influenced due to decreased temperature sensitivity and lower SM (Xu and Qi, 2001; Davidson & Janssens, 2006; Van der Molen et al, 2011). A higher SM can impact soil oxygen diffusion for heterotrophic respiration (Pumpanen et al, 2008).

In 2016, models produced on average a low fit because of low precipitation and subsequently low SM. Additionally, higher yearly temperatures created relatively low Rs compared to previous years causing models dependence on soil temperature and moisture to underestimate. The Rs Ts SM GEP model had large underestimation of Rs throughout the year when combined with low soil temperature and moisture. The NARX neural network and Gaussian – Gamma models both performed well in this year with the neural network following the trends of increasing and decreasing Rs during the summer and the Gaussian – Gamma model underestimating (especially during fall). This is probably due to a series of precipitation events including a period of high precipitation followed by a drought and another, slightly lower precipitation event. The neural network accounts for the spike in Rs after the event, causing a closer yearly fit (6.61 µmol CO_2 $m^{-2}s^{-}1$ modeled vs 6.59 µmol CO_2 $m^{-2}s^{-1}$ observed) while the rest of the models produce a significantly lower Rs (~4.50 µmol CO_2 $m^{-2}s^{-1}$). This could be due to the inclusion of multiple variables that may influence Rs while other models incorporated Ts and SM.

In 2017, models produced a slightly better fit compared to 2016, however because of an extremely high precipitation event, the overall fit is comparably less than 2014

and 2015. All models have a close relationship with Ts and follows the Ts curve accordingly each year. However, because of the high amount of Ts early within the season due to a high precipitation event (57.39 mm), the models based on only Ts overestimated Rs early within the growing season (Rs Ts, Rs Q10). This event was closely followed with another, slightly lower precipitation event (39.70 mm) which caused Rs to rapidly increase and models to underestimate (except Rs Ts SM GEP and NARX neural network). In October 9th, there was an extreme precipitation event of 81.44 mm causing Rs to spike to 11.86 µmol CO_2 $m^{-2}s^{-1}$. However, because the soil moisture did not increase as high due to excess saturation of the ground and runoff, models dependent on both soil temperature and soil moisture underestimated Rs (Rs Ts SM, Bunnell model, Gaussian – Gamma model). The Rs Ts SM GEP model fit the initial precipitation event well, however the model underestimated Rs during the October rainfall event. This is probably due to GEP or photosynthesis being affected by precipitation. An increase in precipitation causes a decrease in PAR resulting in lower photosynthesis occurring within the forest stand. With the addition of PPT within the model, the NARX neural network is able to accurately follow measured Rs during the early growing season and during the October precipitation event, however the model still underestimates Rs (10.96 86 µmol CO_2 $m^{-2}s^{-1}$ observed vs. 6.15 86 µmol CO_2 $m^{-2}s^{-1}$ modeled). However, the inclusion may account for large and intense PPT events because the model reflects a larger increase in Rs for the October 9^{th} precipitation event compared to other models.

In 2018, models were able to produce a better yearly fit because of a one measurement chamber being re-introduced increasing the amount of training data. The year showed relatively similar soil temperature and moisture to 2014 and 2015 with no extreme precipitation events. There were two spikes in Rs in July and September corresponding to two precipitation events the first of which (July) caused underestimation in models using only Ts and SM (with the exception of Gaussian – Gamma model). The second spike in Rs (September) was able to be accurately predicted by all models involving soil moisture. The Rs Ts SM GEP model was able to accurately predict Rs for 81% of the observed data. However, like in 2017 the first precipitation event caused the model to underestimate likely due to the same factors. There was a 6-day gap in observed Rs data from (August 8 – 13) which was filled by all models. The models that incorporate SM produced an increase in Rs while the NARX neural network produced decline. The increase in Rs is more plausible when considering soil moisture and precipitation (rainfall of 28.76 mm on August 8). The decline produced by the NARX neural network is probably related to a decline on August 11th of Ta (22.28 to 20.40^{o}C), LH (87.16 to 56.41 W m^{-2}), or PPT (28.76 to 2.17 mm).

Overall, the NARX neural network produced a noisier dataset during periods of non-measurement while the Gaussian – Gamma model produced a consistent Rs. This indicates that neural network prediction outside of the measurement period is inaccurate due to low consistent respiration occurring in the winter (Thorne et al, 2020). The Rs Ts SM GEP model has limitations restricting Rs estimation to the

growing season because of the model's reliance on GEP. Further research is needed to verify this conclusion on the role of model prediction using Rs measurements obtained before and after the growing season.

2.6.2 Comparison of Rs with Ecosystem Respiration

In order to estimate the growing season CO_2 emissions, a yearly model had to be implemented to account for gaps in measured data, in particular in the winter where measurements are commonly not performed. Calculated Rs values using 7 models were compared against ecosystem respiration (RE) measured using an eddy covariance system since RE is measured year-round. Additionally, during the winter where photosynthesis does not occur, primary respiration is assumed to be from the soil. Previous studies have reported Rs values of 800 to 1400 g C m^{-2} in temperate forests (Raich and Schlesinger, 1992; Kishimoto – Mo et al, 2015; Keidel et al, 2015; Liu et al, 2016). Our calculated Rs values from 2014 to 2018 were within this range with an average Rs of 1207.8 g C m^{-2}. Most studies do not include winter measurements because of difficulty in chamber maintenance from snowfall and low contribution compared to total annual Rs. Liu et al, (2016) found winter Rs in a temperate coniferous forest to be 5% of annual emissions but other studies have reported 10 – 50% with around 60 – 90% of total Rs contributing to RE (Davidson et al, 2002; Yuste et al, 2005; Khomik et al, 2006; Schindlbacher et al, 2007; Wei et al, 2010). Our chamber measurements yielded more missing data in the early spring (average 69.35%) than in the summer (10.37%) and autumn (18.90%) (Table 2.6).

In this study, the Gaussian – Gamma model yielded an average of 90.8% of growing season RE and the neural network provided 65.1% (Table 2.7). All models displayed a seasonal bias with overestimation in the summer and underestimation in the winter (Figure 2.7). Errors resulting in overestimation can be caused by methodology such as disturbance of soil pressure gradient caused by chamber closure (Davidson et al, 1998; Koskinen et al, 2014). The absence of data for the first half of 2014 growing season combined with a removal of one chamber from 2014 to 2017 could have led to estimation errors.

This study has provided an important insight into the Rs modeling using different models and the temporal dynamics of Rs. The addition of environmental factors such as SM have shown to increase the accuracy of traditional models such as Rs Ts and the Q10 model. Many climate change models have predicted a shift in weather patterns causing shifts in temperature and precipitation (IPCC, 2014). An understanding of Rs in response to this shift can assist in the development of more accurate global carbon cycle models. Future work can include the development of a more robust model by incorporating multiple chambers measuring the spatial variability and contribution from additional environmental variables to total annual Rs in temperate deciduous forests.

2.7 Conclusion

The assessment of Rs in a temperate deciduous forest was performed using an automated chamber system over a five-year period (2014 to 2018). Our analysis indicated that factors other than Ts such as SM can exert significant control on Rs.

A pulse of Rs during major rainfall events was observed, which increased Rs by 78% in 2017. The average Q_{10} value was 1.91 and R_{10} increased while Q_{10} decreased in response to increasing Ts. Models such as Rs Ts and Q10 were found to improve by incorporating soil moisture. The Gaussian – Gamma provided the highest accuracy when estimating Rs with average yearly R^2 values of 0.60 compared to the Rs Ts and Rs Q10 models (R^2 = 0.55 for both). Application of both models indicated that Rs accounted for 65 – 90% of ecosystem respiration for the growing season as measured by the eddy covariance system.

This study provided understanding of the temporal dynamics of Rs in a temperate deciduous forest as well as the functioning of the various Rs models in simulating Rs dynamics. Findings highlight the importance of multiple environmental factors such as precipitation, temperature, soil moisture on Rs. Observed and modeled results suggest that extreme weather events could have major implications on Rs in the future.

2.8 References

Apps, M. J., & Price, D. T. (1996). *Forest ecosystems, forest management, and the global carbon cycle*. *NATO ASI series. Series I, Global environmental change: vol. 40*. Berlin, New York: Springer. https://doi.org/10.1007/978-3-642-61111-7

Atkin, O. K., Edwards, E. J., & Loveys, B. R. (2000). Response of root respiration to changes in temperature and its relevance to global warming. *New Phytologist*, *147*(1), 141–154. https://doi.org/10.1046/j.1469-8137.2000.00683.x

Beamesderfer, E. R., Arain, M. A., Khomik, M., Brodeur, J. J., & Burns, B. M. (2020). Response of carbon and water fluxes to meteorological and phenological variability in two eastern North American forests of similar age but contrasting species composition – a multiyear comparison. *Biogeosciences*, *17*(13), 3563–3587. https://doi.org/10.5194/bg-17-3563-2020

Borken, W., Xu, Y.-J., Brumme, R., & Lamersdorf, N. (1999). A Climate Change Scenario for Carbon Dioxide and Dissolved Organic Carbon Fluxes from a Temperate Forest Soil Drought and Rewetting Effects. *Soil Science Society of America Journal*, *63*(6), 1848–1855. https://doi.org/10.2136/sssaj1999.6361848x

Borken, W., Savage, K., Davidson, E. A., & Trumbore, S. E. (2006). Effects of experimental drought on soil respiration and radiocarbon efflux from a temperate forest soil. *Global Change Biology*, *12*(2), 177–193. https://doi.org/10.1111/j.1365-2486.2005.001058.x

Boussaada, I., & Niculescu, S.-I. (2018). On the Dominancy of Multiple Spectral Values for Time-delay Systems with Applications. *IFAC-PapersOnLine*, *51*(14), 55–60. https://doi.org/10.1016/j.ifacol.2018.07.198

Bowden, R. D., Davidson, E., Savage, K., Arabia, C., & Steudler, P. (2004). Chronic nitrogen additions reduce total soil respiration and microbial respiration in temperate forest soils at the Harvard Forest. *Forest Ecology and Management*, *196*(1), 43–56. https://doi.org/10.1016/j.foreco.2004.03.011

Brady, N. C., & Weil, R. R. (2017). *The nature and properties of soils* (Global edition). Boston: Pearson.

Burba, G. (2013). *Eddy Covariance Method for Scientific, Industrial, Agricultural and Regulatory Applications: A Field Book on Measuring Ecosystem Gas*

Exchange and Areal Emission Rates: LI-COR Biosciences. https://doi.org/10.13140/RG.2.1.4247.8561

Craine, J. M., Fierer, N., & McLauchlan, K. K. (2010). Widespread coupling between the rate and temperature sensitivity of organic matter decay. *Nature Geoscience*, *3*(12), 854–857. https://doi.org/10.1038/ngeo1009

Cigizoglu, H. K., Alp, K., & Kömürcü, M. (2005). Estimation of Air Pollution Parameters Using Artificial Neural Networks. In I. Faragó, K. Georgiev, & Á. Havasi (Eds.), *NATO science series. Series IV, Earth and environmental sciences: v. 54. Advances in air pollution modeling for environmental security* (Vol. 54, pp. 63–75). Dordrecht, Great Britain: Springer. https://doi.org/10.1007/1-4020-3351-6_7

Curiel Yuste, J., Janssens, I. A., Carrara, A., & Ceulemans, R. (2004). Annual Q10 of soil respiration reflects plant phenological patterns as well as temperature sensitivity. *Global Change Biology*, *10*(2), 161–169. https://doi.org/10.1111/j.1529-8817.2003.00727.x

Curiel Yuste, J., Nagy, M., Janssens, I. A., Carrara, A., & Ceulemans, R. (2005). Soil respiration in a mixed temperate forest and its contribution to total ecosystem respiration. *Tree Physiology*, *25*(5), 609–619. https://doi.org/10.1093/treephys/25.5.609

Daly, K. (2016). An Analysis of Soil Respiration in a Temperate Deciduous Forest Ecosystem (Doctoral dissertation).

Dan Foresee, F., & Hagan, M. T. (1997). Gauss-Newton approximation to Bayesian learning. In *The 1997 IEEE International Conference on Neural Networks, June 9-12, 1997, Westin Galleria Hotel, Houston, Texas, USA* (pp. 1930–1935). New York: Institute of Electrical and Electronics Engineers. https://doi.org/10.1109/ICNN.1997.614194

Davidson, E.A., Savage, K., Verchot, L.V., & Navarro, R. (2002). Minimizing artifacts and biases in chamber-based measurements of soil respiration. *Agricultural and Forest Meteorology*, *113*(1-4), 21–37. https://doi.org/10.1016/S0168-1923(02)00100-4

Davidson, E. A., & Janssens, I. A. (2006). Temperature sensitivity of soil carbon decomposition and feedbacks to climate change. *Nature*, *440*(7081), 165–173. https://doi.org/10.1038/nature04514

Davidson, E. A., Belk, E., & Boone, R. D. (1998). Soil water content and temperature as independent or confounded factors controlling soil respiration in a temperate mixed hardwood forest. *Global Change Biology*, *4*(2), 217–227. https://doi.org/10.1046/j.1365-2486.1998.00128.x

Delgrosso, S., Mosier, A., Parton, W., & Ojima, D. (2005). DAYCENT model analysis of past and contemporary soil NO and net greenhouse gas flux for major crops in the USA. *Soil and Tillage Research*, *83*(1), 9–24. https://doi.org/10.1016/j.still.2005.02.007

Fadare, D. A. (2009). Modelling of solar energy potential in Nigeria using an artificial neural network model. *Applied Energy*, *86*(9), 1410–1422. https://doi.org/10.1016/j.apenergy.2008.12.005

Gao, Y., & Er, M. J. (2005). NARMAX time series model prediction: feedforward and recurrent fuzzy neural network approaches. *Fuzzy Sets and Systems*, *150*(2), 331–350. https://doi.org/10.1016/j.fss.2004.09.015

Gaumont-Guay, D., Black, T. A., Griffis, T. J., Barr, A. G., Jassal, R. S., & Nesic, Z. (2006). Interpreting the dependence of soil respiration on soil temperature and water content in a boreal aspen stand. *Agricultural and Forest Meteorology*, *140*(1-4), 220–235. https://doi.org/10.1016/j.agrformet.2006.08.003

Geider, R. J., Delucia, E. H., Falkowski, P. G., Finzi, A. C., Grime, J. P., Grace, J., . . . Woodward, F. I. (2001). Primary productivity of planet earth: biological determinants and physical constraints in terrestrial and aquatic habitats. *Global Change Biology*, *7*(8), 849–882. https://doi.org/10.1046/j.1365-2486.2001.00448.x

Gholamy, A., Kreinovich, V., & Kosheleva, O. (2018). Why 70/30 or 80/20 Relation Between Training and Testing Sets: A Pedagogical Explanation.

Goulden, M. L., Munger, J. W., Fan, S.-M., Daube, B. C., & Wofsy, S. C. (1996). Exchange of Carbon Dioxide by a Deciduous Forest: Response to Interannual Climate Variability. *Science*, *271*(5255), 1576–1578. https://doi.org/10.1126/science.271.5255.1576

Greco, S., & Baldocchi, D. D. (1996). Seasonal variations of CO2 and water vapour exchange rates over a temperate deciduous forest. *Global Change Biology*, *2*(3), 183–197. https://doi.org/10.1111/j.1365-2486.1996.tb00071.x

Hagan, M. T., & Menhaj, M. B. (1994). Training feedforward networks with the Marquardt algorithm. *IEEE Transactions on Neural Networks*, *5*(6), 989–993. https://doi.org/10.1109/72.329697

Hanson, P. J., Edwards, N. T., Garten, C. T., & Andrews, J. A. (2000). Separating root and soil microbial contributions to soil respiration: A review of methods and observations. *Biogeochemistry*, *48*(1), 115–146. https://doi.org/10.1023/A:1006244819642

Hebb, D. O. (1949). *The organization of behavior: A neuropsychological theory*. Mahwah N.J.: L. Erlbaum Associates.

Hinton, G. E. (2002). Training products of experts by minimizing contrastive divergence. *Neural Computation*, *14*(8), 1771–1800. https://doi.org/10.1162/089976602760128018

Hochreiter, S., & Schmidhuber, J. (1997). Long short-term memory. *Neural Computation*, *9*(8), 1735–1780. https://doi.org/10.1162/neco.1997.9.8.1735

Högberg, P., Nordgren, A., Buchmann, N., Taylor, A. F., Ekblad, A., Högberg, M. N., . . . Read, D. J. (2001). Large-scale forest girdling shows that current photosynthesis drives soil respiration. *Nature*, *411*(6839), 789–792. https://doi.org/10.1038/35081058

Hollinger, D. Y., & Richardson, A. D. (2005). Uncertainty in eddy covariance measurements and its application to physiological models. *Tree Physiology*, *25*(7), 873–885. https://doi.org/10.1093/treephys/25.7.873

Huang, N., Gu, L., & Niu, Z. (2014). Estimating soil respiration using spatial data products: A case study in a deciduous broadleaf forest in the Midwest USA. *Journal of Geophysical Research: Atmospheres*, *119*(11), 6393–6408. https://doi.org/10.1002/2013JD020515

Ignace, D. D. (2019). Determinants of temperature sensitivity of soil respiration with the decline of a foundation species. *PloS One*, *14*(10), e0223566. https://doi.org/10.1371/journal.pone.0223566

IEEE, 1997. *The 1997 IEEE International Conference on Neural Networks, June 9-12, 1997, Westin Galleria Hotel, Houston, Texas, USA*. New York: Institute of Electrical and Electronics Engineers.

IPCC, 2014: Climate Change 2014: Synthesis Report. Contribution of Working Groups I, II and III to the Fifth Assessment Report of the Intergovernmental Panel on Climate Change [Core Writing Team, R.K. Pachauri and L.A. Meyer (eds.)]. IPCC, Geneva, Switzerland, 151 pp.

Janssens, I. A., & Pilegaard, K. I.M. (2003). Large seasonal changes in Q10 of soil respiration in a beech forest. *Global Change Biology*, *9*(6), 911–918. https://doi.org/10.1046/j.1365-2486.2003.00636.x

Jeong, S.-H., Eom, J.-Y., Park, J.-Y., Chun, J.-H., & Lee, J.-S. (2018). Effect of precipitation on soil respiration in a temperate broad-leaved forest. *Journal of Ecology and Environment*, *42*(1). https://doi.org/10.1186/s41610-018-0071-6

Jia, X., Zha, T., Wu, B., Zhang, Y., Chen, W., Wang, X., . . . He, G. (2013). Temperature response of soil respiration in a Chinese pine plantation: Hysteresis and seasonal vs. Diel Q10. *PloS One*, *8*(2), e57858. https://doi.org/10.1371/journal.pone.0057858

Keidel, L., Kammann, C., Grünhage, L., Moser, G., & Müller, C. (2015). Positive feedback of elevated CO 2 on soil respiration in late autumn and winter. *Biogeosciences*, *12*(4), 1257–1269. https://doi.org/10.5194/bg-12-1257-2015

Khomik, Myroslava. (2004). Soil CO2 Efflux From Temperate and Boreal Forests in Ontario (Master's Thesis). McMaster University. Hamilton, Ontario.

Khomik, M., Arain, M. A., Liaw, K.-L., & McCaughey, J. H. (2009). Debut of a flexible model for simulating soil respiration–soil temperature relationship: Gamma model. *Journal of Geophysical Research*, *114*(G3). https://doi.org/10.1029/2008JG000851

Khomik, M., Arain, M. A., Brodeur, J. J., Peichl, M., Restrepo-Coupé, N., & McLaren, J. D. (2010). Relative contributions of soil, foliar, and woody tissue respiration to total ecosystem respiration in four pine forests of different ages. *Journal of Geophysical Research*, *115*(G3). https://doi.org/10.1029/2009JG001089

Khomik, M., Arain, M. A., & McCaughey, J. H. (2006). Temporal and spatial variability of soil respiration in a boreal mixedwood forest. *Agricultural and Forest Meteorology*, *140*(1-4), 244–256. https://doi.org/10.1016/j.agrformet.2006.08.006

Kishimoto-Mo, A. W., Yonemura, S., Uchida, M., Kondo, M., Murayama, S., & Koizumi, H. (2015). Contribution of soil moisture to seasonal and annual variations of soil CO2 efflux in a humid cool-temperate oak-birch forest in central Japan. *Ecological Research*, *30*(2), 311–325. https://doi.org/10.1007/s11284-015-1254-6

Kisi, O., & Uncuoğlu, E. (2005). Comparison of three back-propagation training algorithms for two case studies. *Indian Journal of Engineering and Materials Sciences*, *12*.

Koskinen, M., Minkkinen, K., Ojanen, P., Kämäräinen, M., Laurila, T., & Lohila, A. (2014). Measurements of CO 2 exchange with an automated chamber system throughout the year: challenges in measuring night-time respiration on porous peat soil. *Biogeosciences*, *11*(2), 347–363. https://doi.org/10.5194/bg-11-347-2014

Krasnopol′sky, V. M. (2013). *The application of neural networks in the earth system sciences: Neural networks emulations for complex multidimensional mappings /Vladimir M. Krasnopolsky*. *Atmospheric and oceanographic sciences library: Vol. 46*. Dordrecht: Springer.

LeCun, Y., Boser, B., Denker, J. S., Henderson, D., Howard, R. E., Hubbard, W., & Jackel, L. D. (1989). Backpropagation Applied to Handwritten Zip Code

Recognition. *Neural Computation*, *1*(4), 541–551. https://doi.org/10.1162/neco.1989.1.4.541

LeCun, Y., Jackel, L. D., Bottou, L., Brunot, A., Cortes, C., Denker, J., . . . Sackinger, E. (Eds.) (1995). *Comparison of learning algorithms for handwritten digit recognition*: Perth, Australia.

Lee, M.-S., Nakane, K., Nakatsubo, T., Mo, W.-h., & Koizumi, H. (2002). Effects of rainfall events on soil CO 2 flux in a cool temperate deciduous broad-leaved forest. *Ecological Research*, *17*(3), 401–409. https://doi.org/10.1046/j.1440-1703.2002.00498.x

Lee, X., Wu, H.-J., Sigler, J., Oishi, C., & Siccama, T. (2004). Rapid and transient response of soil respiration to rain. *Global Change Biology*, *10*(6), 1017–1026. https://doi.org/10.1111/j.1529-8817.2003.00787.x

Lin, T., Horne, B. G., Tino, P., & Giles, C. L. (1996). Learning long-term dependencies in NARX recurrent neural networks. *IEEE Transactions on Neural Networks*, *7*(6), 1329–1338. https://doi.org/10.1109/72.548162

Liu, B., Mou, C., Yan, G., Xu, L., Jiang, S., Xing, Y., . . . Wang, Q. (2016). Annual soil CO2 efflux in a cold temperate forest in northeastern China: Effects of winter snowpack and artificial nitrogen deposition. *Scientific Reports*, *6*, 18957. https://doi.org/10.1038/srep18957

Liu, L., Wang, X., Lajeunesse, M. J., Miao, G., Piao, S., Wan, S., . . . Deng, M. (2016). A cross-biome synthesis of soil respiration and its determinants under simulated precipitation changes. *Global Change Biology*, *22*(4), 1394–1405. https://doi.org/10.1111/gcb.13156

Lloyd, J., & Taylor, J. A. (1994). On the Temperature Dependence of Soil Respiration. *Functional Ecology*, *8*(3), 315. https://doi.org/10.2307/2389824

Luan, J.-B., Wang, X.-W., Colvin, J., & Liu, S.-S. (2014). Plant-mediated whitefly-begomovirus interactions: Research progress and future prospects. *Bulletin of Entomological Research*, *104*(3), 267–276. https://doi.org/10.1017/S000748531400011X

Luo, Y., & Zhou, X. (2006). *Soil respiration and the environment*. Amsterdam, London: Academic Press. Retrieved from http://www.loc.gov/catdir/enhancements/fy0665/2006024416-d.html

MacKay, D. J. C. (1992). Bayesian Interpolation. *Neural Computation*, *4*(3), 415–447. https://doi.org/10.1162/neco.1992.4.3.415

Melesse, A. M., & Hanley, R. S. (2005). Artificial neural network application for multi-ecosystem carbon flux simulation. *Ecological Modelling*, *189*(3-4), 305–314. https://doi.org/10.1016/j.ecolmodel.2005.03.014

Mo, W., Lee, M.-S., Uchida, M., Inatomi, M., Saigusa, N., Mariko, S., & Koizumi, H. (2005). Seasonal and annual variations in soil respiration in a cool-temperate deciduous broad-leaved forest in Japan. *Agricultural and Forest Meteorology*, *134*(1-4), 81–94. https://doi.org/10.1016/j.agrformet.2005.08.015

Møller, M. F. (1993). A scaled conjugate gradient algorithm for fast supervised learning. *Neural Networks*, *6*(4), 525–533. https://doi.org/10.1016/S0893-6080(05)80056-5

Moré, J. J. (1978). The Levenberg-Marquardt algorithm: Implementation and theory. In G. A. Watson (Ed.), *Lecture Notes in Mathematics. Numerical analysis: Proceedings of the biennial Conference held at Dundee ... 1977 / edited by G. A. Watson* (Vol. 630, pp. 105–116). Berlin, Heidelberg: Springer Berlin Heidelberg. https://doi.org/10.1007/BFb0067700

Ngao, J., Epron, D., Delpierre, N., Bréda, N., Granier, A., & Longdoz, B. (2012). Spatial variability of soil CO2 efflux linked to soil parameters and ecosystem characteristics in a temperate beech forest. *Agricultural and Forest Meteorology*, *154-155*, 136–146. https://doi.org/10.1016/j.agrformet.2011.11.003

Ohashi, M., & Gyokusen, K. (2007). Temporal change in spatial variability of soil respiration on a slope of Japanese cedar (Cryptomeria japonica D. Don) forest. *Soil Biology and Biochemistry*, *39*(5), 1130–1138. https://doi.org/10.1016/j.soilbio.2006.12.021

Orchard, V. A., & Cook, F. J. (1983). Relationship between soil respiration and soil moisture. *Soil Biology and Biochemistry*, *15*(4), 447–453. https://doi.org/10.1016/0038-0717(83)90010-X

Palm, G., & Aertsen, A. (Eds.) (1986). *Brain Theory: Proceedings of the First Trieste Meeting on Brain Theory, October 1-4, 1984*. Berlin, Heidelberg: Springer Berlin Heidelberg. https://doi.org/10.1007/978-3-642-70911-1

Peng, Y., Thomas, S. C., & Tian, D. (2008). Forest management and soil respiration: Implications for carbon sequestration. *Environmental Reviews*, *16*(NA), 93–111. https://doi.org/10.1139/A08-003

Pumpanen, J., Ilvesniemi, H., Kulmala, L., Siivola, E., Laakso, H., Kolari, P., . . . Hari, P. (2008). Respiration in Boreal Forest Soil as Determined from Carbon Dioxide Concentration Profile. *Soil Science Society of America Journal*, *72*(5), 1187–1196. https://doi.org/10.2136/sssaj2007.0199

Raich, J. W., & Schlesinger, W. H. (1992). The global carbon dioxide flux in soil respiration and its relationship to vegetation and climate. *Tellus B: Chemical and Physical Meteorology*, *44*(2), 81–99. https://doi.org/10.3402/tellusb.v44i2.15428

Raich, J. W., & Potter, C. S. (1995). Global patterns of carbon dioxide emissions from soils. *Global Biogeochemical Cycles*, *9*(1), 23–36. https://doi.org/10.1029/94GB02723

Raich, J. W., Potter, C. S., & Bhagawati, D. (2002). Interannual variability in global soil respiration, 1980-94. *Global Change Biology*, *8*(8), 800–812. https://doi.org/10.1046/j.1365-2486.2002.00511.x

Reichstein, M., & Beer, C. (2008). Soil respiration across scales: The importance of a model–data integration framework for data interpretation. *Journal of Plant Nutrition and Soil Science*, *171*(3), 344–354. https://doi.org/10.1002/jpln.200700075

Restrepo, N. C., & Arain, M. A. (2005). Energy and water exchanges from a temperate pine plantation forest. *Hydrological Processes*, *19*(1), 27–49. https://doi.org/10.1002/hyp.5758

Rosenblatt, F. (1958). The perceptron: A probabilistic model for information storage and organization in the brain. *Psychological Review*, *65*(6), 386–408. https://doi.org/10.1037/h0042519

Running, S. W., Baldocchi, D. D., Turner, D. P., Gower, S. T., Bakwin, P. S., & Hibbard, K. A. (1999). A Global Terrestrial Monitoring Network Integrating Tower Fluxes, Flask Sampling, Ecosystem Modeling and EOS Satellite Data. *Remote Sensing of Environment*, *70*(1), 108–127. https://doi.org/10.1016/S0034-4257(99)00061-9

Russell, S. J., Norvig, P., & Davis, E. (2010). *Artificial intelligence: A modern approach* (3rd ed.). *Prentice Hall series in artificial intelligence*. Upper Saddle River: Prentice Hall.

Savage, K. E., & Davidson, E. A. (2001). Interannual variation of soil respiration in two New England forests. *Global Biogeochemical Cycles*, *15*(2), 337–350. https://doi.org/10.1029/1999GB001248

Schindlbacher, A., Zechmeister-Boltenstern, S., Glatzel, G., & Jandl, R. (2007). Winter soil respiration from an Austrian mountain forest. *Agricultural and Forest Meteorology*, *146*(3-4), 205–215. https://doi.org/10.1016/j.agrformet.2007.06.001

Schlesinger, W. H., & Andrews, J. A. (2000). Soil respiration and the global carbon cycle. *Biogeochemistry*, *48*(1), 7–20. https://doi.org/10.1023/A:1006247623877

Schmidhuber, J. (2015). Deep learning in neural networks: An overview. *Neural Networks : The Official Journal of the International Neural Network Society*, *61*, 85–117. https://doi.org/10.1016/j.neunet.2014.09.003

Shabaga, J. A., Basiliko, N., Caspersen, J. P., & Jones, T. A. (2015). Seasonal controls on patterns of soil respiration and temperature sensitivity in a northern mixed deciduous forest following partial-harvesting. *Forest Ecology and Management*, *348*, 208–219. https://doi.org/10.1016/j.foreco.2015.03.022

Shi, B., & Jin, G. (2016). Variability of soil respiration at different spatial scales in temperate forests. *Biology and Fertility of Soils*, *52*(4), 561–571. https://doi.org/10.1007/s00374-016-1100-1

Sinanoğlu, C. (2004). The analysis of the effects of surface roughness of shafts on journal bearings using recurrent hybrid neural network. *Industrial Lubrication and Tribology*, *56*(6), 324–333. https://doi.org/10.1108/00368790410558239

Skopp, J., Jawson, M. D., & Doran, J. W. (1990). Steady-State Aerobic Microbial Activity as a Function of Soil Water Content. *Soil Science Society of America Journal*, *54*(6), 1619–1625. https://doi.org/10.2136/sssaj1990.03615995005400060018x

Song, X., Peng, C., Zhao, Z., Zhang, Z., Guo, B., Wang, W., . . . Zhu, Q. (2014). Quantification of soil respiration in forest ecosystems across China. *Atmospheric Environment*, *94*, 546–551. https://doi.org/10.1016/j.atmosenv.2014.05.071

Tang, Y., Wen, X., Sun, X., Zhang, X., & Wang, H. (2014). The limiting effect of deep soilwater on evapotranspiration of a subtropical coniferous plantation subjected to seasonal drought. *Advances in Atmospheric Sciences*, *31*(2), 385–395. https://doi.org/10.1007/s00376-013-2321-y

Taylor, A. J., Lai, C.-T., Hopkins, F. M., Wharton, S., Bible, K., Xu, X., . . . Ehleringer, J. R. (2015). Radiocarbon-Based Partitioning of Soil Respiration in an Old-Growth Coniferous Forest. *Ecosystems*, *18*(3), 459–470. https://doi.org/10.1007/s10021-014-9839-4

Thierron, V., & Laudelout, H. (1996). Contribution of root respiration to total CO 2 efflux from the soil of a deciduous forest. *Canadian Journal of Forest Research*, *26*(7), 1142–1148. https://doi.org/10.1139/x26-127

Thorne, R., Khomik, M., Hayman, E., & Arain, A. (2020). Response of Soil CO2 Efflux to Shelterwood Harvesting in a Mature Temperate Pine Forest. *Forests*, *11*(3), 304. https://doi.org/10.3390/f11030304

Van der Molen, M. K., Dolman, A. J., Ciais, P., Eglin, T., Gobron, N., Law, B. E., . . . Wang, G. (2011). Drought and ecosystem carbon cycling. *Agricultural and Forest Meteorology*, *151*(7), 765–773. https://doi.org/10.1016/j.agrformet.2011.01.018

Van Gestel, M., Ladd, J. N., & Amato, M. (1991). Carbon and nitrogen mineralization from two soils of contrasting texture and microaggregate stability: Influence of sequential fumigation, drying and storage. *Soil Biology and Biochemistry*, *23*(4), 313–322. https://doi.org/10.1016/0038-0717(91)90185-M

Van't Hoff, M. J. H. (1884). Etudes de dynamique chimique. *Recueil Des Travaux Chimiques Des Pays-Bas*, *3*(10), 333–336. https://doi.org/10.1002/recl.18840031003

Waibel, A., Hanazawa, T., Hinton, G., Shikano, K., & Lang, K. J. (1989). Phoneme recognition using time-delay neural networks. *IEEE Transactions on Acoustics, Speech, and Signal Processing*, *37*(3), 328–339. https://doi.org/10.1109/29.21701

Wang, C., Yang, J., & Zhang, Q. (2006). Soil respiration in six temperate forests in China. *Global Change Biology*, *12*(11), 2103–2114. https://doi.org/10.1111/j.1365-2486.2006.01234.x

Wang, W., Peng, S., Wang, T., & Fang, J. (2010). Winter soil CO2 efflux and its contribution to annual soil respiration in different ecosystems of a forest-steppe ecotone, north China. *Soil Biology and Biochemistry*, *42*(3), 451–458. https://doi.org/10.1016/j.soilbio.2009.11.028

Watson, G. A. (Ed.) (1978). *Lecture Notes in Mathematics. Numerical analysis: Proceedings of the biennial Conference held at Dundee ... 1977 / edited by G. A. Watson*. Berlin, Heidelberg: Springer Berlin Heidelberg. https://doi.org/10.1007/BFb0067690

Wei, W., Weile, C., & Shaopeng, W. (2010). Forest soil respiration and its heterotrophic and autotrophic components: Global patterns and responses to temperature and precipitation. *Soil Biology and Biochemistry*, *42*(8), 1236–1244. https://doi.org/10.1016/j.soilbio.2010.04.013

Werbos, P. J. (1994). *The roots of backpropagation: From ordered derivatives to neural networks and political forecasting / Paul John Werbos*. *A Wiley-Interscience publication*. New York, Chichester: Wiley.

Xu, L., Baldocchi, D. D., & Tang, J. (2004). How soil moisture, rain pulses, and growth alter the response of ecosystem respiration to temperature. *Global Biogeochemical Cycles*, *18*(4), n/a-n/a. https://doi.org/10.1029/2004GB002281

Xu, M., & Qi, Y. (2001). Soil-surface CO2 efflux and its spatial and temporal variations in a young ponderosa pine plantation in northern California. *Global Change Biology*, *7*(6), 667–677. https://doi.org/10.1046/j.1354-1013.2001.00435.x

Yan, L., Chen, S., Xia, J., & Luo, Y. (2014). Precipitation regime shift enhanced the rain pulse effect on soil respiration in a semi-arid steppe. *PloS One, 9*(8), e104217. https://doi.org/10.1371/journal.pone.0104217

Zhou, Z., Guo, C., & Meng, H. (2013). Temperature sensitivity and basal rate of soil respiration and their determinants in temperate forests of North China. *PloS One, 8*(12), e81793. https://doi.org/10.1371/journal.pone.0081793

Table 2.1. Soil respiration (Rs) models used for modeling and analysis

Model	**Formula**	**Reference**
Rs Ts	$Rs = ae^{Ts}$	Van't Hoff (1884); Lloyd and Taylor (1994)
Rs Q_{10}	$Rs = R_{10}Q_{10}^{\frac{Ts-10}{10}}$	Yuste et al. (2004)
Rs Ts SM	$Rs = R_{10}Q_{10}^{\frac{Ts-10}{10}} * \left(\frac{1}{1+e^{a+b*SM}}\right)$	Peichl et al. (2010)
Rs Ts SM GEP	$Rs = B_0 e^{B_1 Ts} e^{b_2 SM + B_3 SM^2} + B_4 GEP + B_5$	Huang et al. (2014)
Bunnell Model	$Rs = \left(\frac{SM}{a+SM}\right)\left(\frac{b}{b+SM}\right) cd^{\frac{Ts-10}{10}}$	Bunnell et al. (1977)
Gaussian – Gamma Model	$y_i = e^{\beta_0 + \beta_{11}T_i + \beta_{12}T_i^2 + \beta_{21}M_i + \beta_{22}\ln(M_i)}$	Khomik et al. (2009)
NARX Neural Network	$y(t) = f(x(t-1), x(t-2) \dots x(t-D), y(t-1), y(t-2) \dots y(t-D)$	Melesse et al. (2005)

Table 2.2. Training results and coefficient of determination (R^2) for the Rs models from 2014 to 2018.

(a) Rs Ts Model

Year	A	B	R^2
2014	2.29	0.072	0.71
2015	1.79	0.056	0.54
2016	1.67	0.053	0.44
2017	2.61	0.052	0.48
2018	1.49	0.085	0.74
All	2.25	0.054	0.38

(b) Rs Q_{10} Model

Year	R_{10}	Q_{10}	R^2
2014	4.73	2.06	0.71
2015	3.14	1.76	0.54
2016	2.84	1.70	0.44
2017	4.36	1.67	0.48
2018	3.51	2.36	0.75
All	3.87	1.72	0.38

(c) Rs Ts SM Model

Year	R_{10}	Q_{10}	A	B	R^2
2014	6.07	2.51	1.17	-17.67	0.82
2015	3.87	2.32	0.89	-17.55	0.76
2016	2.77	2.03	1.46	-87.91	0.54
2017	4.30	1.89	0.90	-63.23	0.64
2018	3.97	2.76	0.029	-18.65	0.85
All	4.12	2.14	0.49	-26.90	0.52

(d) Rs Ts SM GEP

Year	B_0	B_1	B_2	B_e	B_4	B_5	R^2
2014	-11.05	-0.041	0.42	-27.26	0.46	7.95	0.83
2015	$-2.44*10^{-4}$	34.68	34.67	-228.38	0.12	4.36	0.055
2016	$-3.34*10^{-4}$	0.33	2.26	233.43	0.047	4.67	0.24
2017	-3.59	-0.051	31.99	-1264.79	0.42	3.51	0.59
2018	1.33	0.077	5.67	-10.20	0.16	-1.90	0.87
All	-8.76	-0.026	8.73	20.83	0.43	5.94	0.59

(e) Bunnell Model

Year	A	B	C	D	R^2
2014	0.146	$2.07*10^{4}$	1.55	2.50	0.81
2015	-0.695	0.039	-10.58	2.33	0.77
2016	0.132	0.038	7.71	1.79	0.55
2017	0.044	0.240	2.48	1.89	0.64
2018	-0.891	0.011	-37.8	2.67	0.86
All	-1.984	0.026	-72.29	2.14	0.52

(f) Gaussian – Gamma Model

Year	β_0	β_{11}	β_{12}	β_{21}	β_{22}	R^2
2014	1.80	0.154	$2.15*10^{-3}$	-1.52	0.69	0.82
2015	3.34	0.087	$1.56*10^{-4}$	-6.73	1.07	0.74
2016	5.93	0.036	$-4.34*10^{-4}$	-21.39	1.35	0.62
2017	3.24	0.126	$1.94*10^{-3}$	-9.43	0.83	0.65
2018	3.00	0.088	$-1.88*10^{-6}$	-7.51	0.77	0.83
All	3.00	0.135	$2.02*10^{-3}$	-7.67	0.88	0.53

Table 2.3. Testing slope and intercept results and coefficient of determination (R2) for seven models: Rs Ts, Rs Q10, Rs Ts SM, Rs Ts SM GEP, Bunnell Model, Gaussian – Gamma model, and NARX Neural Network from:

(a) 2014 to 2016.

Year	**2014**		**2015**		**2016**	
Model	Testing Equation	R^2	Testing Equation	R^2	Testing Equation	R^2
Rs Ts	Y = 0.68x + 2.59	0.63	Y = 0.49x + 2.09	0.62	Y = 0.37x + 2.68	0.40
Rs Q_{10}	Y = 0.68x + 2.59	0.63	Y = 0.49x + 2.09	0.62	Y = 0.37x + 2.67	0.40
Rs Ts SM	Y = 0.77x + 1.73	0.74	Y = 0.86x + 0.62	0.83	Y = 0.53x + 2.13	0.48
Rs Ts SM GEP	Y = 0.67x + 3.13	0.57	Y = 0.065x + 4.46	0.056	Y = -0.068x + 4.54	0.016
Bunnell Model	Y = 0.78x + 1.69	0.75	Y = 0.87x + 0.61	0.83	Y = 0.47x + 2.37	0.52
Gaussian – Gamma	Y = 0.77x + 1.81	0.76	Y = 0.84x + 0.68	0.81	Y = 0.86x + 1.83	0.62
NARX Neural Network	Y = 0.25x + 2.62	0.37	Y = 0.94x + 0.13	0.82	Y = 0.65x + 1.40	0.79

(b) 2017 to 2018.

Year	**2017**		**2018**	
Model	Testing Equation	R^2	Testing Equation	R^2
Rs Ts	Y = 0.43x + 3.66	0.41	Y = 0.64x + 1.90	0.72
Rs Q_{10}	Y = 0.47x + 3.66	0.41	Y = 0.64x + 1.90	0.72
Rs Ts SM	Y = 0.56x + 2.67	0.53	Y = 0.73x + 1.27	0.85
Rs Ts SM GEP	Y = 0.56x + 2.85	0.54	Y = 0.74x + 1.27	0.81
Bunnell Model	Y = 0.57x + 2.63	0.53	Y = 0.71x + 1.41	0.86
Gaussian – Gamma	Y = 0.63x + 2.14	0.55	Y = 0.71x + 1.38	0.82
NARX Neural Network	Y = 0.73x + 1.74	0.63	Y = 0.79x + 1.18	0.83

Table 2.4. Statistics for applied Rs models. Error sum of squares (SSE) and standard deviation (STD).

Model	2014		2015		2016		2017		2018	
	SSE	STD	SSE	STD	SSE	STD	SSE	STD	SSE	STD
Rs Ts	86.86	2.49	72.15	1.26	41.32	1.10	57.18	1.56	233.6	2.63
Rs Q10	86.91	2.50	72.23	1.25	41.35	1.10	57.08	1.55	233.4	2.63
Rs Ts SM	111.2	2.63	54.52	1.63	42.16	1.24	56.83	1.68	152.7	2.73
Rs Ts SM GEP	138.4	1.33	15.19	0.25	174.8	0.71	188.5	1.17	133.2	1.51
Bunnell Model	112.0	2.62	53.69	1.63	31.46	1.21	58.27	1.69	138.7	2.68
Gaussian – Gamma	111.1	2.93	69.69	1.66	77.83	1.44	92.62	2.14	181.8	2.66
NARX Neural Network	134.2	1.46	138.7	2.12	75.38	1.47	248.0	2.83	167.6	2.44
Observed Rs STD	1.84		1.41		1.33		1.46		1.89	

Table 2.5. Estimated seasonal and total Rs (g C m^{-2} $year^{-1}$) over the growing season using seven Rs models

Year	2014						
Model	Gaussian Gamma	Rs Ts SM	Bunnell	Rs Q10	Rs Ts	Rs Ts SM GEP	NARX Neural Network
Winter	42±0.26	103±0.33	103±0.33	135±0.22	135±0.22	30±0.52	315±0.41
Spring	177±1.99	219±1.64	221±1.66	222±1.25	222±1.25	172±2.01	252±0.86
Summer	632±1.41	613±1.47	614±1.43	585±0.83	585±0.83	635±1.44	544±1.30
Autumn	376±2.47	393±2.18	393±2.17	362±1.66	362±1.66	379±2.32	321±0.53
Total	1225±2.97	1328±2.60	1330±2.60	1304±2.16	1303±2.15	1216±3.01	1432±1.47

Year	2015						
Model	Gaussian Gamma	Rs Ts SM	Bunnell	Rs Q10	Rs Ts	Rs Ts SM GEP	NARX Neural Network
Winter	55±0.63	101±0.71	100±0.70	149±0.48	149±0.48	32±1.03	107±0.60
Spring	187±2.01	226±1.67	226±1.65	236±1.36	236±1.36	184±2.09	167±1.20
Summer	687±1.22	670±1.30	671±1.28	592±1.00	591±1.00	684±1.21	556±0.98
Autumn	363±1.64	374±1.39	373±1.41	405±1.69	404±1.69	353±1.50	255±1.18
Total	1292±2.94	1370±2.62	1371±2.62	1382±2.20	1381±2.20	1254±3.02	1084±2.13

Year	2016						
Model	Gaussian Gamma	Rs Ts SM	Bunnell	Rs Q10	Rs Ts	Rs Ts SM GEP	NARX Neural Network
Winter	42±0.32	95±0.31	94±0.30	146±0.25	146±0.25	45±0.41	230±1.05
Spring	204±1.44	249±1.13	249±1.12	255±1.04	255±1.04	218±1.37	207±0.83
Summer	526±1.53	533±1.79	533±1.86	652±1.43	651±1.43	541±1.60	439±1.19
Autumn	371±1.90	380±1.65	382±1.68	422±1.80	422±1.79	360±1.77	350±1.21
Total	1143±2.38	1257±2.13	1258±2.16	1475±2.43	1475±2.43	1164±2.37	1226±1.47

Year	2017						
Model	Gaussian Gamma	Rs Ts SM	Bunnell	Rs Q10	Rs Ts	Rs Ts SM GEP	NARX Neural Network
Winter	54±0.30	120±0.31	118±0.31	146±0.25	146±0.25	56±0.43	132±0.59
Spring	222±1.68	261±1.35	260±1.35	259±1.07	259±1.07	231±1.67	214±2.00
Summer	591±1.21	578±1.25	577±1.27	604±0.88	604±0.88	599±1.18	698±1.09
Autumn	362±1.85	369±1.50	367±1.51	402±1.58	402±1.58	355±1.68	391±2.16
Total	1228±2.55	1329±2.17	1323±2.17	1411±2.13	1410±2.13	1241±2.53	1435±2.84

Year	2018						
Model	Gaussian Gamma	Rs Ts SM	Bunnell	Rs Q10	Rs Ts	Rs Ts SM GEP	NARX Neural Network
Winter	48±0.22	114±0.26	114±0.27	139±0.19	139±0.19	47±0.39	194±0.25
Spring	187±1.99	232±1.60	232±1.60	236±1.36	236±1.36	195±1.94	273±1.50
Summer	595±1.67	598±1.90	597±1.93	647±1.14	647±1.14	599±1.69	634±1.66
Autumn	407±2.95	434±2.84	434±2.82	409±2.25	409±2.25	404±2.79	448±2.40
Total	1236±3.00	1377±2.76	1377±2.76	1431±2.54	1430±2.53	1244±2.96	1549±2.45

Table 2.6. Mean seasonal and growing seasonal of ecosystem respiration (RE) and measured soil respiration (Rs) values, in µmol CO_2 m^{-2} s^{-1}, total observed data, and the percentage of missing Rs measurements from RE during the study period.

Year	2014		
Season	RE (µmol CO_2 m^{-2} s^{-1})	Rs Measured (µmol CO_2 m^{-2} s^{-1})	Missing Data from RE (%)
Spring	1.81±1.24	NaN	100%
Summer	5.56±1.20	9.48±1.74	41.30%
Autumn	3.42±1.80	5.02±2.21	14.29%
Total Measured Data	1070.62±2.17	906.19±3.04	63.29%

Year	2015		
Season	RE (µmol CO_2 m^{-2} s^{-1})	Rs Measured (µmol CO_2 m^{-2} s^{-1})	Missing Data from RE (%)
Spring	2.14±1.59	2.64±1.27	69.57%
Summer	6.69±1.21	6.08±1.30	4.35%
Autumn	3.71±1.62	3.36±1.12	6.59%
Total Measured Data	1237.87±2.51	894.61±1.90	44.93%

Year	2016		
Season	RE (µmol CO_2 m^{-2} s^{-1})	Rs Measured (µmol CO_2 m^{-2} s^{-1})	Missing Data from RE (%)
Spring	2.10±1.11	2.11±0.74	51.09%
Summer	5.94±1.80	4.96±1.4	0.00%
Autumn	4.18±1.89	4.68±1.29	29.67%
Total Measured Data	1214.86±2.37	850.55±1.79	44.93%

Year	2017		
Season	RE (µmol CO_2 m^{-2} s^{-1})	Rs Measured (µmol CO_2 m^{-2} s^{-1})	Missing Data from RE (%)
Spring	2.31±1.37	4.21±1.82	68.48%
Summer	6.65±1.34	7.57±1.33	0.00%
Autumn	3.94±1.80	5.39±1.74	29.67%
Total Measured Data	1270.04±2.49	1162.87±2.05	49.32%

Year	2018		
Season	RE ($\mu mol\ CO_2\ m^{-2}\ s^{-1}$)	Rs Measured ($\mu mol\ CO_2\ m^{-2}\ s^{-1}$)	Missing Data from RE (%)
Spring	1.85±1.28	3.99±1.89	58.70%
Summer	5.57±1.51	7.35±184	6.52%
Autumn	3.71±2.36	5.38±2.63	13.19%
Total Measured Data	1103.59±2.36	1208.94±2.53	44.38%

Table 2.7. Estimated ecosystem respiration (RE) by the Gaussian – Gamma model and NARX Neural Network.

Year	2014	2015	2016	2017	2018
Gaussian – Gamma	91.17	87.49	85.77	92.46	97.14
NARX neural network	32.77	63.98	65.56	80.49	82.85

a)

b)

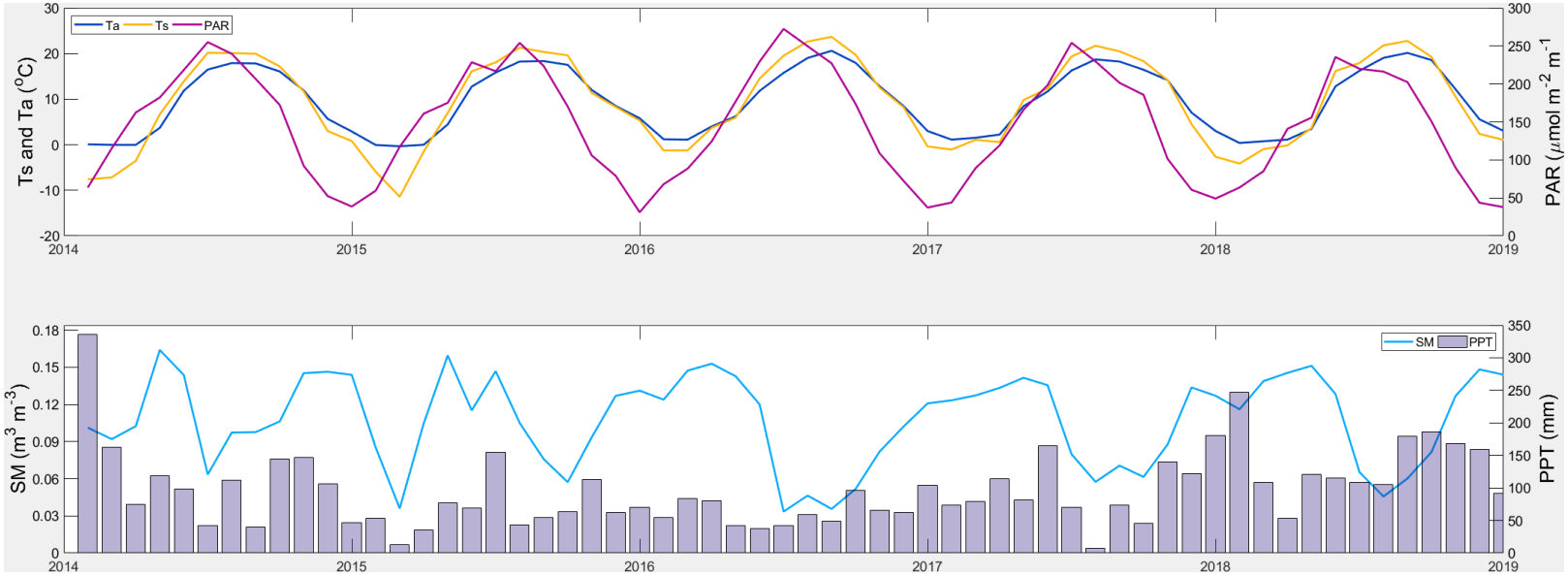

Figure 2.1. Climatic comparison from 2014 to 2018. (a) Monthly average air temperature (Ta), monthly average soil temperature (Ts), and photosynthetically active radiation (PAR); (b) monthly average soil moisture (SM) at 5 cm depth and cumulative monthly precipitation (PPT). Monthly averages are calculated from half-hourly measurements.

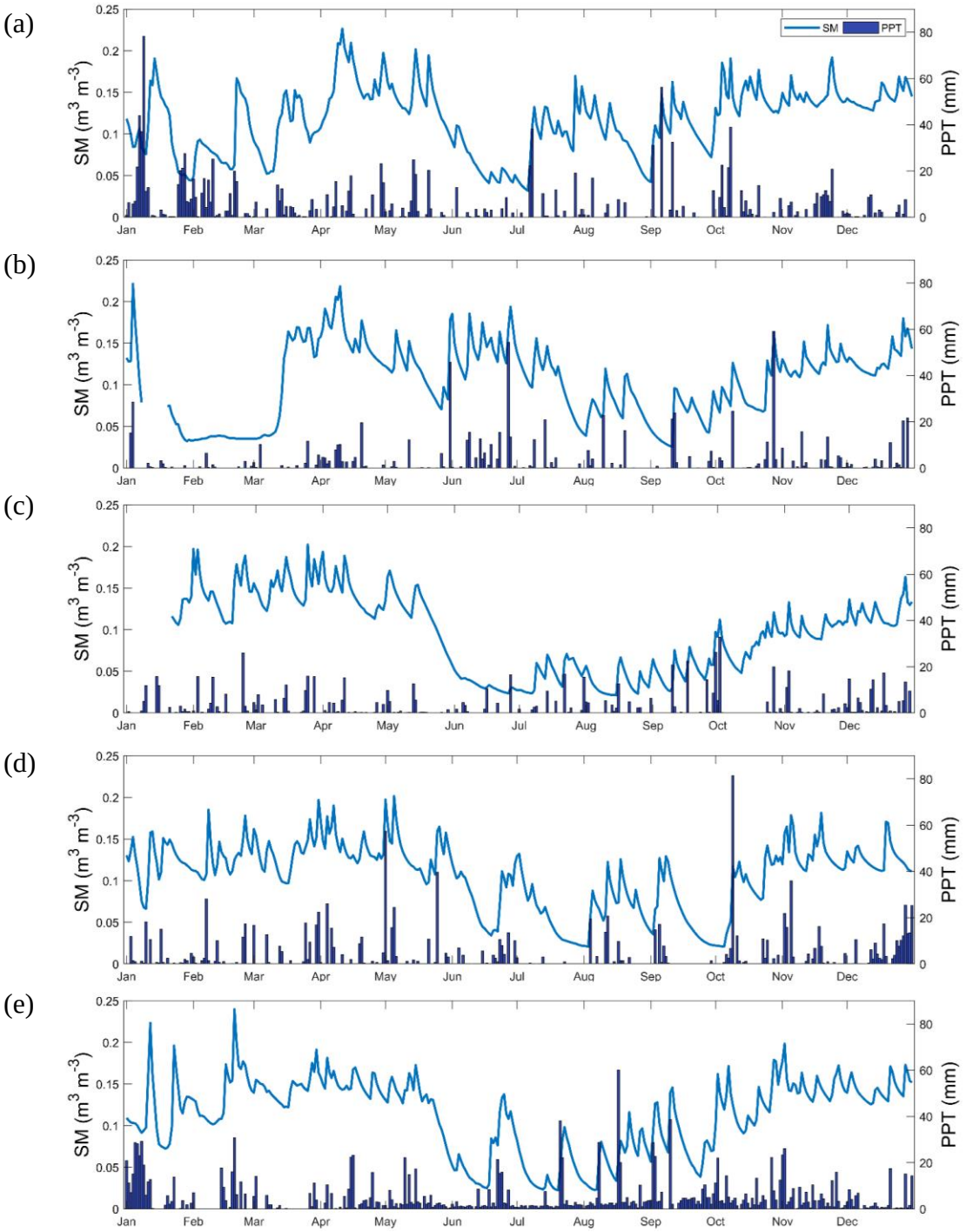

Figure 2.2. Comparison of daily mean soil moisture (SM) at 5 cm depth in m^3m^{-3} and cumulative daily average precipitation (PPT) in mm during (a) 2014, (b) 2015, (c) 2016, (d) 2017, and (e) 2018.

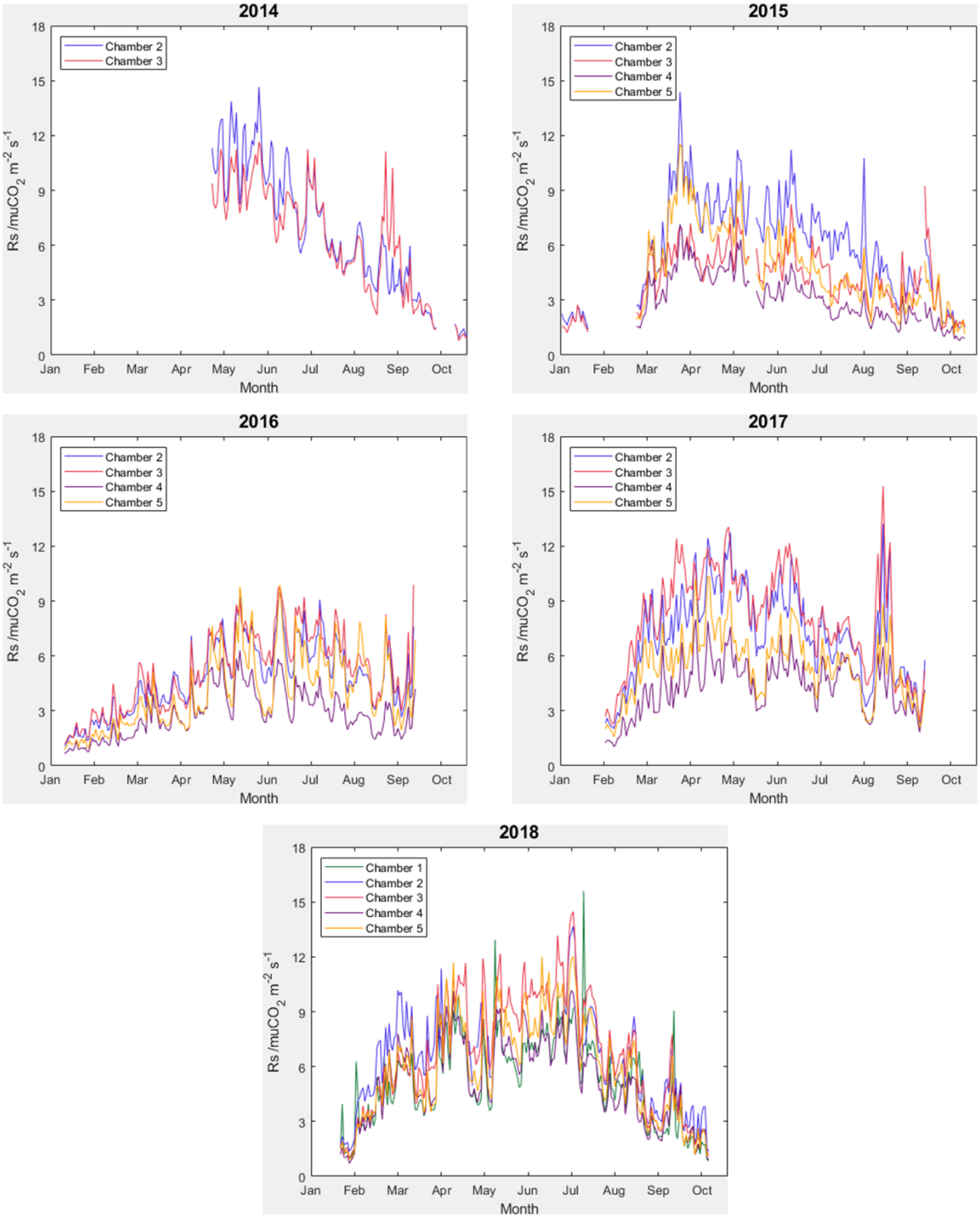

Figure 2.3. Daily average soil respiration (Rs) in µmol CO_2 m^{-2} s^{-1} measured by automated soil CO_2 chamber systems from 2014 to 2018.

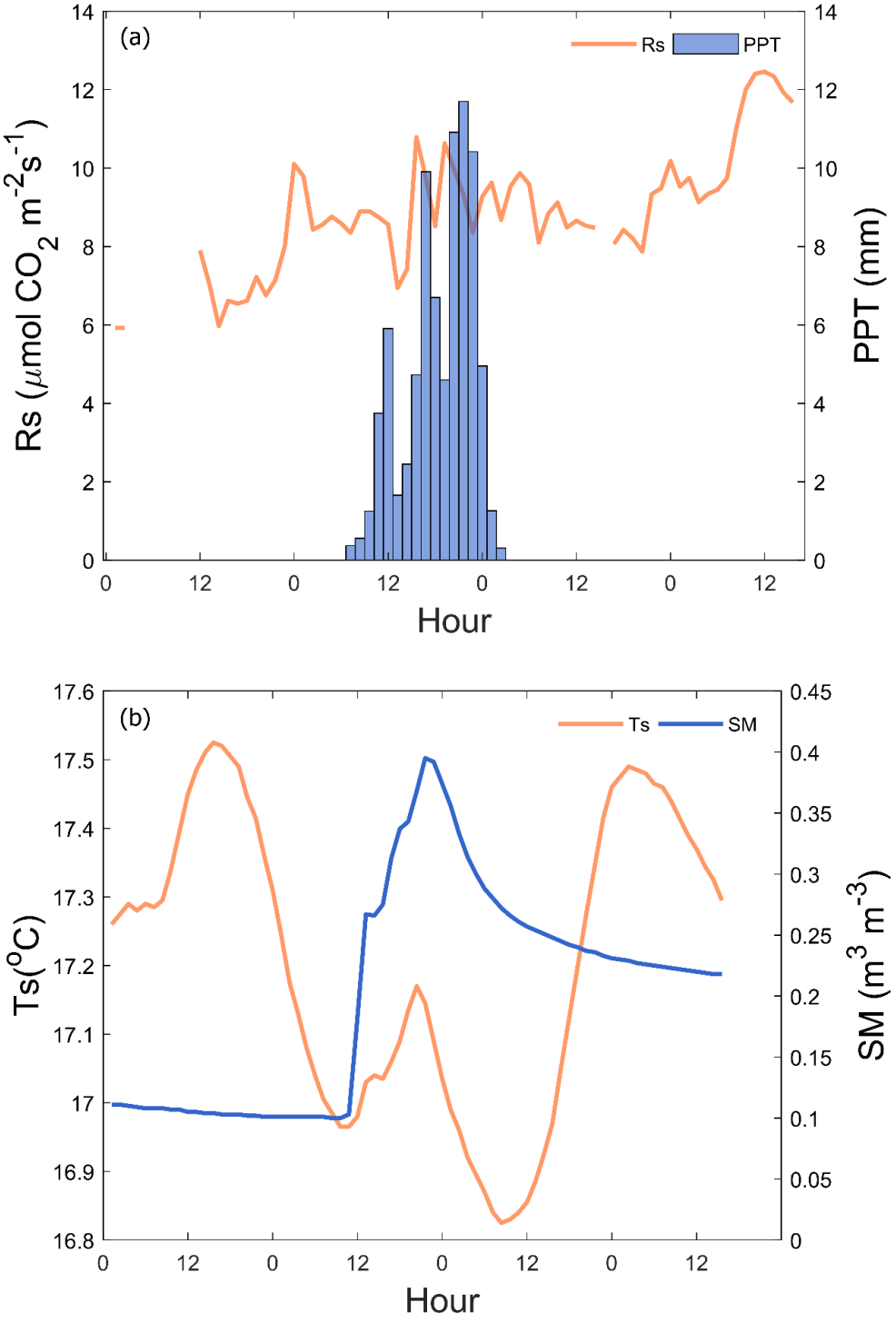

Figure 2.4. (a) Half hourly soil respiration (Rs) and precipitation (PPT) and (b) half hourly soil temperature (Ts) and soil moisture (SM) at 5 cm depth, before, during, and following a 11.7 mm precipitation event on October 9, 2017.

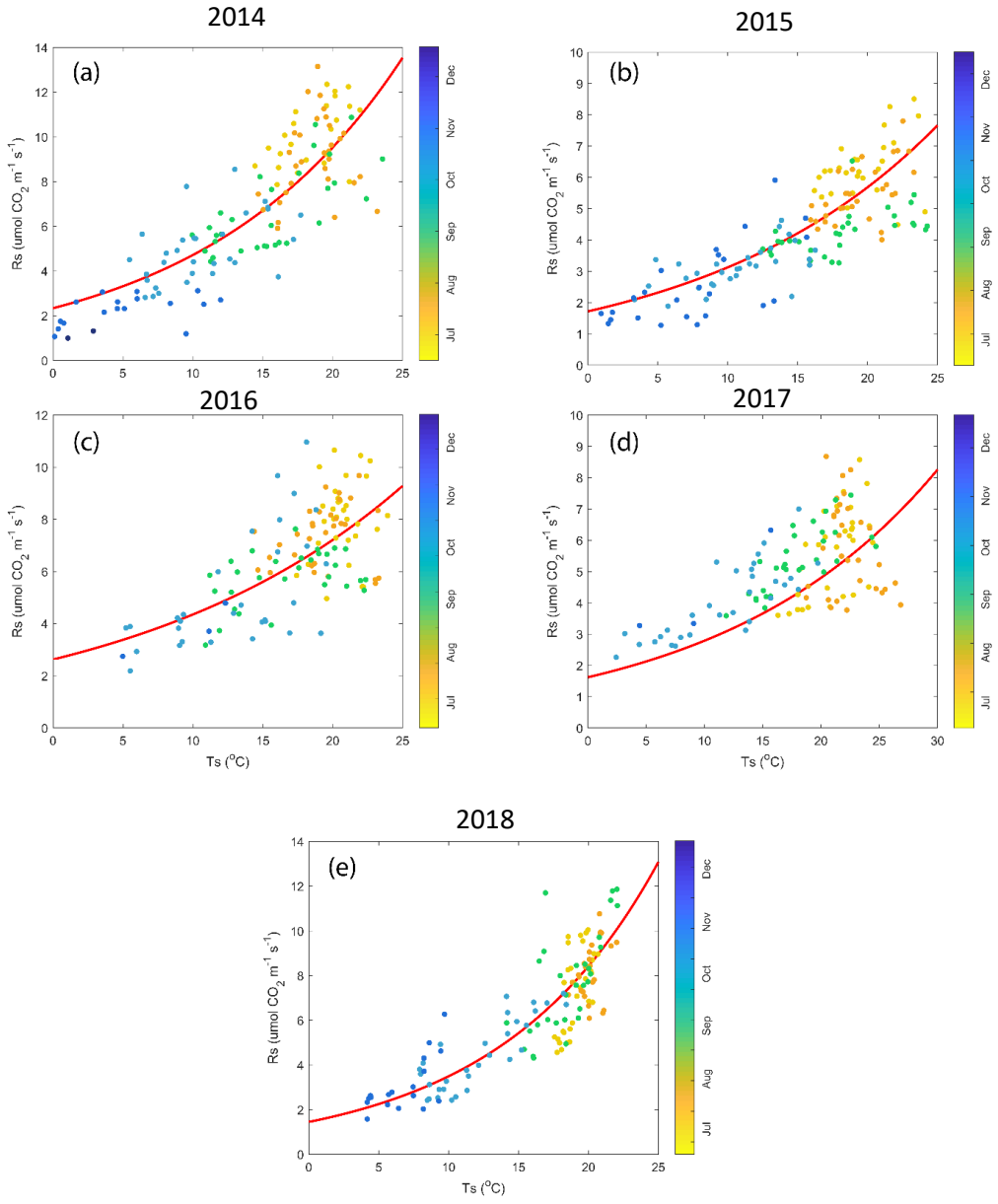

Figure 2.5. The empirical relationship between daily soil respiration (Rs) and soil temperature (Ts) measured with the automated chamber temperature probes at 5 cm depth during the 5-year (2014 to 2018) study period. Rs for each season is also shown (spring – blue dots, summer green dots, and fall – yellow dots). The fitted Rs Ts equations and R^2 are shown in Table 2.3a and 2.3b.

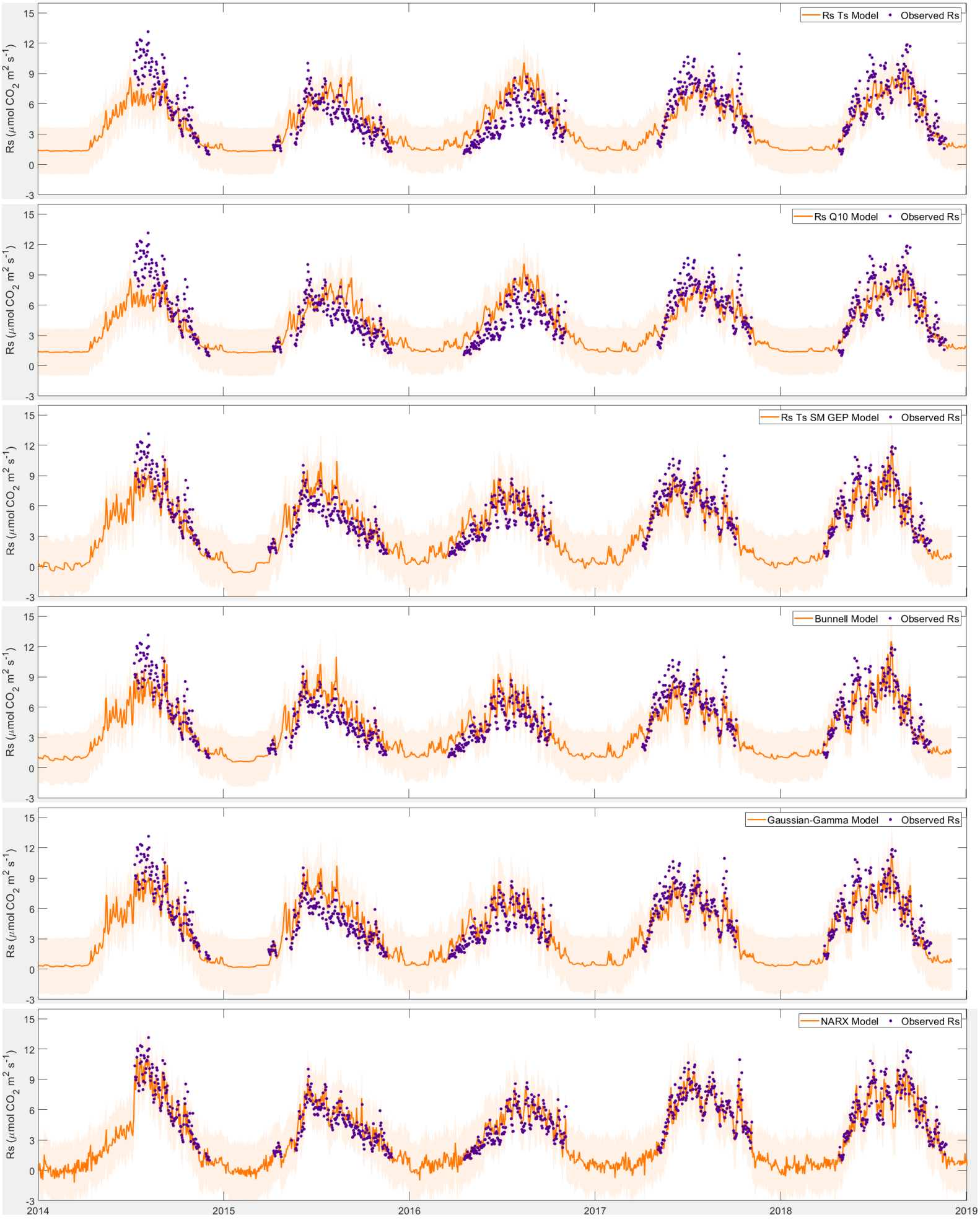

Figure 2.6. Annual observed Rs values compared with predicted values using seven models (Rs Ts, Rs Q10, Rs Ts SM, Rs Ts SM GEP, Bunnell Model, Gaussian – Gamma Model, and NARX Neural Network) from 2014 to 2018.

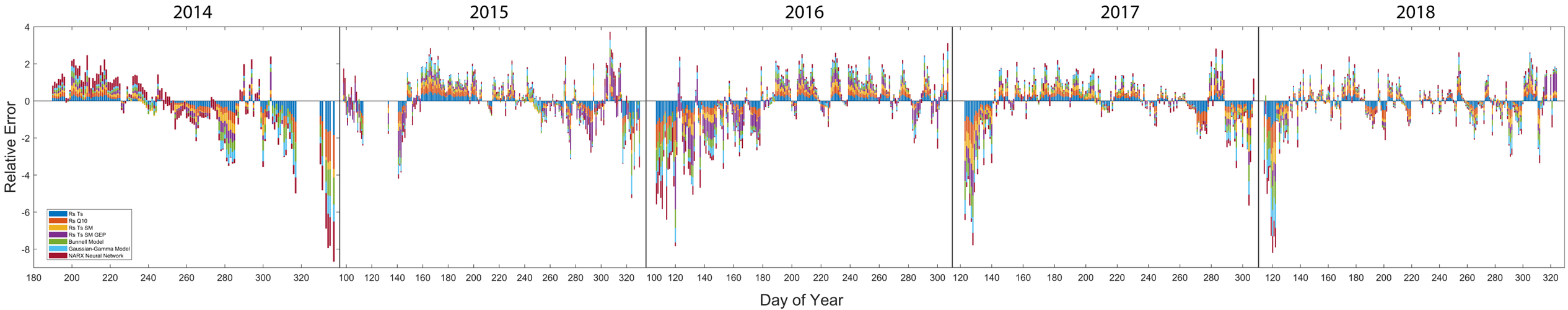

Figure 2.7. Stacked bar plot showing the daily relative error of each of the seven fitted models (Rs Ts, Rs Q_{10}, Rs Ts SM, Rs Ts SM GEP, Bunnell Model, Gaussian – Gamma model, and NARX Neural Network) over the 2014 to 2018 measurement period.

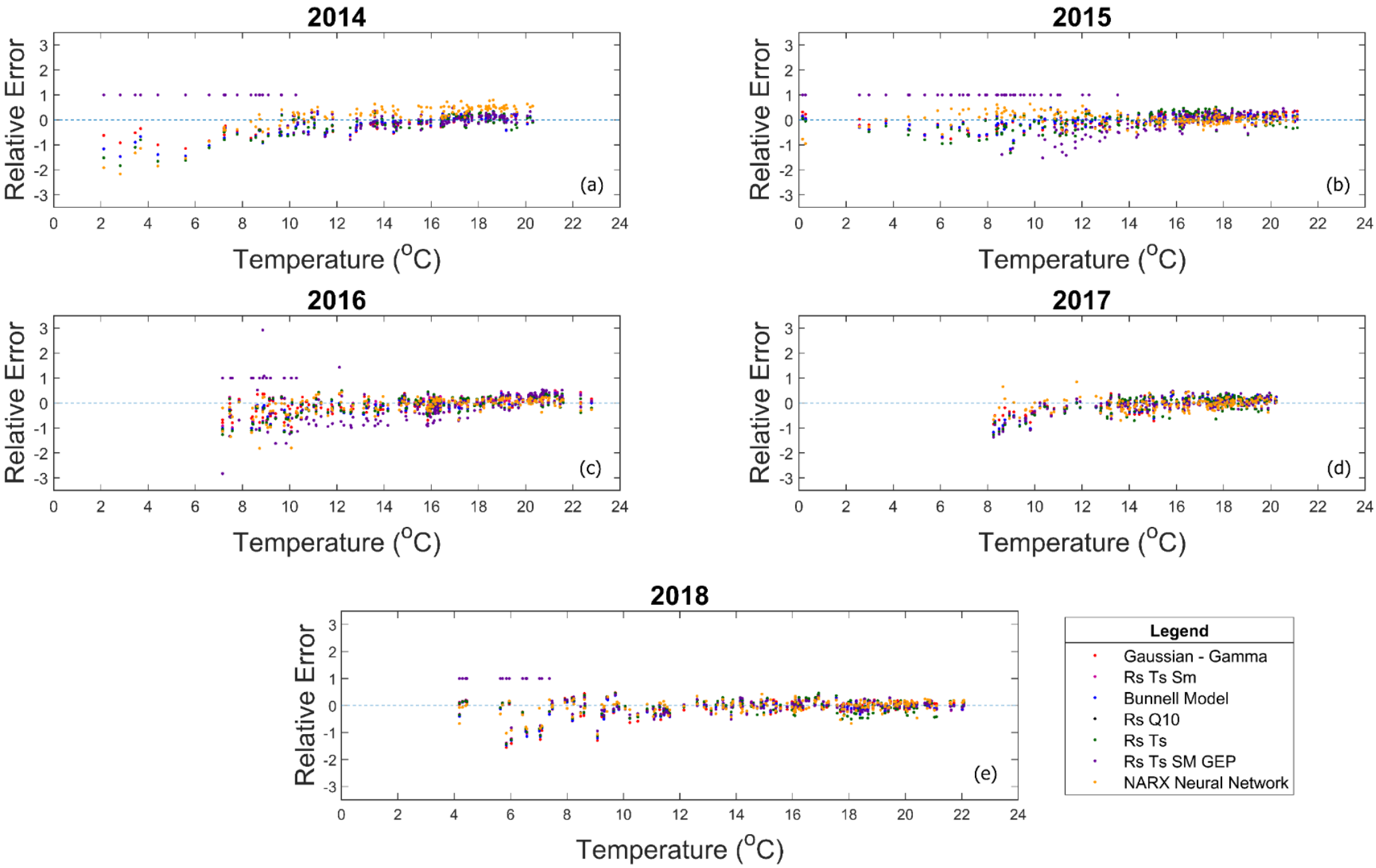

Figure 2.8. The daily relative error of each of the seven fitted models (Rs Ts, Rs Q_{10}, Rs Ts SM, Rs Ts SM GEP, Bunnell Model, Gaussian – Gamma model, and NARX Neural Network) plotted against temperature (°C) for the growing seasons from 2014 to 2018.

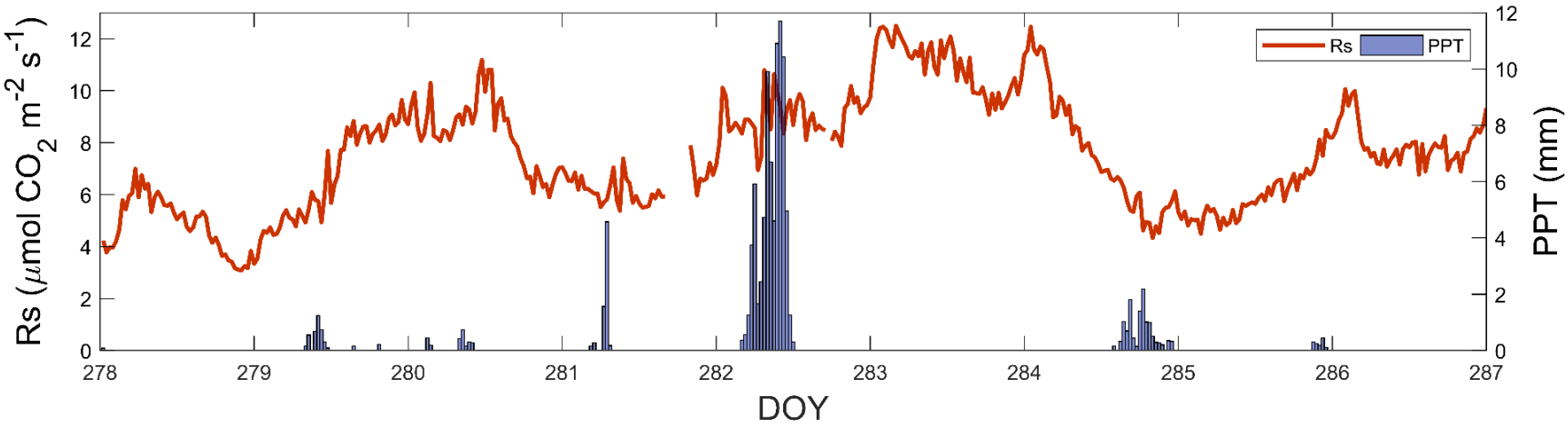

Figure 2.9. Precipitation event (mm) and Rs (µmol CO_2 m^{-2} s^{-1}) from October 5 to 13 in 2017 following a drought of 19 days.

Chapter 3:

Comparing temporal variability of soil CO_2 flux within a temperate coniferous and deciduous forest ecosystem

3.1 Abstract

The forest soil carbon pool accounts for 80% of the carbon within terrestrial ecosystems and contains three times as much carbon compared to the atmosphere (Davidson et al, 2006; Luo and Zhou, 2006). A small change in soil respiration (i.e. soil CO_2 efflux) may either mitigate or increase carbon fluxes into the atmosphere from this soil pool. In this study, temporal dynamics of soil respiration (Rs) and its key environmental controls such as soil temperature (Ts) and soil moisture (SM) was examined in two different species of temperate forests in the Great Lakes region in southern Canada. Automated soil chambers were utilized to continuously monitor soil respiration fluxes (Rs) in a 45-year-old temperate conifer forest (TP74), and a 90-year-old deciduous forest (TPD) in southern Ontario, Canada from 2017 to 2019. Coherence analysis of observed fluxes showed that prolonged periods of drought in the summer had reduced Rs. Large precipitation events and the resulting increase in soil moisture increased Rs. Periods of lag in coherence analysis was observed in the fall season which was primarily caused by soil moisture increases due to large precipitation events which are common in this region. The performance of multiple empirical Rs models (e.g. Rs Ts, Rs Ts SM, Rs Q10, Null Model, Ratkowsky, Stanford and Epstein, Myers, Bunnell, Lloyd and Taylor, Tuomi, and Gaussian – Gamma) showed that the Gaussian – Gamma model produced the best

results with the lowest corrected Akaike Information Criterion (AICc) values and fit with an R^2 of 0.83 and 0.76 for TP74 and TPD forests respectively. Rs was in higher coherence with temperature in the coniferous forest compared to the deciduous forest. Findings indicate that the fluxes of plantation forests may be less resilient to increasing temperatures.

3.2 Introduction

Soil respiration (Rs) is a major component of the carbon cycle, with climate change there are uncertainties that can be caused with extreme climate events. About half the terrestrial carbon sink is located within forests with most carbon residing within forest soils (Canadell et al, 2007; Kinderman et al, 2008). The forest soil carbon pool consists of 691 pentagrams (Pg) in plant biomass and up to 968 Pg in soils which is about 3 times larger than that of the atmosphere (817 Pg) (Lorenz and Lal 2010). Understanding how Rs responds to climate change and extreme weather events is particularly important in southern Canadian forests because most of forests in the region are afforested on plantation stands. Shifts in temperature and soil moisture caused by climate change can negatively affect these plantation stands causing release of Rs. With improper management such as clear cutting, these forests can become carbon sources instead of carbon sinks.

Forest species, canopy cover and structure, age, and soil characteristics can affect Rs. Many temperate coniferous forests, in particular white pine, specialize in growing in nutrient limited soils and can retain their needles for multiple years (Burgess-Conforti et al, 2019). Studies have also shown that higher soil pH from

the needles contributed to overall low Rs (Alban 1982; Binkley and Valentine 1991). Temperate deciduous forests typically drop their leaves in the fall (senescence) and regrow them in the spring. Leaf composition of these broad leaves contain more nutrients than coniferous foliage leading to overall higher Rs (Hanson and Wullschleger, 2003). Canopy cover also affects Rs by affecting the amount of sunlight able to reach the soil and shaded plots have significantly reduced Rs rates in response to decreased Ts (Hartley et al, 2007; Saiz et al, 2006). It is important to understand the differences in Rs dynamics and its controls in different species and characteristic temperate forests in order to explore their responses and long – term survival in the face of climate change.

The main objectives of this study are to: (1) compare temporal dynamics of Rs in a temperate conifer and deciduous forest growing in similar environmental conditions in the Great Lakes region from 2017 to 2019 (2) determine main controlling factors on Rs and how they might differ in these two stands and (3) examine how Rs models may help in simulating Rs and quantify the contribution of major controls and associated uncertainties. This study will help improve our understanding of Rs processes in different temperate forests in Eastern North America.

3.3 Methods

3.3.1 Study Site

The two sites used in this study were a unevenly aged (70 – 110 years old) naturally grown but managed deciduous forest (TPD, 42°38’7.18’’N, 80°33’27.83’W) and a

46-year-old coniferous forest afforested in 1974 (TP74, 42°42’24.52’’N, 80°20’53.93’’W). These forest sites are part of the Global Water Future (GWF) Program’s Turkey Point Observatory and has been associated with AmeriFlux and global Fluxnet initiatives, where they are also known as CA-TPD (Arain, 2012) and CA-TP74 (Arain, 2002).

TPD is dominated by White Oak (Quercus Alba) with scattered native Carolinian species such as Sugar Maple (Acer Saccharum), Red Maple (Acer Rubrum), American Beech (Fagus Grandifolia), Black and Red Oak (Quercus Velutina, Quercus Rubra), and White Ash (Fraxinus Americana). Eastern White Pine (Pinus Strobus) and Red Pine (Pinus Resinosa) compose 5% of the canopy. Average tree height is 25.7 cm with a stand density of 504 ± 18 trees per hectare. Average tree diameter at breast height is 22.3 cm. The understory species include young deciduous trees as well as Canadian mayflower (Maianthemum canadense), putty root (Aplectrum hymale), yellow mandarin (Disporum lanuginosum), red trillium (Trillium erectum), and horsetail (Equistum). Part of this land was on abandoned agricultural land that was previously used for agriculture (Richart and Hewitt, 2008). Previous management practices occurred in 1984 and 1986 that included the removal of 440 and 39.97 m^3 of wood respectively. Harvesting of various pine and dead oak occurred from 1989 to 1994 (Long Point Region Conservation Authority records; Beamesderfer et al, 2020). No management activity has occurred after 1994. Soil layers of consists of over 90% sand and is well drained with low moisture

holding capacity (0.10 cm/cm^3) with less than 2% organic matter. Further details are given in Beamesderfer et al, (2020).

TP74 is a closed canopy forest which was planted in a previously cleared oak savannah land to stabilize local soils. The dominant species is Eastern White Pine (*Pinus Strobus*) with occasional Jack Pine (*Pinus Banksiana*) and Oak (*Quercus Velutina*) trees. Average tree height is 13.5 m with a stand density of 1633 ± 166 trees per hectare. Average tree diameter at breast height is 18.3 cm. Due to high shading in this site, the understory is limited to a few bryophytes and grasses. Soils are 98% sand, 1% silt, and <1% clay and well drained (Peichl et al, 2010).

The climate in the region is humid continental with warm summers and cool winters. The 30-year (1981 to 2010) mean annual air temperature and total precipitation measured at a weather station at Delhi, Ontario (~25 km north of site) is 8.0°C and 997 mm, respectively. Precipitation is evenly distributed over the year, with 13% falling as snow (Environment and Climate Change Canada).

3.3.2 Soil Respiration Flux Measurements

Continuous half-hourly soil respiration (Rs) measurements were recorded using long term LI-COR LI-8100A chamber system. Two measurement chambers were deployed at TPD from July to December 2014 and extended to five in April 2015. TP74 measurements started on May 2017 with four chambers. Each chamber at the sites extended approximately 15 m from the central analyzer control unit and multiplexer and were equipped with a LI-8150-203 soil temperature probe and GS-

1 soil moisture probe. The probes were buried approximately 5 cm outside permanent collars installed in the ground. The collars are comprised of PVC pipe with an internal diameter of 20 cm, a height of 11.5 cm, and a thickness of 1 cm. Each collar is inserted approximately 7 – 8 cm into the soil surface with 3 cm remaining above. During the growing season, the measurement chamber was placed directly above the collars remaining open while not actively taking measurements. Any vegetation growth was removed from inside the collars to eliminate any interference from above-ground autotrophic respiration. The chambers were removed during the winter and stored for use the next growing season.

3.3.3 Data Analysis and Processing

Soil CO_2 emissions data were processed using Soil Flux Pro (4.2.1) from Li-COR Biosciences, Inc. by analyzing the exponential flux and iteration obtained every 3 to 4 min within the measurement period. An exponential curve was fitted and the resulting plot was fit with a non-linear regression equation that solved for C_∞, t_0, and a where C_o is the starting measured CO_2 concentration. The CO_2 flux based on the slope of the regression equation was reported as the exponential flux.

$$C(t) = C_\infty + (C_0 - C_\infty)e^{-a(t-t_0)} \quad (1)$$

Measurements that reported a higher exponential iteration (>10) were processed further by changing the start time affecting the overall t value until the exponential

iteration is less than 10. Measurements from one chamber was removed from 2014 to 2017 due to a wasp nest causing and unusual increase in CO_2 emissions in TPD.

Wavelet coherence analysis can be used for real-time analysis by providing multiple resolutions to analyze complex data (Oh et al, 2019). A wavelet is a mathematical function used to divide continuous data into different scales (Grinsted et al, 2004). In this analysis, a single wavelet is created, dilated or compressed, then shifted along a time scale axis to create multiple smaller wavelets. The small wavelets are expressed with two parameters: scale (s) and time position (n). A larger scale allows more detail to be captured with a wavelet and larger sections of the time series can be analyzed for low-frequency events. A smaller scale captures lower details and can detect low period (high-frequency) events. When a signal wavelet is multiplied by these smaller wavelets, a coefficient is obtained for that frequency. A larger coefficient means that the signal is similar to the wavelet and vice versa. This was repeated for all the smaller wavelets to obtain a set of coefficients or a wavelet transform (Jevrejeva et al, 2003).

Wavelet transforms are separated into continuous or discrete groups (Yates et al, 2006). A discrete wavelet transform restricts the number of dilations and translations so that the number of transforms is the same as the number of samples within the input time series. A continuous wavelet transform allows overlapping of one small wavelet with another so that the similarity between signals can be analyzed (Yates et al, 2006). The equation for the continuous or cross wavelet transform $W_n^X(s)$ is:

$$W_n^X(s) = \sqrt{\frac{\delta t}{S}} \sum_{n'=1}^{N} x_{n'} \psi_0 \left[(n' - n) \frac{\delta t}{s} \right] \quad (2)$$

where s is the scale on a discrete time series ($x_{n'}$) of length N with uniform steps δt and the scaled and translated wavelet function ψ_0 (Grinsted et al, 2004).

The models used in this study are the Rs Ts model (Van't Hoff, 1884), Rs Q_{10} (Yuste et al, 2005), Rs Ts SM (Khomik et al, 2009), Null, Ratkowsky (1982), Stanford and Epstein (1974), Myers (1982), Bunnell (1977), Lloyd and Taylor (1994), Tuomi (2008), and the Gaussian – Gamma (Khomik et al, 2010). Model equations are shown Table 3.1.

For small sample sizes, the Akaike Information Criterion is corrected so that a penalty is assigned to the number of predicted variables in a model such that there is not a bias towards more complex models (Hurvich and Tsai, 1989; Liu et al, 2018). Here AICc was used as a method of comparing the differences between TP74 and TPD from model predictions. The Akaike Information Corrected Criterion (AICc) equation is defined as:

$$AICc = 2k - 2lin\left(\sum_{i=1}^{n} \frac{(o_i - p_i)^2}{n}\right) + \frac{2k^2 + 2k}{n - k - 1} \quad (3)$$

where k is the number of parameters within an equation, n is the sample size, o is the observed values, and p is predicted values.

3.3.4 Dry and Wet Periods

Throughout the world there is no universally accepted definition of drought or excessive precipitation because of differing sites and climate conditions. Based on historical site analysis, precipitation in both sites are evenly distributed throughout the year (Beamesderfer et al, 2020; Barr et al. 2013). Drought periods are related to deficits in precipitation which impose plant stress due to decreased SM (Wolf et al. 2013). To assess dry and wet periods throughout the year, the relative extractable water (REW) was utilized (Black, 1979; Breda et al. 1995). REW is the amount of SM available for plant use, it relates to the pores within the soils and suction that plants utilize to extract water from the soil. As water is depleted from larger pores, more suction force is required. When REW drops below 0.4, large pores are considered empty and water is only contained in micropores which require more suction force causing both gross primary productivity and transpiration to decrease in response to stomatic closure (Ciais et al. 2005; Grainer et al. 1999; Reichstein et al. 2003). REW values above 0.72 were categorized as wet periods. REW is calculated as:

$$REW = \frac{\theta - \theta_{wp}}{\theta_{fc} - \theta_{wp}}$$

Where Θ is the actual soil water content for the root zone from 0 – 20 cm. Θ_{fc} is the soil water content at field capacity and is estimated from periods when soil water content was at its maximum daily mean value after the remove of freely drained water. Θ_{fp} is the soil water content at wilting point and is estimated from the

minimum value observed during a natural drought (McKay et al. 2012). The wilting point and field capacity values were estimated from a long – term soil moisture study performed by Peichl et al. (2010) and are 0.01 – 0.04 and 0.16 respectively. The lower end of the wilting point is utilized since in this study, well – drained sandy soils the wilting point can reach soil hydrophobic values (McKay et al. 2012). For the purpose of this study, Ts and SM was utilized from a nearby pit buried 5 cm below the surface near the chambers. Pit data was selected since it has undergone validation, acclimation to the site over multiple years, is measured throughout the year, and is shown to be similar to chamber data.

3.4 Results

3.4.1 Observed Rs Fluxes

Observed daily values of Rs, Ts, and SM from 2017 to 2019 for both TP74 and TPD are shown in Figure 3.1 and Figure 3.2. Rs was found to follow closely to that of Ts in TPD and displayed similar patterns in TP74. SM was also found to increase after precipitation events in both sites. TPD displayed greater fluctuations compared to TP74 during the spring and summer. Data coverage for TP74 is 44.38%, 53.15%, and 56.71% from 2017 to 2019. Coverage for TPD is 50.68%, 55.62%, and 62.47% from 2017 to 2019.

In 2017, TP74 and TPD showed differences in dry and wet periods during the spring, with a total of 18 wet days at TP74 as compared to a total of 20 wet days at TPD (Figure 3.1a and 3.1b). Both sites experienced four extended dry periods in the

summer and fall comprising a total of 82 and 74 days for TP74 and TPD respectively. TPD received additional wet periods (20 days) in the summer and fall. Observed daily SM and PPT values are shown in Figure 3.2a and 3.2b. Overall, SM values at 5 cm depth at TP74 showed much lower amplitudes as compared to TPD. Accordingly, Rs at TP74 also did not show a large increase in response to rainfall events such as an 81.44 mm event on October 9th at both sites. Seasonal dynamics between both sites showed that TPD had more wet periods (40 vs 18 days) than TP74. Observations for TPD showed sporadic wet periods occurring throughout the year with a 11-day wet period occurring in the fall.

In 2018, there were 12 wet (high SM) days in the spring at TP74 and 31 days at TPD. Observed SM and PPT values for 2018 showed a 60 mm event on August 17th that caused SM at TP74 to increase by 0.03 m^3 m^{-3} over three days and 0.05 m^3 m^{-3} at TPD at the same time period. A later precipitation event of 40 mm caused an increase of 0.02 m^3 m^{-3} in TP74 and 0.08 m^3 m^{-3} at TPD over three days as well. The first PPT event caused an increase of 2.45 µmol CO_2 m^{-2} s^{-1} and 2.08 µmol CO_2 m^{-2} s^{-1} in Rs at TP74 and TPD after this event. Dry events at both sites occurred in the summer (24 and 72 days for TP74 and TPD respectively; Figure 3.1c and 3.1d). Ts at TP74 remained relatively similar at 24.30ºC, but TPD experienced a decline from 20.03ºC to 18.85ºC. The second PPT event caused similar results. Rs increased by 1.32 µmol CO_2 m^{-2} s^{-1} at TP74 and 1.08 µmol CO_2 m^{-2} s^{-1} at TPD after this event. Ts at both sites increased similarly by 0.36ºC (Figure 3.2c and 3.2d). Seasonal dynamics for both sites experienced long wet periods in the fall (33 and

43 days). TPD received long dry periods (63 days) in the summer while TP74 received sparse (24 days) dry periods (Figure 3.3c and 3.3d).

In 2019, there were 54 wet days in the spring and summer for TP74 and 103 days at TPD. Dry periods occurred in the summer (22 and 24 days) and fall (4 and 31 days) for TP74 and TPD, respectively (Figure 3.1e and 3.1f). A 45 mm PPT event occurred on October 27th at both sites that caused SM to increase by 0.02 m^3 m^{-3} in TP74 and 0.06 m^3 m^{-3} in TPD within a day. Rs decreased at TP74 from 2.86 µmol CO_2 m^{-2} s^{-1} to 2.69 µmol CO_2 m^{-2} s^{-1}, while TPD experienced an increase from 3.07 µmol CO_2 m^{-2} s^{-1} to 4.52 µmol CO_2 m^{-2} s^{-1}. Ts at both sites increased by 2^{o}C and 0.78^{o}C at TP74 and TPD, respectively (Figure 3.2e and 3.2f). Overall, Rs in all years at TP74 is shown to be less than that of TPD. Similarly, Rs closely followed Ts for all years at both TP74 and TPD. Seasonal dynamics showed that TPD received a long continuous wet period in the spring followed with two dry periods in the fall. TP74 received a continuous wet period in the spring but sparse dry periods in the summer and fall (Figure 3.3e and 3.3f).

Coherence between Rs and Ts from 2017 to 2019 for TP74 and TPD sites are shown in Figure 3.3. Arrows within coherence figure panels indicate the phase and lag of both time series. Arrows pointing to the right indicate Rs and Ts are in phase with no lags. Left pointing arrows indicate anti-phase when Rs is increasing and Ts decreases. Arrows pointing up or down represents a lead of 90 degrees for Rs or Ts, respectively. Slanted arrows indicate lag where arrows point left to up or right to down show Rs is leading and arrows point left to down or right to up show Ts is

leading. Areas with high coherence are shown in yellow shading, while areas with low coherence are shown in blue. Coherence measurements outside the cone of influence where results are distorted is not considered.

Overall, in 2017, TP74 displayed high coherence between Rs and Ts from the 2 to 8-day scale (mid-August to September; Figure 3.3a). Arrows within the high coherence area primarily point to the bottom right indicating that Rs is leading in front of Ts. From the 0 to 4-day scale, arrows are shown pointing down in June indicating a lead of 90 degrees for Ts. Arrows from mid-August to October are shown to shift from pointing downward to slanted to the bottom right then back pointing downward indicating that the temperature sensitivity of Rs is affected in these months. TPD displayed high coherence from the 0 to 16-day scale from mid-June to October (Figure 3.3b). Arrows in the coherence area point right from mid-June to mid-July and in September at the 4 to 8-day scale. From the 0 to 4-day scale arrows primarily point right and shift to the bottom right in the beginning and end of August before shifting to pointing to the upper right.

In 2018, significant coherence between Rs and was observed in at TP74 from the 1 to 32-day scale (September to November; Figure 3.2c). Arrows within the high coherence area point to the bottom right in the beginning of August and October for ~8 days which show that Rs is leading in front of Ts. This occurs in the period between July and August as well. High coherence hotspots in TPD are shown from the end of May and the beginning of June for ~14 days. Downward arrows are shown in October for ~8 days and arrows that point right to up are shown as well

for ~20 days. From the 0 to 4-day scale arrows primarily point right but shift to bottom right pointing in September, October, and November in TP74. TPD displayed arrows that point to the bottom right in June and arrows that point left in August (anti-phase).

In 2019, high coherence between Rs and Ts was observed from the 0 to 16-day scale from May to June in TP74 (Figure 3.3e). Arrows within the coherence area primarily point to the right with a shift to the upper right in June. Coherence hotspots occur at the end of June and in July for ~5 and ~16 days. From the 0 to 4-day scale, arrows are shown pointing to the right before shifting to the upper right and back. TPD showed a significant coherence from the 0 to 16-day scale and at the 32-day scale (Figure 3.3f). Arrows primarily point right with slanted arrows (upper right) occurring in September at the 16-day scale and in June and September at the 32-day scale. At the 0 to 4-day scale, arrows point right at the end of May, June, September, and October.

Coherence between Rs and SM from 2017 to 2019 is shown in Figure 3.4. In 2017, there was little to no coherence between Rs and SM in TP74 while hotspots from the 4 to 8 days occurred in the spring and at the 16-day scale in the fall (Figure 3.4a and 3.4b). In 2018, in-phase coherence occurred at the 32-day scale from June to August for TP74 and for the entire year in TPD (Figure 3.4c and 3.4d). Numerous coherence hotspots occurred in the summer for TPD compared to TP74. In 2019, there was little coherence at TP74 except from the 0 to 6-day scale from May to

July (Figure 3.4e). Coherence in TPD was similar with a hotspot occurring at the 16-day scale from July to September (Figure 3.4f).

Ts and SM coherence from 2017 to 2019 is shown in Figure 3.5. In 2017, anti-phase coherence occurred from the 16 to 64-day scale for the entire year. Smaller, anti-phase hotspots occurred from the 4 to 16-day scale from August to October for TP74 (Figure 3.2a). TPD had one anti-coherence hotspot from June to July at the ~25-day scale and a hotspot from the 4 to 8-day scale in July (Figure 3.5b). In 2018, anti-phase occurred from August to September at the 64-day scale in TP74. A minor hotspot occurring from the 0 to 4-day scale occurs in late-July with arrows pointing left to up (Rs leading; Figure 3.5c). Minor hotspots occur similarly for TPD such as from June to July at the 16-day scale showing anti-phase (Figure 3.5d) and in August. In 2019, TP74 had multiple minor hotspots scattered throughout the summer with an anti-phase hotspot occurring at the 64-day scale in July and a hotspot with slanted arrows pointing to the bottom right (Rs leading) from August to September (Figure 3.5e). Minor and scattered hotspots occurred from July to October for TPD with primarily bottom-right slanted arrows (Rs leading) throughout the year (Figure 3.5f).

Volumetric water content or SM is shown in Figure 3.6. For all six years, TPD's SM is shown to be higher than TP74 in the spring and fall. TPD had higher SM in the summer in 2014, 2015, and 2019. Both sites recorded similar SM in 2016, 2017, and 2018. A comparison of SM between tower and chamber SM is shown for TPD

in 2018 (Figure 3.8). Linear regression shows that the slope and intercept closely match that of a 1:1 line.

3.4.2 Model Inter-Comparison

Eleven different Rs models were used to simulate soil CO_2 emissions at both sites and their ranking in terms of AICc values is shown in Tables 3.2 to 3.4. The Gaussian – Gamma model was the best predictor for TP74 and TPD with the exception of 2017. The Bunnell model performed well for TPD and poorly for TP74 in all years. The Rs Ts SM model ranked highly for both sites in 2018, but ranked poorly in 2017 and for TPD in 2019. The Rs Q10 model ranked poorly for all years except for TP74 in 2019. The Rs Ts model ranked highly for TP74 in 2017, but poorly for all other years. The Lloyd and Taylor model ranked highly for both sites in 2017 and 2018, but poorly for TP74 in 2019. The Stanford and Epstein model ranked poorly for 2018 and for TPD in 2019. The Ratkowsky model was rated in the middle and remained in similar rankings for all years. The Myers model ranked low and remained poorly for all years. The Tuomi model ranked low, but performed well at TP74 for 2017. The Null model performed poorly in 2018 and for TPD in 2019, but remained in the middle for 2017 and TP74 in 2019. In summary, Gaussian – Gamma model was quite robust in simulating Rs dynamics at both sites.

Linear regression analysis of simulated Rs with observed Rs was also performed from 2017 to 2019 for TP74 and TPD sites (Figure 3.7). Model results showed a

coefficient of determination (R^2) of 0.54 for 2017, 0.77 for 2018, and 0.59 for 2019. Model equations are displayed on the figure for each year.

3.5 Discussion

3.5.1 Observed Fluxes

Environmental factors affecting the soil carbon pool such as air temperature (Ta), Ts, precipitation (PPT), and SM exhibited strong seasonal controls within both conifer and deciduous forests. In both forests' Ts increased during the growing season, peaked during the summer, and decreased during the fall into the winter which is typical for forests located in the temperate regions (Wang et al, 2010; Davidson et al, 1998). The relationship between Rs and Ts is exhibited multiple times in literature (Davidson and Janssens, 2006; Lloyd & Taylor, 1994; Taylor et al, 2015; Shabaga et al, 2015). Sensitivity to temperature change in response to global climate change is one of the uncertainties in empirical Rs models (Jones et al, 2003). The Q_{10} value of a site indicates the temperature sensitivity of Rs, where a lower value represents low sensitivity while higher values indicate more (Meyer et al, 2003).

Annual Q10 values for TP74 and TPD are shown in Table 3.5. Values for TPD are comparable to literature in 2017 and 2018, but all values for TP74 are quite low compared to other studies with similar ecosystems (Raich and Schlesinger, 1992; Quan et al, 2004; Meyer et al. 2018). Multiple factors that may influence this such as substrate disturbance, site specificity, and climate (Davidson et al, 2006). Within literature, Rs is reported to be less sensitive to temperature with lower SM with

sensitivity increasing to a threshold with higher SM and decreasing afterwards (Yuste et al, 2007; Craine and Gelderman, 2011; Illeris et al, 2004; Jassal et al, 2008). However, analysis with wavelet coherence shows a high coherence occurring from August 21, 2018 to the end of the growing season. This is probably due to the effects of the three drought events causing the annual Q_{10} and to decrease overall (Q_{10} outside coherence = 2.02). As SM increased due to precipitation events, a higher threshold was reached causing a higher Q_{10} value (Q_{10} = 2.29) that is more comparable with literature (Table 3.6c). This is reflected within the coherence chart with Ta as well, during the 3 drought periods there was no observed coherence whereas afterwards following a high PPT event (60.13 mm), there was coherence until the rest of the growing season (Figure 3.4). The Q_{10} value in 2019 for TPD is higher compared to literature indicating a greater sensitivity to Ts. This is probably the result of dry periods occurring in the summer (July, August, September). Analysis with the coherence chart reinforces this where both Rs and Ts are in phase. Temperature sensitivity is also represented by the 0 to 4-day scale on coherence graphs. In 2018, temperature sensitivity from the 0 to 4-day scale is abnormal for TP74 compared to TPD. Dry/wet period analysis shows a high coherence occurring from September to the November indicating temperature sensitivity not that does not coincide with dry periods. Analysis of Rs showed a similar trend early within the growing season. However, as the year progressed, there were more fluctuations from Rs throughout the summer that were not consistent with observed Ts values notably in TPD. This can be accounted by other environmental controls such as SM

and in many studies in literature (Davidson et al, 1998; Xu and Qi, 2001; Pumpanen et al, 2008; Van der Molen et al, 2011). High SM content can limit the diffusion of oxygen into the soil reducing Rs (Alexander, 1977). As soils dry due to higher temperatures, Rs decreases from microbial death. Following rewetting events there is an increase in Rs (Orchard and Cook, 1983). This process is primarily exhibited within between July and August for both sites. During the second dry period, Rs decreased to 1.93 and 4.98 µmol CO_2 m^{-2} s^{-1}, following a PPT event of 7.54 mm, Rs rapidly increased to 5.94 and 9.80 µmol CO_2 m^{-2} s^{-1} within 3 days for TP74 and TPD respectively. Afterwards, there was a sharp decline back to previous Rs levels in 4 days. A second, much greater PPT event occurred (38.02 mm) at the end of the second dry period causing Rs increase back to levels from the first PPT event for TPD. There was a second increase following a PPT event of 22.2 mm at TP74.

Temperature sensitivity in 2019 at TP74 in the 0 to 4-day scale functions similarly to that of 2018, where Rs is shown to be sensitive to temperature in a wet period instead of a dry period. This could be the result of environmental factors from the previous year influencing Rs and its sensitivity to Ts. TPD's temperature sensitivity in the 0 to 4-day scale is shown to occur in May, September, and October. Sensitivity in September and October coincides with dry periods but May does not. This could be the result of understory vegetation development causing an increase in heterotrophic respiration coinciding with increases in Ts. In TP74, because of the presence of a closed canopy and lack of nutrition, the understory consists of lichen and small shrubs causing low Rs. TPD's rich understory consists of many

deciduous woody species which facilitate Rs increase as the year progresses These impacts would be indirect through more root biomass in the soil because any vegetation growing inside the chamber colors was removed. These findings are similar a study produced by Yuste et al (2014) which suggests that Q_{10} is influenced by seasonal plant growth in both a coniferous and deciduous forest.

SM comparison for both sites showed that TPD consistently measured higher SM in the spring and winter. This is probably due to canopy and understory differences between both sites. During the summer, both sites' vegetation is well developed and are show similar coverage affecting the amount of precipitation that percolates within the soil. During the spring and winter, the deciduous understory and canopy in TPD are greatly reduced during senescence in the fall. This causes TPD to become an open canopy instead of a closed canopy which allows more precipitation to permeate the soil.

3.5.2 Chamber Uncertainty

Automatic soil chambers can have both uncertainty and variability associated with Rs measurements. One of the downsides of automated chambers is poor spatial resolution causing higher variability (Khomik, 2014; Wei-Yu et al. 2015). In a comprehensive study performed by Khomik, 2014, 50 collars were utilized in a square grid design and were installed along a 2 m transect at a 60-year-old coniferous stand located 20 km away from both sites. It was determined that chambers located near tree trunks (~50 cm) consistently produced higher Rs compared to the rest of the chambers. Furthermore, measurements performed ~2.5

m from tree trunks reported increased Rs which was most likely caused due to increased density of fine roots. Several other factors have also been identified to contribute to variability in the study such as tree root density, litter thickness, and availability of soil nutrients. Uncertainty for automatic chambers can be caused by microclimates, differences in gas pressures inside and outside the bell, site carbon capacity and specificity (Livingston and Hutchinson, 1995; Welles et al. 2001; Hou et al. 2013)

The standard deviation for both sites' mean chamber Rs is 2.51 and 1.62 for TPD and TP74, respectively. Differences between both sites can be caused by understory, shade, and chamber locations. TPD's understory is dominated by deciduous shrubs while TP74 has little understory except for moss and lichen. Chambers within TP74 are located close to plantation tree trunks that receive occasional lighting while TPD chambers are located at the bottom of a slope surrounded by shrubs inhibiting the amount of sunlight received daily.

3.5.3 Wavelet Coherence

Wavelet coherence performed on accumulated long-term Rs measurements can provide opportunities to analyze time lags and the effects of Ts and SM spatially and temporally (Vargas et al, 2010; Oh et al, 2019). There are a few wavelet coherence studies done between Rs, Ts, and SM. Vargas et al (2010) examined a mixed conifer-oak forest and reported high correlation for Rs and SM between 2 and 32 days with high correlation between summer rainfalls. For TP74, all years showed non-similar results to Vargas et al (2010) mainly because the soil structure

within both sites are formed from Glaciolacustrine sand deposits (Brunisolic Gray Brown Luvisol). Savage et al (2009) reported a significant coherence between Rs and Ts within a 70-year-old deciduous forest at the diel frequency.

Coherence in 2017 between Rs and Ts occurred primarily during fall for TP74 and summer to fall in TPD from the 0 to 8-day period. This shows that Rs in TPD is sensitive to Ts in the summer and that Rs in both sites are sensitive to Ts in the fall during this period. However, further analysis of SM at a depth of 5 cm shows that SM did not increase significantly due to large precipitation events at TP74 site. This is probably the result of the soil type causing PPT to drain rapidly such that the moisture probe could not maintain contact or the result of litterfall obstructing the sensor. Deeper SM measurements (20 cm) show higher response to PPT. In both plots at the 16-day period, coherence is shown to lag which indicates SM influence on Rs. In 2018, there were three abnormally long dry periods throughout the growing season. Coherence for Rs and SM in TPD showed a high phase for 32 days for the whole measurement period. TP74 displayed similar results between June and August, but disappeared during the same period for Rs and Ts coherence. This is probably due to the differences in canopy between both sites affecting the amount of PPT that the soil receives.

Coherence within TPD in 2019 showed a similar result from that of Savage et al (2009) at the diel frequency in spring but deviated to the 5 to 16-day scale in the summer. This is probably due to the differences in precipitation causing dry periods to occur which caused a close relationship between Rs and Ts. Longer impacts of

Ts on Rs is also reflected within longer periods of coherence such as from the 32 scale for the entire year which could be caused by diminished PPT. Coherence analysis for Ts and SM across all years for both sites showed little to no correlation between Ts and SM except for 2017 in TP74 where a high anti-phase coherence was observed. This is to be expected since higher temperatures result in greater evapotranspiration and thus diminished SM.

3.5.4 Rs Modelling Analysis

To further analyze the relationship between Rs, Ts, and SM various empirical models were compared and the AICc calculated. In 2017, models that utilized Ts produced a higher fit than those SM models for TP74 (Table 3.2). In TPD the Bunnell model produced the highest fit and the Gaussian – Gamma model had a worse fit. The differences between these years can be explained by the reaction of the SM sensor within both sites. During the year, the SM at 5 cm did not respond to high PPT events at TP74 compared to TPD. This phenomenon throughout the year caused models that primarily utilized Ts to predict Rs to become more accurate at Rs prediction compared to models that utilized SM. TPD's Bunnell model ranked higher than the rest of the models is primarily because the SM exerted more influence on Rs while Ts was not a dominate factor. This is explained by the large differences between Bunnell model, a model that favors SM but incorporates Ts, and other models that rely heavily on Ts or SM.

In 2018, models that utilized primarily Ts were able to produce a higher fit than those that utilized only SM which further emphasizes the importance of Ts on Rs

at TP74 (Table 3.3). Similarly, models that incorporated primarily SM produced a higher fit than those that used Ts in TPD. Models that had both Ts and SM were higher than those that utilized only a single variable in TPD suggesting that throughout the year multiple influences of these variables. As expected, TP74 models produced similar results for Rs Ts SM and the Gaussian – Gamma model similarly to previous studies (Vargas and Allen, 2008; Khomik et al, 2009; Lellei – Kovács et al, 2011). However, the Bunnell model produced a significant difference (184.81 vs 23.21 for TP74 and TPD respectively). This is probably due to how the Bunnell model is structured leaning heavily on the influence of SM on Rs.

In 2019, much like the previous year, models that utilized primarily Ts displayed a lower difference and AICc compared to models that utilized SM in TP74. Models for TPD increased dramatically to models utilizing SM (Table 3.4). This change is also reflected within the coherence plot for this year where Ts is shown to have a greater impact on Rs from July to October. Coherence changes can be explained by the dry periods present within the year which coincide with increases in Ts and consequently Rs. For all years, the Gaussian – Gamma model is shown to closely model Rs for both sites following dry/wet years.

Linear regression of Rs between TP74 and TPD for all three years showed a consistent relationship between TP74 and TPD in 2017. This shows that Rs displays a similar pattern for both sites which is expected since AICc model ranking are similar showing comparable reactions to changes in environmental variables. In 2018, equation analysis shows that at lower Rs (<8 μmol CO_2 m^{-3} s^{-2}), TP74 is more

affected and at higher Rs, TPD is more affected. This can be explained by Rs responses to extreme weather events during this year. In dry periods in the summer, Rs lowers dramatically causing fluctuations due to increases in PPT and SM. In a study performed by Carlyle and Bathan (1988) where Rs is shown to be more sensitive at higher Ts (10 – 20^{o}C) and SM. Throughout the year, there are consistent PPT events which caused SM to periodically increase. Since TP74 has a higher Ts than TPD (mean of 16.88^{o}C vs 14.69^{o}C), and Rs values for TP74 does not increase beyond 8 µmol CO_2 m^{-3} s^{-2}, This can explain why TP74 is seen to have more extreme fluctuations and more sensitivity to changes in Ts. TPD also had more fluctuations in Rs at higher measurements due to differences in stand type and increases in SM in the summer which can explain why TPD is more affected by Rs at higher levels (>8 µmol CO_2 m^{-3} s^{-2}). In 2019, equation analysis shows the opposite from that of 2018, where at lower Rs (~3.2 µmol CO_2 m^{-3} s^{-2}) TPD is more affected and at higher Rs, TP74 is affected. This can be explained by differences in Rs, TPD has consistently high Rs due to accelerated rates of decomposition and greater fluctuations of SM in the summer where Rs is the largest. Rs variations for TP74 are consistent in the spring and until July for TP74 due to differences in canopy and consistent Ts.

With extreme weather patterns such as in 2018, TP74's soil carbon pool is influenced more by temperature than with SM and that TPD's soil carbon pool seems more resilient. Carbon fluxes from soils are closely related to plant growth (Raich and Schlesinger, 1992). With addition of organic carbon from litterfall, the

rate of Rs increases with largest increases observed underground (Hogberg and Ekblad, 1996; Rogers et al, 1994). Additionally, about 30 – 50% of Rs is derived from root respiration and the remainder from microorganisms (Bowden et al, 1993; Andrews et al, 1999). Based on a study in North Carolina in a 15-year-old loblolly pine forest stand there was an increase in pore space and Rs of ~30% following elevated CO_2 for three years (Schlesinger and Andrews, 2000). Plant growth at higher CO_2 and temperature levels can add additional carbon to the soil where most of it can return to the atmosphere. A comparison for both sites from 2017 to 2019 shows that TP74 is more wet in 2018 compared to TPD (Figure 3.2). If additional moisture along with increased temperature changes were to occur at TP74 with climate change, there can be a potentially large increase in Rs because of stand instability.

3.6 Conclusion

This study demonstrates the influence of Ts on Rs within two forest stands from 2017 to 2019. Extreme weather events were observed in 2018. Study results showed that by applying spectral analysis to measured Rs data for multiple years, variations in Rs in 2018 were shown to be closely linked to Ts at diel timescales in TP74 and in at both sites in 2019. SM fluctuated with increases in PPT in both sites and corresponded with wet periods in the spring and fall. Increases in SM in the summer caused Rs oscillations. Furthermore, by comparing multiple models with their AICc, the Gaussian – Gamma model was able to rank consistently high for all years (with the exception of TPD in 2017) which reinforces the importance of Ts and SM

within both conifer and deciduous forests. Findings indicate that the soil CO_2 emissions in plantation conifer forests may be less resilient to increasing temperatures in extreme weather events. Future studies should examine the relationship between Ts, SM, and Rs during extreme weather years in managed forest ecosystems.

3.7 References

Alban, D. H. (1982). Effects of Nutrient Accumulation by Aspen, Spruce, and Pine on Soil Properties. *Soil Science Society of America Journal*, *46*(4), 853–861. https://doi.org/10.2136/sssaj1982.03615995004600040037x

Alexander, M. (1977). *Introduction to soil microbiology* (2nd ed.). New York, London: Wiley.

Andrews, J. A., Harrison, K. G., Matamala, R., & Schlesinger, W. H. (1999). Separation of Root Respiration from Total Soil Respiration Using Carbon-13 Labeling during Free-Air Carbon Dioxide Enrichment (FACE). *Soil Science Society of America Journal*, *63*(5), 1429–1435. https://doi.org/10.2136/sssaj1999.6351429x

Arain, M. A. (2002). *Fluxnet2015 CA-TP3 Ontario - Turkey Point 1974 Plantation White Pine.* https://doi.org/10.18140/FLX/1440052

Arain, M. A. (2012). *Fluxnet2015 CA-TPD Ontario - Turkey Point Mature Deciduous.* https://doi.org/10.18140/FLX/1440112

Barr, A. G., Ricciuto, D. M., Schaefer, K., Richardson, A., Agarwal, D., Thornton, P. E., . . . Verma, S. B. (2013). *Nacp Site: Tower Meteorology, Flux Observations with Uncertainty, and Ancillary Data.* https://doi.org/10.3334/ORNLDAAC/1178

Bauer, J., Weihermüller, L., Huisman, J. A., Herbst, M., Graf, A., Séquaris, J. M., & Vereecken, H. (2012). Inverse determination of heterotrophic soil respiration response to temperature and water content under field conditions. *Biogeochemistry*, *108*(1-3), 119–134. https://doi.org/10.1007/s10533-011-9583-1

Beamesderfer, E. R., Arain, M. A., Khomik, M., Brodeur, J. J., & Burns, B. M. (2020). Response of carbon and water fluxes to meteorological and phenological variability in two eastern North American forests of similar age but contrasting species composition – a multiyear comparison. *Biogeosciences*, *17*(13), 3563–3587. https://doi.org/10.5194/bg-17-3563-2020

Binkley, D., & Valentine, D. (1991). Fifty-year biogeochemical effects of green ash, white pine, and Norway spruce in a replicated experiment. *Forest Ecology and Management*, *40*(1-2), 13–25. https://doi.org/10.1016/0378-1127(91)90088-D

Bjorn Berg, Gunnar Ekbohm, & Charles McClaugherty. Lignin and holocellulose relations during long-term decomposition of some forest litters. Long-term decomposition in a Scots pine forest. IV.

Bowden, R. D., Nadelhoffer, K. J., Boone, R. D., Melillo, J. M., & Garrison, J. B. (1993). Contributions of aboveground litter, belowground litter, and root respiration to total soil respiration in a temperate mixed hardwood forest. *Canadian Journal of Forest Research*, *23*(7), 1402–1407. https://doi.org/10.1139/x93-177

Bunnell, F. L., Tait, D.E.N., & Flanagan, P. W. (1977). Microbial respiration and substrate weight loss—II. *Soil Biology and Biochemistry*, *9*(1), 41–47. https://doi.org/10.1016/0038-0717(77)90059-1

Canadell, J. G., Le Quéré, C., Raupach, M. R., Field, C. B., Buitenhuis, E. T., Ciais, P., . . . Marland, G. (2007). Contributions to accelerating atmospheric CO2 growth from economic activity, carbon intensity, and efficiency of natural sinks. *Proceedings of the National Academy of Sciences of the United States of America*, *104*(47), 18866–18870. https://doi.org/10.1073/pnas.0702737104

Carlyle, J. C., & Than, U. B. (1988). Abiotic Controls of Soil Respiration Beneath an Eighteen-Year-Old Pinus Radiata Stand in South-Eastern Australia. *The Journal of Ecology*, *76*(3), 654. https://doi.org/10.2307/2260565

Craine, J. M., & Gelderman, T. M. (2011). Soil moisture controls on temperature sensitivity of soil organic carbon decomposition for a mesic grassland. *Soil Biology and Biochemistry*, *43*(2), 455–457. https://doi.org/10.1016/j.soilbio.2010.10.011

Curiel Yuste, J., Baldocchi, D. D., Gershenson, A., Goldstein, A., Misson, L., & Wong, S. (2007). Microbial soil respiration and its dependency on carbon inputs, soil temperature and moisture. *Global Change Biology*, *13*(9), 2018–2035. https://doi.org/10.1111/j.1365-2486.2007.01415.x

Curiel Yuste, J., Janssens, I. A., Carrara, A., & Ceulemans, R. (2004). Annual Q10 of soil respiration reflects plant phenological patterns as well as temperature sensitivity. *Global Change Biology*, *10*(2), 161–169. https://doi.org/10.1111/j.1529-8817.2003.00727.x

Curiel Yuste, J., Nagy, M., Janssens, I. A., Carrara, A., & Ceulemans, R. (2005). Soil respiration in a mixed temperate forest and its contribution to total ecosystem respiration. *Tree Physiology*, *25*(5), 609–619. https://doi.org/10.1093/treephys/25.5.609

Davidson, E. A., & Janssens, I. A. (2006). Temperature sensitivity of soil carbon decomposition and feedbacks to climate change. *Nature*, *440*(7081), 165–173. https://doi.org/10.1038/nature04514

Davidson, E. A., Belk, E., & Boone, R. D. (1998). Soil water content and temperature as independent or confounded factors controlling soil respiration in a temperate mixed hardwood forest. *Global Change Biology*, *4*(2), 217–227. https://doi.org/10.1046/j.1365-2486.1998.00128.x

Environment and Climate Change Canada (2020, July 30). Hourly Data Report for December 31, 2019 - Climate - Environment and Climate Change Canada. Retrieved from https://climate.weather.gc.ca/climate_data/hourly_data_e.html?hlyRange=1999-07-16%7C2020-07-29&dlyRange=1997-06-01%7C2020-07-29&mlyRange=1997-06-01%7C2006-12-01&StationID=27528&Prov=ON&urlExtension=_e.html&searchType=stnName&optLimit=yearRange&StartYear=1840&EndYear=2020&selRowPerPage=25&Line=1&searchMethod=contains&txtStationName=delhi&timeframe=1&Year=2019&Month=12&Day=31#

Gabriel, C. E., & Kellman, L. (2011). Examining moisture and temperature sensitivity of soil organic matter decomposition in a temperate coniferous forest soil. *Biogeosciences Discussions*, *8*(1), 1369–1409. https://doi.org/10.5194/bgd-8-1369-2011

Grinsted, A., Moore, J. C., & Jevrejeva, S. (2004). Application of the cross wavelet transform and wavelet coherence to geophysical time series. *Nonlinear Processes in Geophysics*, *11*(5/6), 561–566. https://doi.org/10.5194/npg-11-561-2004

Hanson, P. J., & Wullschleger, S. D. (Eds.) (2012], 2003). *Ecological Studies: v. 166. North American temperate deciduous forest responses to changing precipitation regimes*. New York: Springer. https://doi.org/10.1007/978-1-4613-0021-2

Harpold, A. A. (2016). Diverging sensitivity of soil water stress to changing snowmelt timing in the Western U.S. *Advances in Water Resources*, *92*, 116–129. https://doi.org/10.1016/j.advwatres.2016.03.017

Hartley, I. P., Heinemeyer, A., & Ineson, P. (2007). Effects of three years of soil warming and shading on the rate of soil respiration: substrate availability and not thermal acclimation mediates observed response. *Global Change Biology*, *13*(8), 1761–1770. https://doi.org/10.1111/j.1365-2486.2007.01373.x

Högberg, P., & Ekblad, A. (1996). Substrate-induced respiration measured in situ in a C3-plant ecosystem using additions of C4-sucrose. *Soil Biology and Biochemistry*, *28*(9), 1131–1138. https://doi.org/10.1016/0038-0717(96)00124-1

Hou, Z., Engel, D. W., Lin, G., Fang, Y., & Fang, Z. (2013). An Uncertainty Quantification Framework for Studying the Effect of Spatial Heterogeneity in Reservoir Permeability on CO2 Sequestration. *Mathematical Geosciences*, *45*(7), 799–817. https://doi.org/10.1007/s11004-013-9459-0

Hurvich, C. M., & Tsai, C.-L. (1989). Regression and time series model selection in small samples. *Biometrika*, *76*(2), 297–307. https://doi.org/10.1093/biomet/76.2.297

Illeris, L., Christensen, T. R., & Mastepanov, M. (2004). Moisture Effects on Temperature Sensitivity of CO2 Exchange in a Subarctic Heath Ecosystem. *Biogeochemistry*, *70*(3), 315–330. https://doi.org/10.1007/s10533-003-0855-2

Jassal, R. S., Black, T. A., Novak, M. D., Gaumont-Guay, D., & Nesic, Z. (2008). Effect of soil water stress on soil respiration and its temperature sensitivity in an 18-year-old temperate Douglas-fir stand. *Global Change Biology*, *14*(6), 1305–1318. https://doi.org/10.1111/j.1365-2486.2008.01573.x

Jevrejeva, S., Moore, J. C., & Grinsted, A. (2003). Influence of the Arctic Oscillation and El Niño-Southern Oscillation (ENSO) on ice conditions in the Baltic Sea: The wavelet approach. *Journal of Geophysical Research*, *108*(D21). https://doi.org/10.1029/2003JD003417

Jia, X., Zha, T., Wang, S., Bourque, C. P.-A., Wang, B., Qin, S., & Zhang, Y. (2018). Canopy photosynthesis modulates soil respiration in a temperate semi-arid shrubland at multiple timescales. *Plant and Soil*, *432*(1-2), 437–450. https://doi.org/10.1007/s11104-018-3818-z

Jones, C. D., Cox, P., & Huntingford, C. (2003). Uncertainty in climate-carbon-cycle projections associated with the sensitivity of soil respiration to temperature. *Tellus B*, *55*(2), 642–648. https://doi.org/10.1034/j.1600-0889.2003.01440.x

Khomik, Myroslava. (2004). Soil CO2 Efflux From Temperate and Boreal Forests in Ontario (Master's Thesis). McMaster University. Hamilton, Ontario.

Khomik, M., Arain, M. A., Brodeur, J. J., Peichl, M., Restrepo-Coupé, N., & McLaren, J. D. (2010). Relative contributions of soil, foliar, and woody tissue respiration to total ecosystem respiration in four pine forests of different ages. *Journal of Geophysical Research*, *115*(G3), 237. https://doi.org/10.1029/2009JG001089

Khomik, M., Arain, M. A., Liaw, K.-L., & McCaughey, J. H. (2009). Debut of a flexible model for simulating soil respiration–soil temperature relationship: Gamma model. *Journal of Geophysical Research*, *114*(G3), 912. https://doi.org/10.1029/2008JG000851

Kindermann, G., Obersteiner, M., Sohngen, B., Sathaye, J., Andrasko, K., Rametsteiner, E., . . . Beach, R. (2008). Global cost estimates of reducing carbon emissions through avoided deforestation. *Proceedings of the*

National Academy of Sciences of the United States of America, *105*(30), 10302–10307. https://doi.org/10.1073/pnas.0710616105

Lellei-Kovács, E., Kovács-Láng, E., Botta-Dukát, Z., Kalapos, T., Emmett, B., & Beier, C. (2011). Thresholds and interactive effects of soil moisture on the temperature response of soil respiration. *European Journal of Soil Biology*, *47*(4), 247–255. https://doi.org/10.1016/j.ejsobi.2011.05.004

Liu, Y.-R., Delgado-Baquerizo, M., Wang, J.-T., Hu, H.-W., Yang, Z., & He, J.-Z. (2018). New insights into the role of microbial community composition in driving soil respiration rates. *Soil Biology and Biochemistry*, *118*, 35–41. https://doi.org/10.1016/j.soilbio.2017.12.003

Livingston, G. P. and Hutchinson, G. L.: Enclosure-based measurement of trace gas exchange: applications and sources of error, in: Biogenic Trace Gases: Measuring Emissions from Soil and Water, edited by: Matson, P. A. and Harriss, R. C. , Blackwell Scientific Publications, Oxford, 14–51, 1995

Lloyd, J., & Taylor, J. A. (1994). On the Temperature Dependence of Soil Respiration. *Functional Ecology*, *8*(3), 315. https://doi.org/10.2307/2389824

Lorenz, K., & Lal, R. (2010). *Carbon Sequestration in Forest Ecosystems*. Dordrecht: Springer Netherlands. https://doi.org/10.1007/978-90-481-3266-9

Lowman, M., & Rinker, H. B. (2004). *Forest canopies* (2nd ed.). *Physiological Ecology*. Amsterdam, Boston: Elsevier Academic Press. Retrieved from http://site.ebrary.com/lib/alltitles/docDetail.action?docID=10186345

Luo, Y., & Zhou, X. (2006). *Soil respiration and the environment*. Amsterdam, London: Academic Press. Retrieved from http://www.loc.gov/catdir/enhancements/fy0665/2006024416-d.html

MacKay, S. L., Arain, M. A., Khomik, M., Brodeur, J. J., Schumacher, J., Hartmann, H., & Peichl, M. (2012). The impact of induced drought on transpiration and growth in a temperate pine plantation forest. *Hydrological Processes*, *26*(12), 1779–1791. https://doi.org/10.1002/hyp.9315

McLaren, J. D., Arain, M. A., Khomik, M., Peichl, M., & Brodeur, J. (2008). Water flux components and soil water-atmospheric controls in a temperate pine forest growing in a well-drained sandy soil. *Journal of Geophysical Research: Biogeosciences*, *113*(G4), 237. https://doi.org/10.1029/2007JG000653

Meyer, N., Welp, G., & Amelung, W. (2018). The Temperature Sensitivity (Q10) of Soil Respiration: Controlling Factors and Spatial Prediction at Regional Scale Based on Environmental Soil Classes. *Global Biogeochemical Cycles*, *32*(2), 306–323. https://doi.org/10.1002/2017GB005644

Myers, R. J. K., Weier, K. L., & Campbell, C. A. (1982). QUANTITATIVE RELATIONSHIP BETWEEN NET NITROGEN MINERALIZATION AND MOISTURE CONTENT OF SOILS. *Canadian Journal of Soil Science*, *62*(1), 111–124. https://doi.org/10.4141/cjss82-013

Neumann, J. (1956). On the Incidence of Dry and Wet Years. *Israel Exploration Journal*, *6*(1), 58–63. Retrieved from www.jstor.org/stable/27924644

Oh, Y.-Y., Yun, S.-T., Yu, S., Kim, H.-J., & Jun, S.-C. (2019). A novel wavelet-based approach to characterize dynamic environmental factors controlling short-term soil surface CO2 flux: Application to a controlled CO2 release test site (EIT) in South Korea. *Geoderma*, *337*, 76–90. https://doi.org/10.1016/j.geoderma.2018.09.017

Orchard, V. A., & Cook, F. J. (1983). Relationship between soil respiration and soil moisture. *Soil Biology and Biochemistry*, *15*(4), 447–453. https://doi.org/10.1016/0038-0717(83)90010-X

Pangle, R., Kavanagh, K., & Duursma, R. (2015). Decline in canopy gas exchange with increasing tree height, atmospheric evaporative demand, and seasonal drought in co-occurring inland Pacific Northwest conifer species. *Canadian Journal of Forest Research*, *45*(8), 1086–1101. https://doi.org/10.1139/cjfr-2014-0551

Peichl, M., Arain, M. A., & Brodeur, J. J. (2010). Age effects on carbon fluxes in temperate pine forests. *Agricultural and Forest Meteorology*, *150*(7-8), 1090–1101. https://doi.org/10.1016/j.agrformet.2010.04.008

Pumpanen, J., Ilvesniemi, H., Kulmala, L., Siivola, E., Laakso, H., Kolari, P., . . . Hari, P. (2008). Respiration in Boreal Forest Soil as Determined from Carbon Dioxide Concentration Profile. *Soil Science Society of America Journal*, *72*(5), 1187–1196. https://doi.org/10.2136/sssaj2007.0199

Quan, Q., Wang, C., He, N., Zhang, Z., Wen, X., Su, H., . . . Xue, J. (2014). Forest type affects the coupled relationships of soil C and N mineralization in the temperate forests of northern China. *Scientific Reports*, *4*, 6584. https://doi.org/10.1038/srep06584

Raich, J. W., & Schlesinger, W. H. (1992). The global carbon dioxide flux in soil respiration and its relationship to vegetation and climate. *Tellus B*, *44*(2), 81–99. https://doi.org/10.1034/j.1600-0889.1992.t01-1-00001.x

Ratkowsky, D. A., Olley, J., McMeekin, T. A., & Ball, A. (1982). Relationship between temperature and growth rate of bacterial cultures. *Journal of Bacteriology*, *149*(1), 1–5.

Reichstein, M., & Beer, C. (2008). Soil respiration across scales: The importance of a model–data integration framework for data interpretation. *Journal of Plant Nutrition and Soil Science*, *171*(3), 344–354. https://doi.org/10.1002/jpln.200700075

Richart, M., & Hewitt, N. (2008). Forest remnants in the Long Point region, Southern Ontario: Tree species diversity and size structure. *Landscape and*

Urban Planning, *86*(1), 25–37. https://doi.org/10.1016/j.landurbplan.2007.12.005

Rogers, H. H., Runion, G.B., & Krupa, S. V. (1994). Plant responses to atmospheric CO2 enrichment with emphasis on roots and the rhizosphere. *Environmental Pollution*, *83*(1-2), 155–189. https://doi.org/10.1016/0269-7491(94)90034-5

Rustad, L., Campbell, J., Marion, G., Norby, R., Mitchell, M., Hartley, A., . . . Gurevitch, J. (2001). A meta-analysis of the response of soil respiration, net nitrogen mineralization, and aboveground plant growth to experimental ecosystem warming. *Oecologia*, *126*(4), 543–562. https://doi.org/10.1007/s004420000544

Saiz, G., Byrne, K. A., Butterbach-Bahl, K., Kiese, R., Blujdea, V., & Farrell, E. P. (2006). Stand age-related effects on soil respiration in a first rotation Sitka spruce chronosequence in central Ireland. *Global Change Biology*, *12*(6), 1007–1020. https://doi.org/10.1111/j.1365-2486.2006.01145.x

Samuels-Crow, K. E., Ryan, E., Pendall, E., & Ogle, K. (2018). Temporal Coupling of Subsurface and Surface Soil CO 2 Fluxes: Insights From a Nonsteady State Model and Cross-Wavelet Coherence Analysis. *Journal of Geophysical Research: Biogeosciences*, *123*(4), 1406–1424. https://doi.org/10.1002/2017JG004207

Savage, K., Davidson, E. A., Richardson, A. D., & Hollinger, D. Y. (2009). Three scales of temporal resolution from automated soil respiration measurements. *Agricultural and Forest Meteorology*, *149*(11), 2012–2021. https://doi.org/10.1016/j.agrformet.2009.07.008

Schlesinger, W. H., & Andrews, J. A. (2000). Soil respiration and the global carbon cycle. *Biogeochemistry*, *48*(1), 7–20. https://doi.org/10.1023/A:1006247623877

Shabaga, J. A., Basiliko, N., Caspersen, J. P., & Jones, T. A. (2015). Seasonal controls on patterns of soil respiration and temperature sensitivity in a northern mixed deciduous forest following partial-harvesting. *Forest Ecology and Management*, *348*, 208–219. https://doi.org/10.1016/j.foreco.2015.03.022

Shi, W.-Y., Su, L.-J., Song, Y., Ma, M.-G., & Du, S. (2015). A Monte Carlo approach to estimate the uncertainty in soil CO2 emissions caused by spatial and sample size variability. *Ecology and Evolution*, *5*(19), 4480–4491. https://doi.org/10.1002/ece3.1729

Singh, N., Parida, B. R., Charakborty, J. S., & Patel, N. R. (2019). Net Ecosystem Exchange of CO2 in Deciduous Pine Forest of Lower Western Himalaya, India. *Resources*, *8*(2), 98. https://doi.org/10.3390/resources8020098

Stanford, G., & Epstein, E. (1974). Nitrogen Mineralization-Water Relations in Soils. *Soil Science Society of America Journal*, *38*(1), 103–107. https://doi.org/10.2136/sssaj1974.03615995003800010032x

Taylor, A. J., Lai, C.-T., Hopkins, F. M., Wharton, S., Bible, K., Xu, X., . . . Ehleringer, J. R. (2015). Radiocarbon-Based Partitioning of Soil Respiration in an Old-Growth Coniferous Forest. *Ecosystems*, *18*(3), 459–470. https://doi.org/10.1007/s10021-014-9839-4

Tuomi, M., Vanhala, P., Karhu, K., Fritze, H., & Liski, J. (2008). Heterotrophic soil respiration—Comparison of different models describing its temperature dependence. *Ecological Modelling*, *211*(1-2), 182–190. https://doi.org/10.1016/j.ecolmodel.2007.09.003

Ullah, S., Frasier, R., King, L., Picotteanderson, N., & Moore, T. (2008). Potential fluxes of N2O and CH4 from soils of three forest types in Eastern Canada. *Soil Biology and Biochemistry*, *40*(4), 986–994. https://doi.org/10.1016/j.soilbio.2007.11.019

Ullah, S., Breitenbeck, G. A., & Faulkner, S. P. (2005). Denitrification and N2O emission from forested and cultivated alluvial clay soil. *Biogeochemistry*, *73*(3), 499–513. https://doi.org/10.1007/s10533-004-1565-0

Van der Molen, M. K., Dolman, A. J., Ciais, P., Eglin, T., Gobron, N., Law, B. E., . . . Wang, G. (2011). Drought and ecosystem carbon cycling. *Agricultural and Forest Meteorology*, *151*(7), 765–773. https://doi.org/10.1016/j.agrformet.2011.01.018

Van't Hoff, M. J. H. (1884). Etudes de dynamique chimique. *Recueil Des Travaux Chimiques Des Pays-Bas*, *3*(10), 333–336. https://doi.org/10.1002/recl.18840031003

Vargas, R., & Allen, M. F. (2008). Diel patterns of soil respiration in a tropical forest after Hurricane Wilma. *Journal of Geophysical Research*, *113*(G3), 859. https://doi.org/10.1029/2007JG000620

Vargas, R., Detto, M., Baldocchi, D. D., & Allen, M. F. (2010). Multiscale analysis of temporal variability of soil CO 2 production as influenced by weather and vegetation. *Global Change Biology*, *16*(5), 1589–1605. https://doi.org/10.1111/j.1365-2486.2009.02111.x

Wang, X., Jiang, Y., Jia, B., Wang, F., & Zhou, G. (2010). Comparison of soil respiration among three temperate forests in Changbai Mountains, China. *Canadian Journal of Forest Research*, *40*(4), 788–795. https://doi.org/10.1139/X10-010

Welles, J.M., Demetriades-Shah, T.H., & McDermitt, D.K. (2001). Considerations for measuring ground CO2 effluxes with chambers. *Chemical Geology*, *177*(1-2), 3–13. https://doi.org/10.1016/S0009-2541(00)00388-0

Woo, M.-k., Arain, M. A., Mollinga, M., & Yi, S. (2004). A two-directional freeze and thaw algorithm for hydrologic and land surface modelling. *Geophysical Research Letters*, *31*(12), n/a-n/a. https://doi.org/10.1029/2004GL019475

Xu, M., & Qi, Y. (2001). Spatial and seasonal variations of Q10 determined by soil respiration measurements at a Sierra Nevadan Forest. *Global*

Biogeochemical Cycles, *15*(3), 687–696. https://doi.org/10.1029/2000GB001365

Yates, T. T., Si, B. C., Farrell, R. E., & Pennock, D. J. (2006). Wavelet Spectra of Nitrous Oxide Emission from Hummocky Terrain during Spring Snowmelt. *Soil Science Society of America Journal*, *70*(4), 1110–1120. https://doi.org/10.2136/sssaj2005.0264

Table 3.1. Soil respiration (Rs) prediction models used for AICc analysis where lower alphabetical variables (a, b, etc.) are estimated values, Ts is soil temperature, and SM is soil moisture.

Model	Estimated Parameters	Formula	Reference
Rs Ts	2	$Rs = ae^{bTs}$	Van't Hoff (1884)
Rs Q10	2	$Rs = a * b^{\frac{Ts-10}{10}}$	Yuste et al (2005)
Rs Ts SM	4	$Rs = a * b^{\frac{Ts-10}{10}} * \left(\frac{1}{1+e^{c+d*SM}}\right)$	Khomik et al (2009)
Null	0	$Rs = mean(Rs)$	None
Ratkowsky	1	$Rs = a * [Ts - \min(Ts)]^2$	Ratkowsky (1982)
Stanford and Epstein	2	$Rs = a * SM + b$	Stanford and Epstein (1974)
Myers	3	$Rs = \frac{SM - a}{SM + b}$	Myers et al (1982)
Bunnell	5	$Rs = \left(\frac{SM}{a+SM}\right)\left(\frac{b}{b+SM}\right) cd^{\frac{Ts-10}{10}}$	Bunnell et al (1977)
Lloyd and Taylor	3	$Rs = a * e^{\frac{b}{c+Ts}}$	Lloyd and Taylor (1994)
Tuomi	3	$Rs = a * e^{b*Ts} + c$	Tuomi et al (2008)
Gaussian – Gamma	5	$Rs = e^{a+b*Ts+c*Ts^2+d*SM+e*\ln(SM)}$	Khomik et al (2010)

Table 3.2. Sample – corrected Akaike Information Criterion (AICc) for TP74 and TPD in 2017 with ranking.

2017

TP74			TPD		
Model	AICc	Difference	Model	AICc	Difference
Gaussian - Gamma	70.28	0	Bunnell	-14.68	0
Lloyd and Taylor	96.82	26.54	Lloyd and Taylor	98.76	113.45
Rs Ts	99.2	28.91	Rs Q10	112.69	127.38
Tuomi	99.57	29.29	Rs Ts	112.69	127.38
Stanford and Epstein	115.14	44.86	Stanford and Epstein	263.76	278.44
NULL	123.07	52.78	NULL	266.66	281.34
Ratkowsky	218.11	147.82	Ratkowsky	321.58	336.26
Bunnell	250.97	180.69	Rs Ts SM	608.97	623.66
Rs Q10	462.97	392.69	Gaussian - Gamma	705.43	720.12
Myers	479.17	408.89	Myers	709.68	724.36
Rs Ts SM	479.38	409.09	Tuomi	1837.03	1851.72

Table 3.3. Sample – corrected Akaike Information Criterion (AICc) for TP74 and TPD in 2018 with ranking.

2018

TP74			TPD		
Model	AICc	Difference	Model	AICc	Difference
Gaussian - Gamma	-78.39	0	Gaussian - Gamma	92.77	0
Rs Ts SM	-72.47	5.92	Rs Ts SM	113.38	20.61
Lloyd and Taylor	77.45	155.84	Bunnell	115.98	23.21
Tuomi	78.59	156.98	Lloyd and Taylor	169.63	76.86
Rs Ts	85.57	164.26	Tuomi	170.63	77.86
Rs Q10	85.57	164.26	Rs Q10	174.17	81.4
Bunnell	106.42	184.81	Rs Ts	174.17	81.4
Ratkowsky	180.36	258.75	Ratkowsky	300.89	208.12
Stanford and Epstein	211.84	290.23	Stanford and Epstein	355.95	263.18
Myers	217.14	295.53	NULL	378.99	286.22
NULL	237.73	316.12	Myers	386.02	293.25

Table 3.4. Sample – corrected Akaike Information Criterion (AICc) for TP74 and TPD in 2019 with ranking.

2019					
TP74			TPD		
Model	AICc	Difference	Model	AICc	Difference
Gaussian - Gamma	-131.16	0	Gaussian - Gamma	-134.69	0
Rs Ts SM	-128.39	2.76	Bunnell	-96.33	38.35
Rs Q10	-118.5	12.65	Lloyd and Taylor	14.74	149.43
Rs Ts	-118.5	12.65	Rs Q10	15.12	149.81
Stanford and Epstein	-28.11	103.04	Rs Ts	15.12	149.81
Ratkowsky	105.82	236.98	Rs Ts SM	19.24	153.93
NULL	121.12	252.28	Ratkowsky	71.03	205.72
Lloyd and Taylor	124.71	255.87	Tuomi	415.21	549.9
Tuomi	352.86	484.02	Stanford and Epstein	418.72	553.41
Myers	565.32	696.48	NULL	453.03	587.72
Bunnell	866.61	997.77	Myers	815.55	950.24

Table 3.5. Q10 values at TP74 and TPD forest site from 2017 to 2019.

Year	TP74 Q10 Value	TPD Q10 Value
2017	1.87	2.40
2018	1.88	2.12
2019	1.86	2.88
Mean	**1.87**	**2.47**

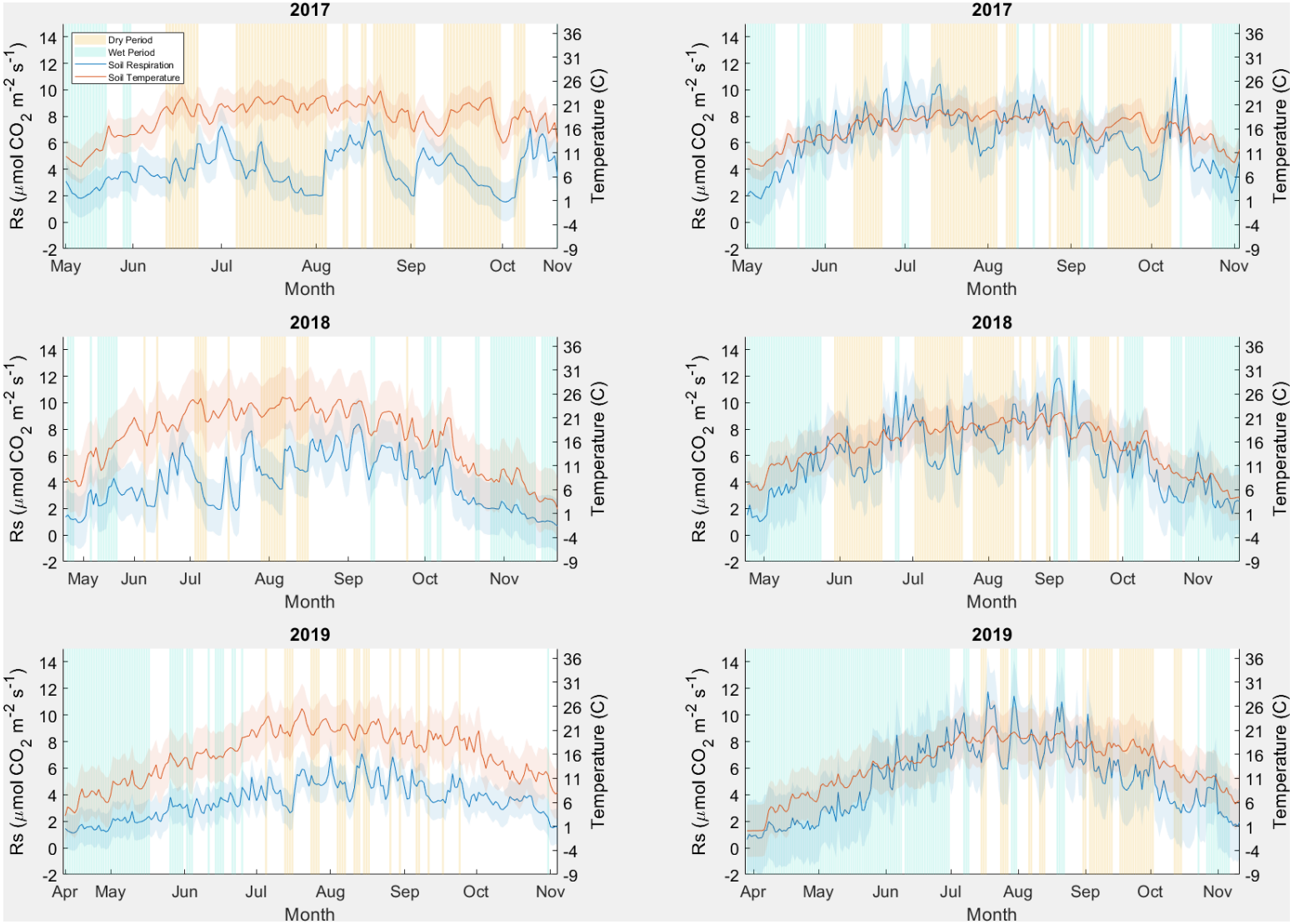

Figure 3.1. Observed daily soil respiration (Rs) and soil temperature values with dry (orange) and wet (blue) periods for TP74 (left) and TPD (right) from 2017 to 2019. Dry periods were calculated from the standard deviation below the mean soil moisture (SM) and wet periods were calculated from the standard deviation above the mean SM.

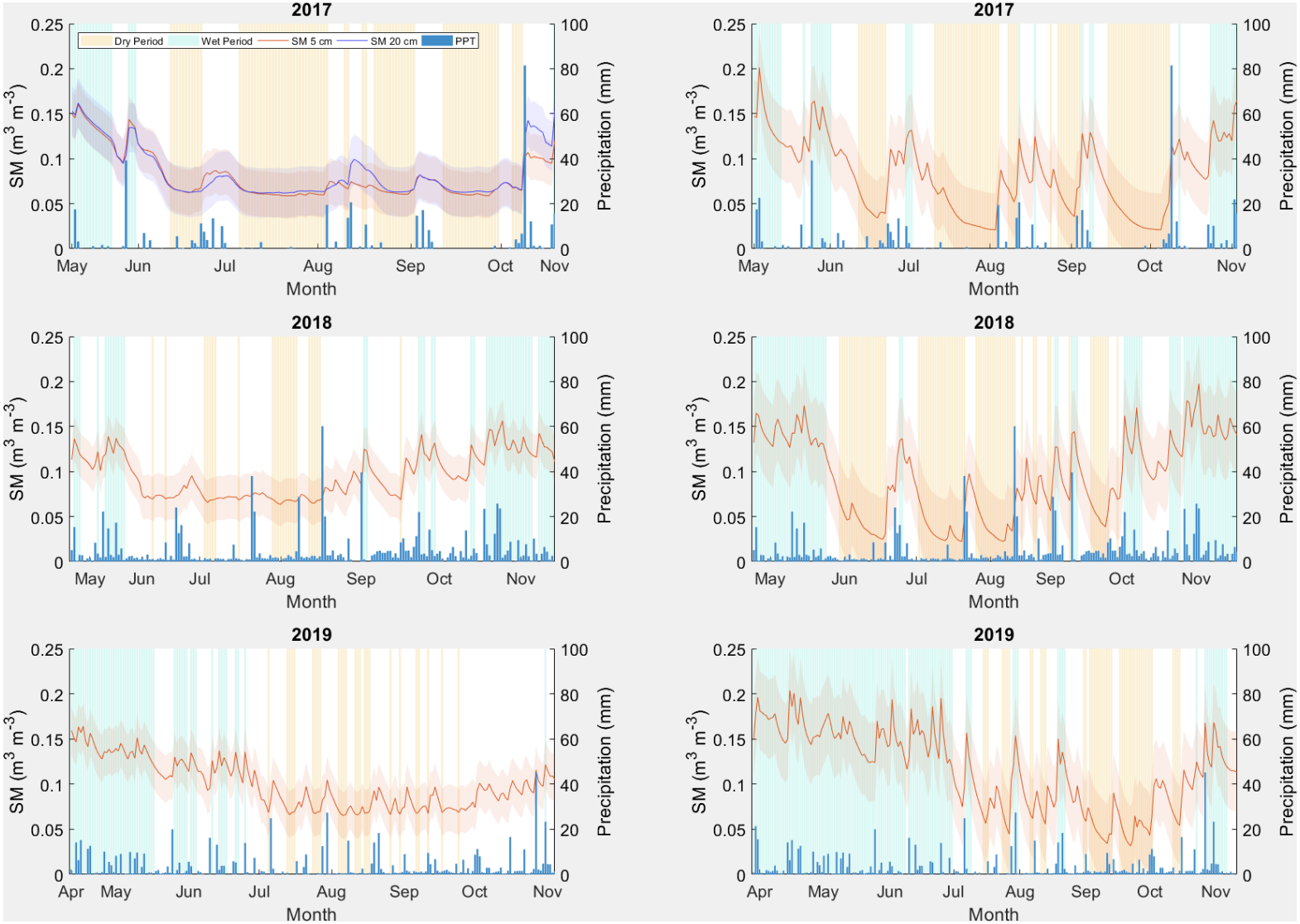

Figure 3.2. Observed soil moisture (SM) at 5 cm along with precipitation for TP74 (left) and TPD (right) from 2017 to 2019. Dry periods are highlighted in orange, while wet periods are highlighted in blue. Dry periods were calculated from the standard deviation below the mean soil moisture (SM) and wet periods were calculated from the standard deviation above the mean SM

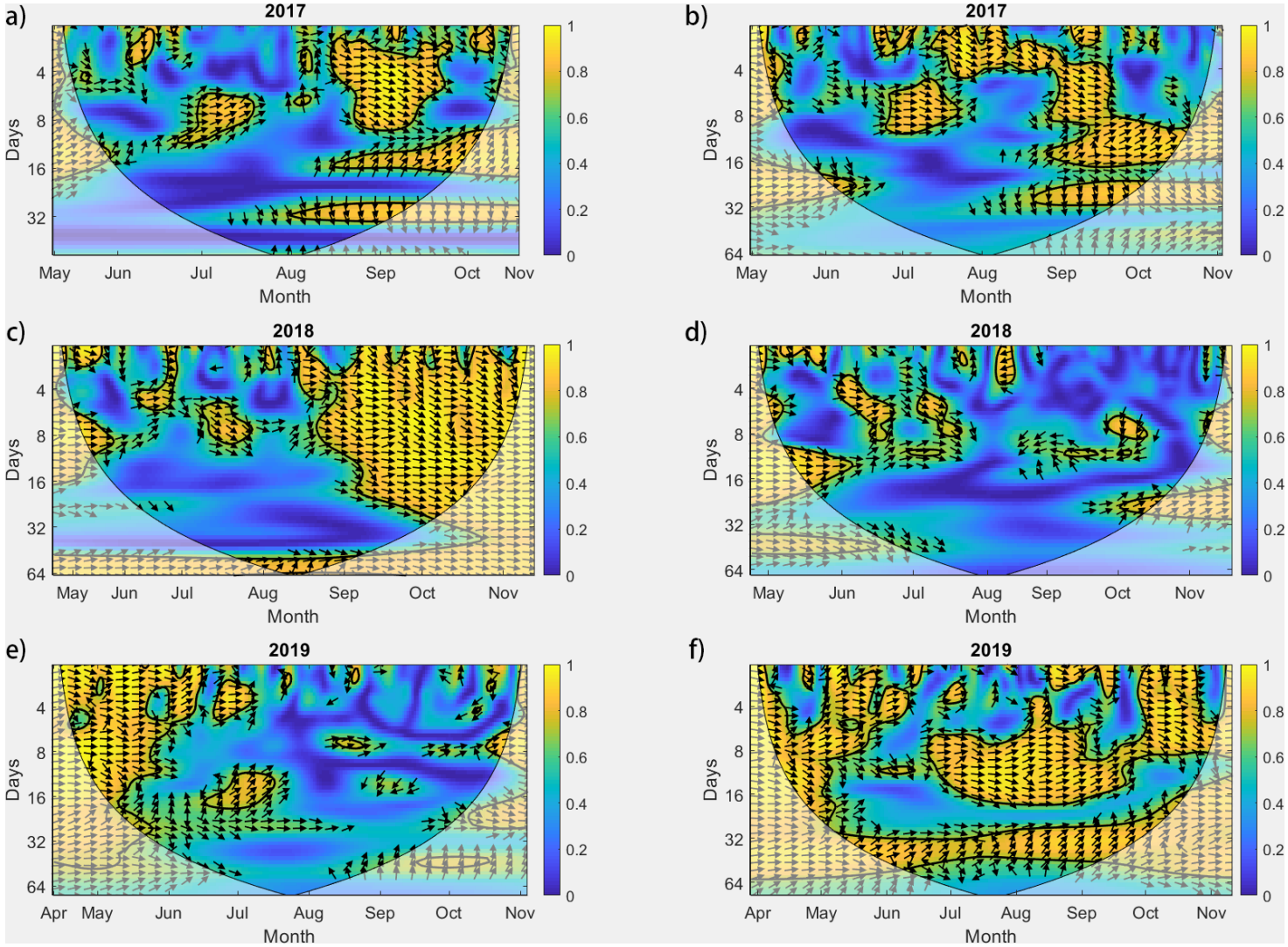

Figure 3.3. Cross – wavelet coherence between soil respiration (Rs) and soil temperature (Ts) for TP74 (left) and TPD (right) in from 2017 to 2019. Areas of yellow indicate high coherence while areas in blue indicate no coherence. Arrows indicate the phase and lag between the time series.

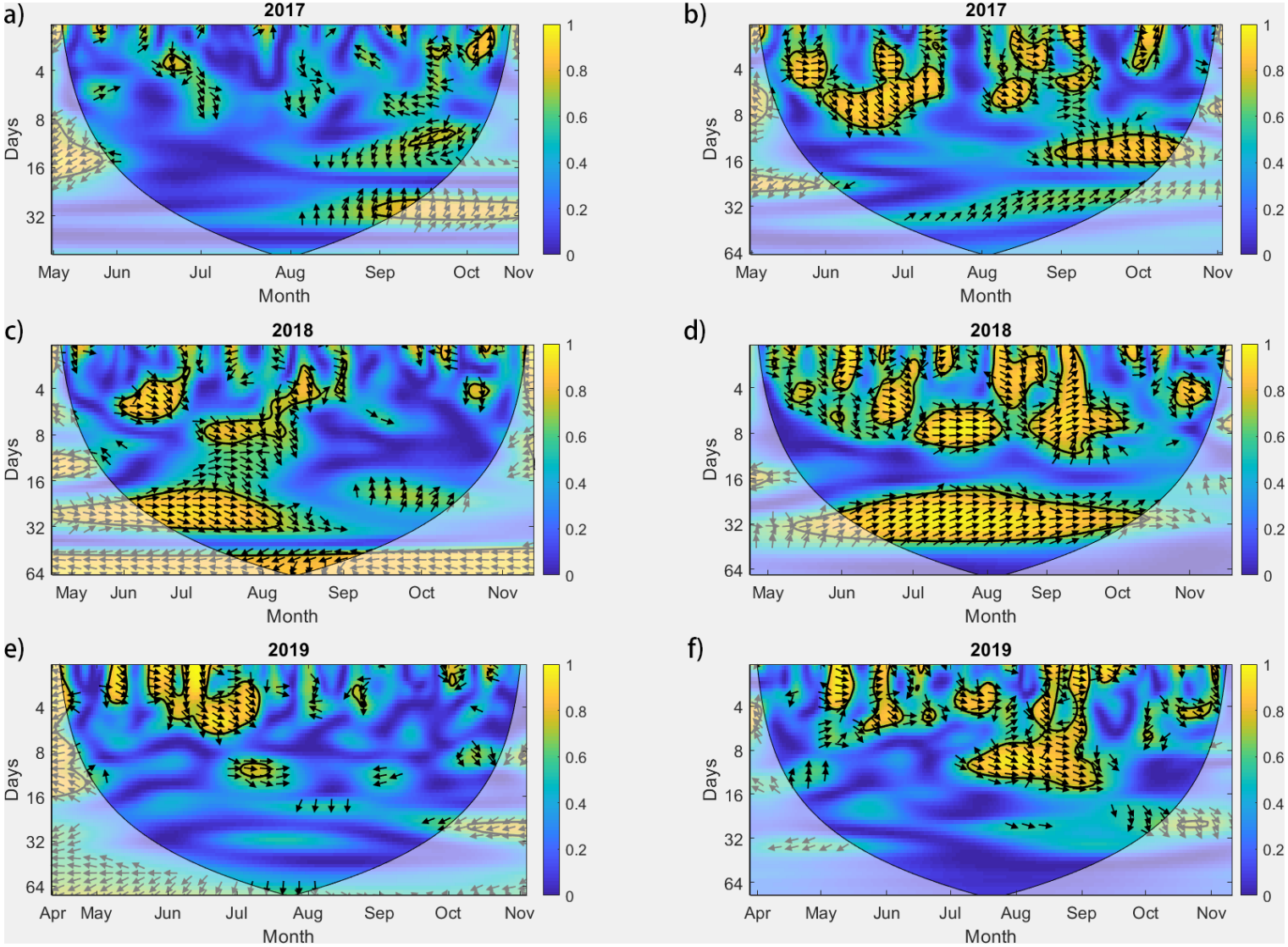

Figure 3.4. Cross – wavelet coherence between soil respiration (Rs) and soil moisture (SM) for TP74 (left) and TPD (right) from 2017 to 2019.

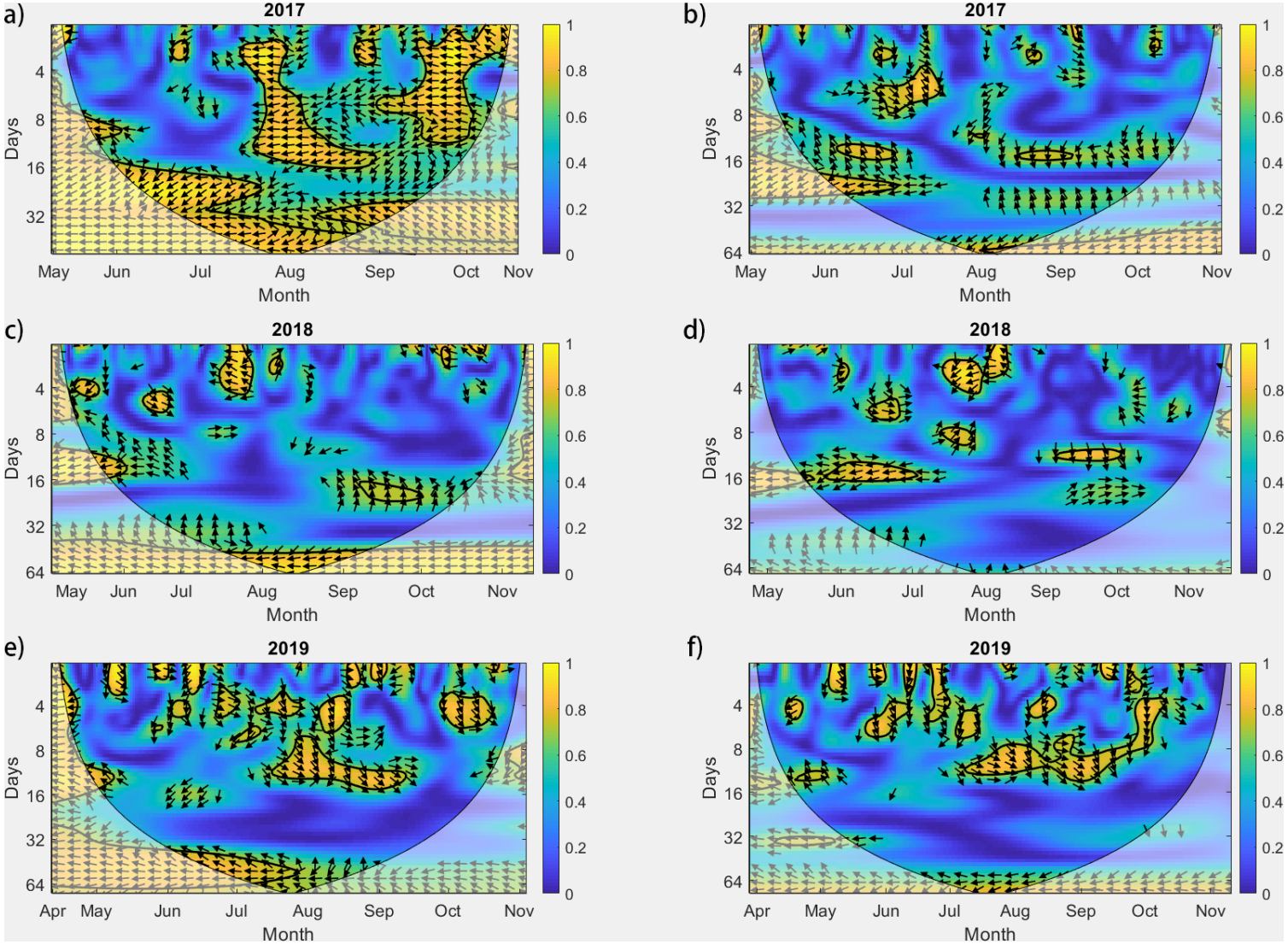

Figure 3.5. Cross – wavelet coherence between soil temperature (Ts) and soil moisture (SM) for TP74 (left) and TPD (right) from 2017 to 2019.

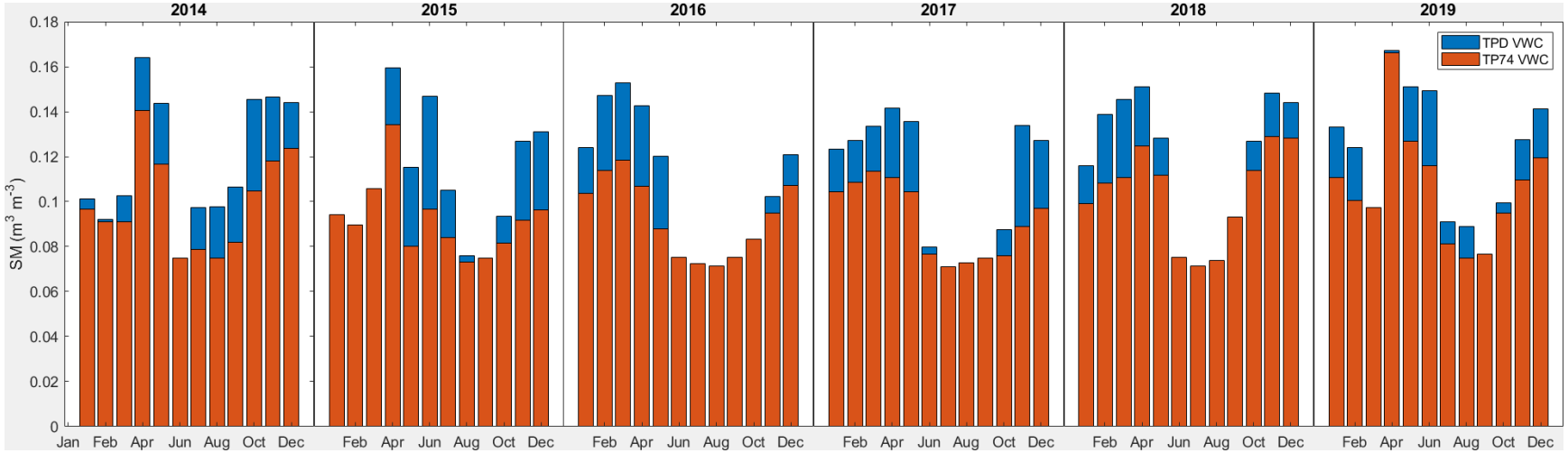

Figure 3.6. Volumetric soil water content or soil moisture (SM) at 5 cm depth in $m^3\ m^{-3}$ for TPD and TP74 from 2014 to 2019.

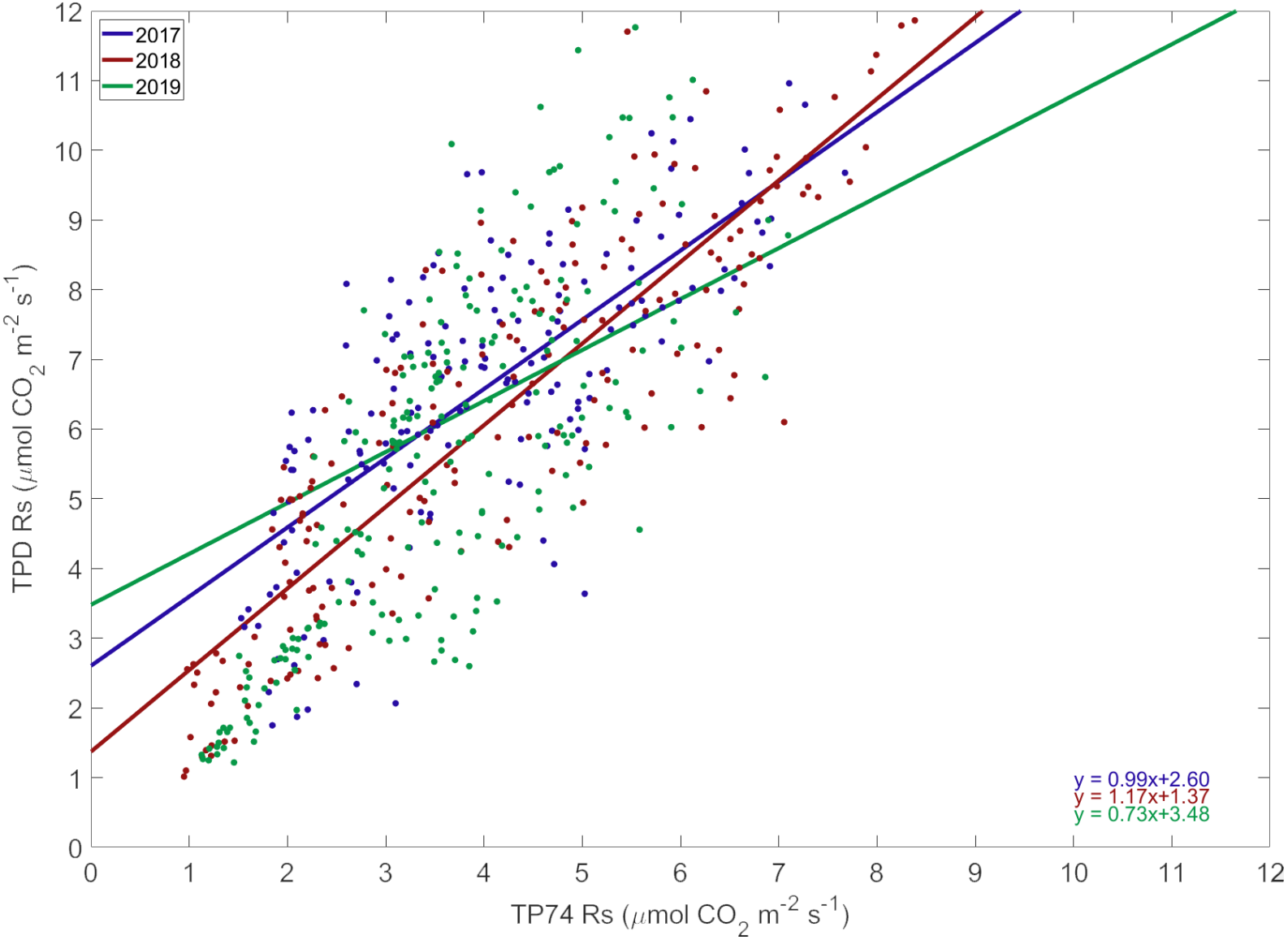

Figure 3.7. Linear regression between daily mean values of soil respiration (Rs) at TP74 and TPD forest sites from 2017 (blue), 2018 (red), 2019 (green), and Y = x (black).

Chapter 4: Conclusions

4.1 Major Findings

This dissertation evaluated the response of soil respiration to environmental controls such as soil temperature (Ts) and soil moisture (SM) in a temperate coniferous and deciduous forests in southern Ontario, Canada using measurements, modeling and spectral analysis. Study results revealed that Ts was the main driving factor for soil respiration. Variations in Ts in June, July, and August were found to be a significant controlling factor for the annual carbon budget of soil respiration. Empirical model testing using the corrected Akaike Information Criterion (AICc) showed that the Gaussian – Gamma model which incorporated both Ts and SM displayed the lowest value with the highest coefficient of determination. This study found that the conifer plantation forest (TP74) was much more sensitive to temperature compared to the deciduous stand (TPD), in particular during years that experienced extreme weather events such as in 2018. This implies that with increasing temperatures from climate change, that conifer plantation forests may be less resilient in this region. The reason for this is likely due to soil structure, canopy composition, and sensitivity of conifer species to warmer temperatures as compared to mixed deciduous stands. In both forest stands, the soil structure consists of over 90% sand causing precipitation to rapidly percolate. However, differences in canopy composition and water use by coniferous and deciduous species impacted SM.

Study results at TPD from 2014 to 2018 using eight different models showed that the Gaussian – Gamma model produced the best coefficient of determination, slope and y-intercept. Overall, models that incorporated SM predicted a better fit to observed data compared to Ts-only models suggesting that apart from Ts, SM and possibly other environmental variables was a major driving factor of soil respiration in these forest stands. The study showed that annual soil respiration accounted for 65 – 90% of observed eddy covariance ecosystem respiration for the growing season in the deciduous forest. Examining multiple Rs models can assist in understanding uncertainties associated with environmental variables and improve ecosystem models.

4.2 Future Considerations

In this study, multiple models were utilized to predict soil respiration and evaluate their performance. These models are utilized to gap fill missing data, in particular during winter periods when measurements are sparse or not measured. However, other studies report a wide variation (10 – 50%) of winter soil respiration contribution towards annual ecosystem respiration (Schindlbacher et al, 2017; Brooks et al, 2011; Contosta et al, 2016; Khomik, 2004). More future winter soil respiration measurements within the conifer and deciduous forest stands could be performed to determine winter contributions.

It is difficult to determine the source and depth of where soil respiration occurs in a soil column (Fang and Moncrieff, 2005; Kellman et al, 2015). Therefore, it is not possible to differentiate recalcitrant and labile carbon production because of

different depths of litter decomposition and time of CO_2 movement to the surface (Ryan and Law, 2005). Chamber measurements can be combined with soil organic matter content analysis and isotopic tracing to determine the source of carbon production in both sites (Pett-Ridge and Firestone, 2017).

4.3 References

Brooks, P. D., Grogan, P., Templer, P. H., Groffman, P., Öquist, M. G., & Schimel, J. (2011). Carbon and Nitrogen Cycling in Snow-Covered Environments. *Geography Compass*, *5*(9), 682–699. https://doi.org/10.1111/j.1749-8198.2011.00420.x

Contosta, A. R., Burakowski, E. A., Varner, R. K., & Frey, S. D. (2016). Winter soil respiration in a humid temperate forest: The roles of moisture, temperature, and snowpack. *Journal of Geophysical Research: Biogeosciences*, *121*(12), 3072–3088. https://doi.org/10.1002/2016JG003450

Fang, C., & Moncrieff, J. B. (2005). The variation of soil microbial respiration with depth in relation to soil carbon composition. *Plant and Soil*, *268*(1), 243–253. https://doi.org/10.1007/S11104-004-0278-4

Kellman, L., Myette, A., & Beltrami, H. (2015). Depth-Dependent Mineral Soil CO2 Production Processes: Sensitivity to Harvesting-Induced Changes in Soil Climate. *PloS One*, *10*(8), e0134171. https://doi.org/10.1371/journal.pone.0134171

Khomik, Myroslava. (2004). Soil CO2 Efflux From Temperate and Boreal Forests in Ontario (Master's Thesis). McMaster University. Hamilton, Ontario.

Pett-Ridge, J., & Firestone, M. K. (2017). Using stable isotopes to explore root-microbe-mineral interactions in soil. *Rhizosphere*, *3*, 244–253. https://doi.org/10.1016/j.rhisph.2017.04.016

Ryan, M. G., & Law, B. E. (2005). Interpreting, measuring, and modeling soil respiration. *Biogeochemistry*, *73*(1), 3–27. https://doi.org/10.1007/s10533-004-5167-7

Schindlbacher, A., Zechmeister-Boltenstern, S., Glatzel, G., & Jandl, R. (2007). Winter soil respiration from an Austrian mountain forest. *Agricultural and Forest Meteorology*, *146*(3-4), 205–215. https://doi.org/10.1016/j.agrformet.2007.06.001